University of Nevada, Reno

Direct-Contact Membrane Distillation: Simplified Flux Prediction, Mass Transfer Mechanisms, and Membrane Cleaning

A dissertation submitted in partial fulfillment of the requirements for the degree of Doctor of Philosophy in Civil and Environmental Engineering

By
Guiying Rao

Dr. Amy E. Childress and Dr. Sage R. Hiibel / Dissertation Advisors

August 2014

University of Nevada, Reno
Statewide • Worldwide

THE GRADUATE SCHOOL

We recommend that the dissertation
prepared under our supervision by

GUIYING RAO

entitled

Direct-Contact Membrane Distillation: Simplified Flux Prediction, Mass Transfer Mechanism, and Membrane Cleaning

be accepted in partial fulfillment of the
requirements for the degree of

DOCTOR OF PHILOSOPHY

Amy E. Childress, Advisor

Sage R. Hiibel, Committee Member

Keith E. Dennett, Committee Member

Chanwoo Park, Committee Member

Alan Fuchs, Graduate School Representative

Marsha H. Read, Ph. D., Dean, Graduate School

August, 2014

ABSTRACT OF THE DISSERTATION

Direct-Contact Membrane Distillation: Simplified Flux Prediction, Mass Transfer Mechanisms, and Membrane Cleaning

by

Guiying Rao

Doctor of Philosophy in Civil and Environmental Engineering

University of Nevada, Reno, 2014

Professor Amy E. Childress, Chair

Membrane distillation (MD) is a thermally-driven membrane separation process that uses the temperature difference at the membrane surfaces as the driving force to separate contaminants from potable water. The capability of MD to be combined with low-grade thermal energies to generate temperature gradients makes MD an attractive water treatment technology compared to the pressure-driven membrane processes, which utilize electricity as the power source. MD has versatile applications because it can achieve near 100% removal of salt and organic matter and the driving force of MD does not fluctuate significantly with variations in feed-water salinity.

Low water flux of MD is desirable when treating feed waters with high fouling potentials, while high water flux of MD is desirable when treating feed waters with low fouling potentials. Therefore, the ability to select a MD membrane with proper (high or low) water flux is useful. Although several mass transfer models are available for flux prediction of MD membranes, the models are generally cumbersome and require

information related to membrane properties. To overcome these issues, a simplified flux prediction model for direct-contact MD (DCMD) was developed using experimental flux and 28 structural parameters derived from physical properties of ten single-layer MD membranes. The membrane water fluxes were determined at the same experimental conditions, and the membrane properties included average pore size, porosity, tortuosity, thickness, liquid entry pressure, and contact angle. Additionally, an innovative membrane structural parameter, the membrane constant (C_m), that contains non-coupled membrane properties while still carrying the physical meaning of a relationship between thickness and porosity was developed. The correlation between water flux and C_m suggested that C_m is a good structural parameter for the prediction of MD flux. The flux prediction errors for membranes with pore sizes from 0.1 to 0.9 μm were generally smaller for the model developed with C_m than for the commonly used dusty gas model.

Because high water flux of MD is desirable when treating feed waters with low fouling potentials, the fundamental principles of mass transfer mechanisms in MD were investigated to provide insight into methods for flux improvement. The performances of three DCMD systems were investigated: 1) traditional DCMD, 2) pressure-enhanced DCMD (PEDCMD), and 3) vacuum-enhanced DCMD (VEDCMD). VEDCMD was found experimentally to have the highest water flux, followed by DCMD and PEDCMD, which had similar water fluxes. The main factors leading to the higher water flux of VEDCMD were membrane compaction and the air pressure inside the membrane pores. The pressure gradient across the membrane was also found to have minimal effect on water flux.

Membrane fouling has been recognized as one of the main obstacles inhibiting the full-scale implementation of DCMD, and can be an issue when treating feed waters with both high and low fouling potentials. The efficiency of several membrane cleaning solutions was investigated for removal of commonly observed scalants (e.g., $CaCO_3$, $CaSO_4$, SiO_2, and NaCl) in DCMD. Experimental results suggested that a citric acid solution could effectively remove $CaCO_3$ scalant, while de-ionized water alone could effectively remove $CaSO_4$ scalant. SiO_2 scaling was more difficult to remove, and a two-stage cleaning procedure using NaOH solution at 40 ^oC followed by Na_2EDTA solution was necessary to fully clean SiO_2 scaled membranes. An HCl solution was found to fully remove the scalants (mainly NaCl) from a hypersaline solution, however membrane wetting occurred after membrane cleaning leading to incomplete restoration of membrane performance. By drying the membranes after HCl cleaning, more than 90% restoration of the maximum water flux and batch recovery was achieved. The identification of effective membrane cleaning solutions in this study is applicable to the full-scale implementation of MD in the future.

The development of the simplified flux prediction model will make a contribution for MD membrane selection since membranes with different fluxes are suitable for specific applications. Besides membrane properties, experimental conditions also affected water flux; therefore, the investigation of the fundamental principles of mass transfer mechanisms in MD has helped to clarify confusions and contradictions about factors affecting water flux in the literature and direct the way for flux improvement in future. The identification of the effective membrane cleaning solutions for typical scales removal

in MD will improve the full-scale implementation of MD since membrane scaling is one of the crucial problems affecting water flux.

AKNOWLEGEMENTS

I would like to express my deepest gratitude to my major advisor Prof. Amy Childress for her patience, her push for professionalism, her efforts for my paper publication, and her financial support during the three and a half years. I am grateful to my co-advisor Dr. Sage R. Hiibel for his advice and guidance in both my academic and professionalism.

I would like to thank my other committee members, Prof. Keith Dennett, Prof. Alan Fuchs, and Prof. Chanwoo Park for their support, inspiration, and constant enthusiasm for my research. Special thanks will be given to Prof. Chanwoo Park for opening the window to the world of Mechanical Engineering. I built my understandings of the principles involved in heat transfer and energy consumptions in engineering processes.

I also give my thanks to Prof. Mariah Evans, for opening the window to the world of Applied Statistics. Thank you, Dr. Deyu Pan, for your suggestions and supports to my research.

Thank you, Dr. Andrea Achilli; you proposed interesting research topics, which shaped one of my manuscripts. Thank you, Dr. Jiangyong Hu and Dr. Ed Kolodziej, for your consistent support of my academic career. Thank you, Viktoriya Weirauch, for being always there and assisting in so many ways. Thank you, Mark Lattin, for assisting to solve technical problems.

I also wish to thank my colleagues in the Civil and Environmental Engineering Department, who have showed their care and shared their knowledge. A special shout out

goes to Katie Bowden, Jeffrey Ruskowitz, Jeri Prante, Wes Helander, Tony Dimpel, and Ally Freitas.

I am thankful to David Bain, Karen Bain, John Grant, Kris Lahti, David Lahti, Mike Culter, and John Volk for their friendship, support, and dedicated assistance.

Finally, I thank my boyfriend, Haohan Li, for his consistent help and encouragement. Without his support, I would not be where I am today.

TABLE OF CONTENTS

LIST OF FIGURES

LIST OF TABLES

Chapter 1

1 INTRODUCTION

1.1. Problem statement and significance

One-third of the world's population currently lives in countries with insufficient freshwater production and two-thirds of the world population will face water scarcity by 2025 [2]. Approximately 97.5% of the world's water is seawater [3]; thus, seawater desalination has become one of the most sustainable alternatives to provide freshwater for communities and industrial sectors [2]. Improved wastewater treatment technologies can also enable the reclamation of wastewater to provide an additional source of potable water [4].

1.2. Processes for drinking water production

Based on the driving forces of water separation, technologies for drinking water production can be classified into thermal and non-thermal processes [5]. Fig. 1.1 gives a summary of some of the technologies currently available for drinking water production. Among all the treatment processes, reverse osmosis (RO) is most commonly used for drinking water production from saline feed waters (e.g., seawater and brackish groundwater) [6, 7], because RO has the benefits of high water flux and low energy consumption. However, some contaminants such as boron, endocrine-disrupting compounds, and radionuclides have been reported to pass through RO membranes [5, 8, 9]. In addition, RO requires electrical energy consumption (2-10 kWh/m^3 [6, 10]), which is directly linked to the depletion of fossil fuels and increased CO_2 in the atmosphere.

Using RO to treat feed waters with high fouling potentials (e.g., brines, salty lake water, mining drainage, and process waters from oil and gas industry) for drinking water production is theoretically feasible. However, high pressure conditions requires membranes, modules, pumps, and pipes that can tolerate the high pressures. In addition, more electricity is required to operate the high pressure pumps needed for the RO system. Furthermore, membrane fouling may occur due to the clogging of the effective membrane surface area caused by the foulants in the feed solutions [11].

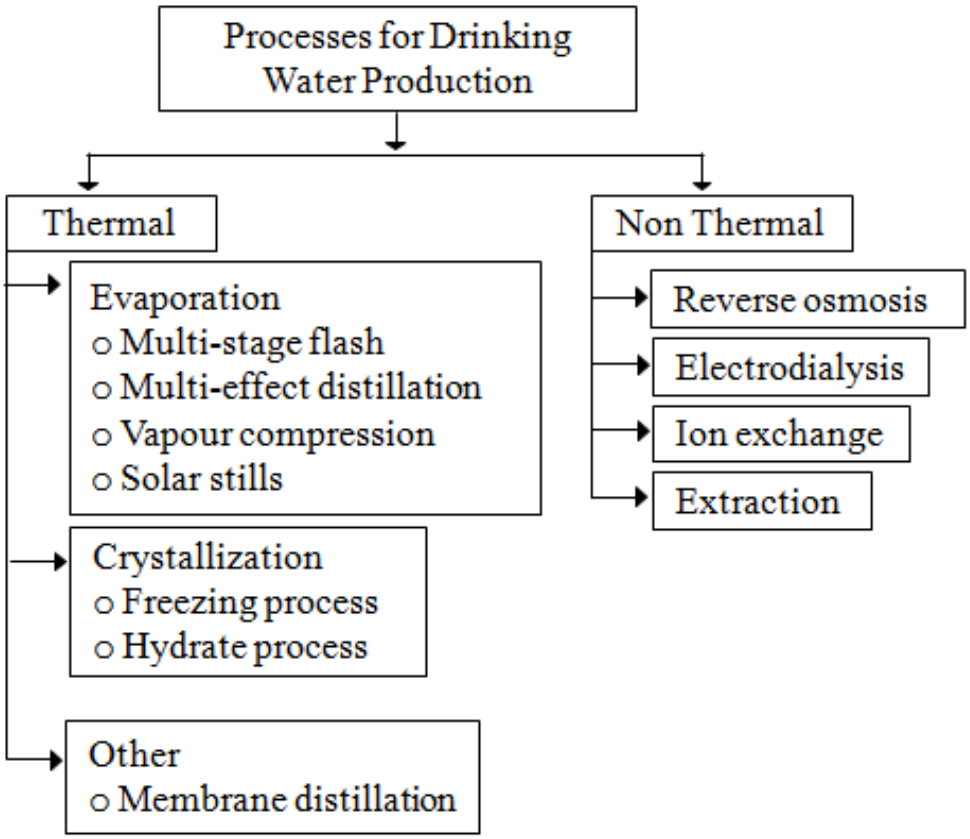

Figure 1.1 A summary of some drinking water production processes (adapted from [12]).

Besides RO desalination, thermal processes (e.g., multi-stage flashing (MSF) and multi-effect distillation (MED)) are also used for seawater desalination in places such as the countries in the Middle East [13]. Seawaters in these regions can have higher salinities and temperatures than the other places, and periodically have higher concentrations of organics, the removal of which can be challenging for the RO desalination process [12]. The low rejection of boron is another key reason that the facilities in the Middle East prefer MSF and MED rather than RO. Operation temperatures up to 120 and 70 ^{o}C are required for MSF and MED, thus, they are capable of using low-grade thermal energies (< 150 ^{o}C), such as the low-temperature heat from the solar system, industrial waste heat, and geothermal energy [12]. Proper pressure controls are needed to properly operate the systems [14]. High water recoveries from MSF and MED are not economical due to the increased boiling point caused by increased feed water salinity at greater water recoveries. For this reason, MSF and MED typically have water recoveries in the range of 35 to 45% [12].

Compared to MSF and MED, membrane distillation (MD) is a relatively new thermally-driven desalination technology that has mostly been studied in bench-scale investigations [15], and very little pilot-scale research has been conducted for MD. MD has a simpler system configuration than MSF and MED and can also utilize low-grade thermal energy. MD has been reported to have nearly 100% salt and non-volatile organic rejection regardless of feed-water salinity [16-18], and thus, has been used to treat feed waters with both high and low fouling potentials [11, 19-21]. More details about the MD process will be given in the following section.

1.3. Membrane distillation (MD)

The driving force in MD is the vapor pressure gradient resulting from the temperature difference across the membrane. MD can be used for stripping volatile organics from aqueous solutions and for concentrating non-volatile solutes by evaporation of the solvent [22]. MD is receiving more interest because the feed side of the membrane module can be operated at atmospheric pressure (unlike pressure-driven membrane processes) and low-grade thermal energies (waste heat or low-temperature heat from solar or geothermal systems) can be used to drive the process. It has been reported that low-grade thermal energies comprise more than 50% of total thermal energies generated worldwide [23]. In remote areas with limited electricity, MD can be used for water production with thermal energy from renewable sources.

In MD, an aqueous feed solution with an elevated temperature is circulated on the feed-side of a hydrophobic, microporous membrane. MD membranes are typically made of polyvinylidenefluoride, polypropylene, or polytetrafluoroethylene with pore sizes ranging from 0.2 to 1.0 μm [15, 24, 25], porosities from 30 to 85% [26, 27], tortuosities from 1.21 to 6.84 [28], and thickness from 40 to 250 μm [15]. The hydrophobic property of the membranes (given by contact angles near 120^{o}) prevents penetration of the feed solution into the membrane pores, leading to a liquid-vapor interface at each pore entrance. Thus, non-volatile contaminants in the feed solution are not transported to the distillate side of the membrane.

1.3.1. Configurations of MD systems

There are four main configurations of MD, which differ based on the condensation mode, including: 1) vacuum MD (VMD), 2) sweep-gas MD (SGMD), 3) air-gap MD (AGMD), and 4) direct-contact MD (DCMD).

In VMD, water vapor transported to the distillate side is removed continuously from the vacuum chamber; this maintains a reduced pressure condition on the distillate side of the membrane. The lower pressure on the distillate side creates a pressure gradient, which facilitates mass transfer. Because the vapor pressure on the distillate side can be reduced to near zero, this configuration can provide the greatest driving force at the same feed temperature compared to the other three MD configurations [15]. The heat loss by membrane conduction is negligible in VMD [27]. Vapor condensation takes place externally in a chemical or physical trap [22]. This configuration is useful when volatiles are being removed from an aqueous solution [15, 27].

In SGMD, a stream of stripping gas (normally air) serves as a carrier for the vapor on the distillate side of the membrane. The gas barrier on the distillate side may reduce the membrane conductive heat loss and the flowing gas may enhance the mass transfer coefficient [27]. An external condenser is needed for vapor condensation and an air blower or compressed air is needed to maintain the flowing gas stream, both leading to higher capital costs of this configuration [15]. Similar to VMD, SGMD is generally used for removing volatile compounds from aqueous solution [15, 27].

In AGMD, an air gap is present between the distillate-side of the membrane surface and a cold condensation surface, where vapor condensation occurs. This configuration generally has low membrane conductive heat loss [27] and high energy

efficiency [15]. However, water flux in this configuration is generally low due to the small temperature difference across the membrane and the additional mass and heat transfer resistances from the air gap (with thickness of 2,000-10,000 μm) [15, 27]. AGMD can be used for most membrane distillation applications. Field trials of AGMD desalination are being performed by MEMSTILL®, Keppel Seghers, Fraunhofer ISE, Scarab AB, and Memsys [15].

In DCMD, both the feed and distillate sides of the membrane are in direct contact with liquid phases. The main disadvantage of DCMD in commercial applications is its low energy efficiency due to the relatively high conductive heat loss through the membrane. The heat loss makes only a portion of the supplied heat useable for water production [15]. However, DCMD has the simplest configuration and is capable of producing reasonably high water flux; thus, it is frequently used in bench-scale studies [15, 27]. More details of the DCMD system will be given in the following section.

1.3.2. DCMD

In DCMD, two solutions with different bulk temperatures are circulated on either side of the membrane. Temperatures of the feed solution typically range from 30-90 ^{o}C [16, 29], which makes it feasible to be combined with low-grade heat sources. DCMD has been used to treat feed solutions with high fouling and scaling potentials, such as industrial wastewater [4, 5], water from salt lakes [6], RO brines [7, 8], and process water from the oil and gas industry [9-11] because the driving force of DCMD does not decrease significantly with increasing water salinity. DCMD is also well suited to treat feed solutions with low fouling and scaling potentials where targeted removal or

polishing is desired because DCMD achieves near 100% rejection of salt and organic compounds [12, 13]. Examples include impaired water containing endocrine disrupting compounds [14], brackish water contaminated with fluoride [15], groundwater with heavy metals [16], and feed solutions with urine and hygiene wastewater [17]. In some DCMD applications (particularly with low fouling and scaling feed waters), achieving high water flux is desirable while in other applications (with high fouling and scaling feed waters) it is not.

1.3.3. Vacuum-enhanced DCMD (VEDCMD)

High water flux is desirable using DCMD when treating feed solutions with low fouling potentials. Traditional approaches to improve water flux of DCMD include operating at greater temperature differences, using more turbulent flows, inventing better membranes and membrane modules, and deaerating the feed waters [30-32]. In the early 2000s, membrane researchers at the University of Nevada, Reno invented vacuum-enhanced DCMD (VEDCMD) [33]. VEDCMD was shown to achieve up to 80% higher fluxes compared to DCMD. Salt rejection during the process was greater than 99.9%. Similar phenomena were observed later by Zhang et al. [34]. In the process, a vacuum is created on the distillate side by placing the distillate-side pump at the outlet of the membrane module to pull water from the membrane module (rather than pushing water into the module as in the case of DCMD). Decreased air pressure inside the membrane pores, decreased membrane conductive heat loss, decreased temperature polarization, and increased pressure gradient across the membrane have all been proposed as possible

mechanisms for flux improvement in VEDCMD [31, 34, 35]. However, these mechanisms have not been systematically investigated.

1.4. Prediction of membrane flux

In some DCMD applications (particularly with low fouling and scaling feed waters) achieving high water flux is desirable while in other applications (with high fouling and scaling feed waters) it is not. The prediction of water flux prediction is desirable for selecting the appropriate membrane and identifying the mass and heat transfer mechanisms. Mass transfer in DCMD includes four steps. First, water is transferred from the feed bulk solution to the membrane surface by crossing the feed-side boundary layer. Second, water evaporates at the feed-side membrane surface and water vapor transfers across the membrane. Third, the vapor condenses at the distillate-side membrane surface. And fourth, the condensed water transfers to the distillate bulk by crossing the distillate-side boundary layer [36]. The mass transfer mechanisms for water vapor transport vapor through a MD membrane can be described by the following processes [37, 38]: 1) Knudsen diffusion, in which the gas density is so low or the membrane pore size is so small that collisions between molecules are negligible compared to the collisions between molecules and the inner walls of the membrane; 2) molecular diffusion, in which molecule-molecule collisions dominate over molecule-wall collisions, and different species of the gas mixture (air and vapor) move relative to each other under the influence of concentration gradients; and 3) viscous flow, in which the air and vapor mixture behave as a continuous fluid driven by a pressure gradient.

The mass transfer mechanism that dominates depends on the configuration of the membrane system and the ratio of membrane pore size (d) to the mean free path of water (λ), or the average distance the diffusing molecules travel between two successive collisions [39] (0.11 μm at a feed water temperature of 60 ^{o}C in DCMD [40]). If $d < \lambda$, Knudsen diffusion dominates; if $d > 100\ \lambda$, both molecular diffusion and viscous flow play important roles; and if $\lambda < d < 100\ \lambda$, all three mass transfer mechanisms may be important [40-42].

The dusty-gas model (DGM) is a general model describing the mass transport in porous media and has been applied to MD by Lawson et al. [11]. The thermal circuit of the DGM describing water vapor passing through an MD membrane is given in Fig. 1.2. The DGM includes a vapor transfer pathway for surface diffusion, but this mechanism only occurs when membrane pore sizes are smaller than 0.02 μm, thus surface diffusion is generally neglected in MD modeling [39]. The Schofield model (Fig. 1.3) is another mass transfer model typically employed in MD. A fundamental difference between the dusty-gas model and Schofield model is where viscous flow is considered in the thermal circuit. However, viscous flow is generally neglected in traditional DCMD because no hydraulic pressure gradient exists [17, 40] and therefore, for DCMD, both models have the same thermal circuit. The expressions of the mass transfer models are complicated: membrane properties have to be characterized and dynamic conditions inside the membrane module have to be considered [37, 43-45]. Also, some studies used membrane pore size distribution instead of the average pore size for mass transfer modeling [40, 46, 47], which further complicates flux prediction using existing mass transfer models.

Therefore, a simplified water flux prediction model is needed to facilitate the application of DCMD.

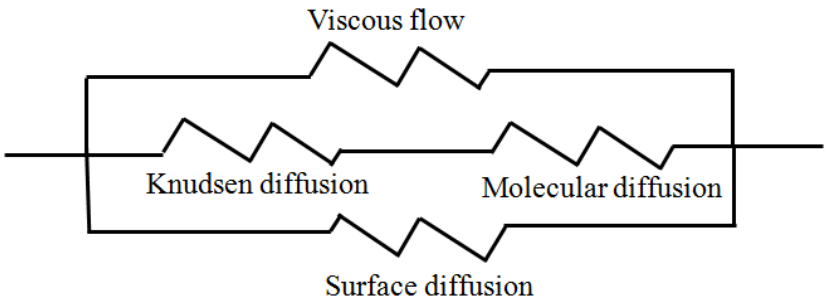

Figure 1.2 Thermal circuit of the dusty-gas model [16].

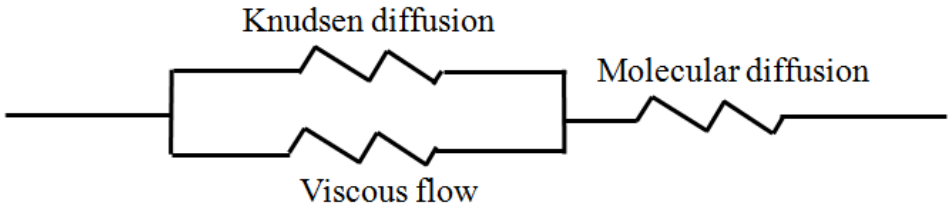

Figure 1.3 Thermal circuit of the Schofield model [52].

1.5. Membrane fouling and cleaning in DCMD

Similar to pressure-driven membrane processes, where membrane fouling is a significant obstacle to the efficient operation of the systems [50], membrane fouling in MD is also recognized as one of the main obstacles impeding the implementation of full-scale MD [51, 52]. Membrane fouling is defined as the accumulation of foulants (organics, inorganics, and/or microorganisms) at the membrane surface or inside the

pores of a membrane [13]. Membrane fouling caused by inorganics is also called membrane scaling [13]. Most literature reports concerning membrane fouling deal with pressure-driven membrane processes that are operated under hydraulic pressures using different membranes and feed waters than are used with DCMD. Thus, pressure-driven membrane processes are expected to have different fouling phenomena than DCMD processes. Membrane fouling in DCMD has been observed when treating tap water [15], groundwater [16], reverse osmosis brines [17, 18], and other specialized solutions [19]. Foulants on the membrane surface may alter the surface properties (e.g., hydrophobicity) and pore structures of the membrane, hinder water transport to the membrane surface, and add an additional thermal resistance factor that in turn lowers the temperature at the membrane surface [12, 20, 21]. Membrane fouling caused by organics does not typically result in a significant decline in flux in DCMD and organic foulants were found to be loosely packed on the membrane surface [22]. Inorganics, such as iron and manganese, reportedly have minimal effects on water flux [18, 23]. Sparingly soluble salts, such as calcium carbonate ($CaCO_3$), calcium sulfate ($CaSO_4$), and silica (SiO_2) were frequently observed as major scalants leading to flux decline and ultimately lower water recovery [12, 13, 18, 24]. When treating hypersaline solutions, sodium chloride (NaCl) was observed as the major scalant [12].

Although the typical foulants in DCMD are different from the typical foulants in pressure-driven membrane processes, the principles used to remove foulants in pressure-driven membrane processes may be applied to DCMD. In pressure-driven membrane processes, alkaline solutions (e.g., sodium hypochlorite and sodium hydroxide solutions) are typically used to remove organic and bio-fouls [55, 60]; acidic solutions (e.g., the

hydrochloric acid solution) and metal chelating agents (e.g., ethylenediaminetetraacetic acid and citric acid) are typically used to remove calcium scalants [50, 55]. The removal of silica scalants using de-ionized water and cleaners did not fully restore the maximum water flux of RO [61]; thus, antiscalants [62] and membrane pretreatments [63] were used. Ultrasound was also successfully applied in microfiltration for the removal of silica scalants, but increased solute permeation occurred [60]. In DCMD, hydrochloric acid solutions have been used to remove the calcium carbonate scalant but increased distillate conductivity was observed [58, 59, 64]. Both metal chelating agents [65] and sodium chloride solutions [64, 66] have been used to remove the calcium sulfate scalant in DCMD. There has been no current study specifically on the removal of silica and sodium chloride scalants using chemical cleaning methods.

1.6. Research objectives

The overall objective of this research was to facilitate the application of DCMD in treating a range of feed waters (those that have both high and low fouling potentials). Three sub-objectives were included. The first sub-objective targeted the development of a simplified flux prediction model to easily identify MD membranes with desirable water fluxes. To achieve this, a novel membrane structural parameter was proposed first, which was highly correlated with water flux, contained non-coupled membrane property parameters, and required simple and reliable laboratory measurements with low costs. Next, an empirical model based on the new structural parameter was also developed for flux prediction and the flux prediction performance was compared to the performance with the existing mass transfer models. At last, the application of this model to

membranes with a wider range of pore sizes was explored. The second sub-objective was aimed at mechanistically evaluating the factors attributing to the improved water flux in VEDCMD in order to provide insight for water flux improvement. To achieve this, the traditional DCMD and pressure-enhanced DCMD (PEDCMD) were studied for comparison with VEDCMD. The dominant factors contributing to higher water flux in VEDCMD were first theoretically identified. Next, membrane compaction phenomena in all three DCMD systems was investigated. At last, the magnitude of the air pressure inside the membrane pores for each DCMD system was quantified. The third sub-objective focused on identifying effective membrane cleaning solutions for the removal of typical scalants ($CaCO_3$, $CaSO_4$, SiO_2, and NaCl) in DCMD in order to facilitate the application of DCMD in long-term operations when treating various feed waters. To achieve this, four feed solutions containing different scalants were collected or synthesized and tested in bench-scale DCMD systems. Membrane performances for each feed solution before and after membrane cleaning were compared to estimate the effectiveness of the cleaning solutions. The scaled membrane surface before membrane cleaning was analyzed using the scanning electron microscopy (SEM) coupled with energy dispersive spectrometry (EDS) to identify the components of the scalants. Membrane surface analysis after cleaning was also performed when necessary to identify the effectiveness of scale removal.

1.7. Dissertation organization

This dissertation is a compilation of papers written over the course of the

dissertation research. Chapter 2 is a manuscript that has been accepted for publication in the *Desalination.* Chapter 3 is a manuscript that has been submitted for publication in the *Journal of Membrane Science*. Chapter 4 is a manuscript that has been submitted for publication in the *Desalination.*

References

[1] M. Shatat, M. Worall, S. Riffat, Opportunities for solar water desalination worldwide: Review, Sustainable cities and society, 9 (2013) 67-80.

[2] S.P. Bindra, W. Abosh, Recent developments in water desalination, Desalination, 136 (2000) 49-56.

[3] M. Wilf, S. Alt, Application of low fouling RO membrane elements for reclamation of municipal wastewater, Desalination, 132 (2000) 11-19.

[4] S. Loo, A.G. Fane, W.B. Krantz, T. Lima, Review: Emergency water supply: A review of potential technologies and selection criteria, Water Res, 46 (2012) 3125-3151.

[5] J. MacHarg, R. Truby, West coast researchers seek to demonstrate SWRO affordability, Desalination & Water Reuse, 14(3) (2004) 10-16.

[6] L.F. Greenlee, D.F. Lawler, B.D. Freeman, B. Marrot, P. Moulin, Reverse osmosis desalination: Water sources, technology, and today's challenges, Water Res., 43 (2009) 2317-2348.

[7] K. Kimura, S. Toshima, G. Amy, Y. Watanabe, Rejection of neutral endocrine disrupting compounds (EDCs) and pharmaceutical active compounds (PhACs) by RO membranes, J. Membr. Sci., 245 (2004) 71-78.

[8] M. Busch, W.E. Mickols, Reducing energy consumption in seawater desalination Desalination, 165 (2004) 299-312.

[9] M. Thomson, M. S. Miranda, D. Infield, A small-scale seawater reverse-osmosis system with excellent energy efficiency over a wide operating range, Desalination, 153 (2002) 229-236.

[10] K. W. Lawson, D.R. Lloyd, Review: Membrane distillation, J. Membr. Sci. , 124 (1997) 1-25.

[11] Division of Water Resource Management, F.D.o.E. Protection, Desalination in Florida: A Brief Review of the Technology, Environmental Issues and its Implementation., in, Tallahassee, Florida, 2010.

[12] H.E.S. Fath, S.M. Elsherbiny, A.A. Hassan, M. Rommel, M. Wieghaus, J. Koschikowski, M. Vatansever, PV and thermally driven small-scale, stand-alone solar desalination systems with very low maintenance needs, Desalination, 225 (2008) 58-69.

[13] G. Raluy, L. Serra, J. Uche, Life cycle assessment of MSF, MED and RO desalination technologies, Energy, 31 (2006) 2361-2372.

[14] L.M. Camacho, L. Dumée, J. Zhang, J. Li, M. Duke, J. Gomez, S. Gray, Review: Advances in Membrane Distillation for Water Desalination and Purification Applications, Water, 5 (2013) 94-196.

[15] K.W. Lawson, D.R. Lloyd, Review: Membrane distillation, J. Membr. Sci. , 124 (1997) 1-25.

[16] K.W. Lawson, D.R. Lloyd, Membrane Distillation. II. Direct contact MD, J. Membr.Sci. , 120 (1996) 123-133.

[17] J.L. Cartinella, T.Y. Cath, M.T. Flynn, G.C. Miller, K.W. Hunter, A.E. Childress, Removal of natural steroid hormones from wastewater using membrane contactor processes, Environ. Sci. Technol., 40 (2006) 7381-7386.

[18] S. Lee, J. Choa, M. Elimelech, Influence of colloidal fouling and feed water recovery on salt rejection of RO and NF membranes, Desalination, 160 (2004) 1-12.

[19] E. Curcio, E. Drioli, Membrane Distillation and Related Operations - A Review, Sep. Purif. Rev., 34 (2005) 35-86.

[20] M. Khayet, Membranes and theoretical modeling of membrane distillation: A review, Adv. Colloid Interface Sci., 164 (2011) 56-88.

[21] T.Y. Cath, Membrane Contactor Processes for Seawater Desalination and Wastewater Reclamation, in: Civil Engineering, University of Reno, Nevavda, Reno, Nevada, 2003.

[22] T. C. Hung, T. Y. Shai, S.K. Wang, A review of organic rankine cycles (ORCs) for the recovery of low-grade waste heat, Energy, 22 (1997) 661-667.

[23] A.M. Alklaibi, N. Lior, Membrane-distillation desalination: status and potential, Desalination, 171 (2004) 111-131.

[24] J. Zhang, N. Dow, M. Duke, E. Ostarcevic, J. Li, S. Gray, Identification of material and physical features of membrane distillation membranes for high performance desalination, J. Membr. Sci. , 349 (2010) 295-303.

[25] M.S. El-Bourawi, Z. Ding, R. Ma, M. Khayet, A framework for better understanding membrane distillation separation process, J. Membr. Sci., 285 (2006) 4-29.

[26] A. Alkhudhiri, N. Darwish, N. Hilal, Membrane distillation: A comprehensive review, Desalination 287, (2012) 2-18.

[27] S. B. Iversen, V. K. Bhatia, K .Dam-Johansen, G. Jonsson, Characterization of microporous membranes for use in membrane contactors, J. Membr. Sci., 130 (1997) 205-217.

[28] A.M. Alklaibi, N. Lior, Transport analysis of air-gap membrane distillation, J. Membr. Sci. 255 (2005) 239-253.

[29] A.G. Fane, R.W. Schofield, C.J.D. Fell, The efficient use of energy in membrane distillation, Desalination, 64 (1987) 231-243.

[30] R.W.Schofield, G. A, Fane,, C.J.D. Fell, Gas and vapour transport through microporous membranes. II. Membrane distillation, Journal of Membrane Science, 53 (1990) 173-185.

[31] R.W. Schofield, A. G. Fane, C. J. D. Fell, R. Macoun, Factors affecting flux in membrane distillation, Desalination, 77 (1990) 279-294.

[32] T.Y. Cath, V.D. Adams, A.E.Childress, Vacuum enhanced direct contact membrane distillation, in, Board of Regents of the Nevada System of Higher Education, U.S.A, 2006.

[33] J. Zhang, J. D. Li, M. Duke, Z. Xie, S. Gray, Performance of asymmetric hollow fiber membranes in membrane distillation under various configurations and vacuum enhancement, J. Membr.Sci., (2010) 517-528.

[34] T.Y. Cath, V.D. Adams, A.E. Childress, Experimental study of desalination using direct contact membrane distillation: a new approach to flux enhancement, J. Membr.Sci., 228 (2004) 5-16.

[35] S. Srisurichan, R. Jiraratananon, A.G. Fane, Mass transfer mechanisms and transport resistances in direct contact membrane distillation process, J. Membr. Sci., 277 (2006) 186-194.

[36] R.W. Schofield, A.G. Fane, C.J.D. Fell, Heat and mass transfer in membrane distillation, J. Membr. Sci., 33 (1987) 299-313.

[37] Z. Ding, R. Ma, A.G. Fane, A new model for mass transfer in direct contact membrane distillation, Desalination 151, (2002) 217-227.

[38] A.O. Imdakm, T. Matsuura, A Monte Carlo simulation model for membrane distillation processes: direct contact (MD), J. Membr. Sci., 237 (2004) 51-59.

[39] J. Phattaranawik, R. Jiraratananon, A.G. Fane, Effect of pore size distribution and air flux on mass transport in direct contact membrane distillation, J. Membr. Sci., 215 (2003) 75-85.

[40] E.A. Mason, A.P. Malinauskas, Gas transport in porous media: the dusty gas model, Elsevier, Amsterdam, Netherlands, 1983.

[41] R.W.Schofield, A.G.Fane, C.J.D.Fell, Heat and mass transfer in membrane distillation, Journal of Membrane Science, 33 (1987) 299-313.

[42] A.R.D. Costa, A.G. Fane, D.E. Wiley, Spacer characterization and pressure drop modelling in spacer-filled channels for ultrafiltration, J. Membr. Sci., 87 (1994) 79-98.

[43] J. Phattaranawik, R. Jiraratananon, A.G. Fane, C. Halim, Mass flux enhancement using spacer filled channels in direct contact membrane distillation, J. Membr. Sci., 187 (2001) 193-201.

[44] L. Martínez, J.M. Rodríguez-Maroto, Characterization of membrane distillation modules and analysis of mass flux enhancement by channel spacers, J. Membr. Sci., 274 (2006) 123-137.

[45] A. Hernfindez, J.I. Calvo, P. Prfidanos, F. Tejerina, Pore size distributions in microporous membranes: A critical analysis of the bubble point extended method, J. Membr. Sci., 112 (1996) 1-12.

[46] J. Woods, J. Pellegrino, J. Burch, Generalized guidance for considering pore-size distribution in membrane distillation, J. Membr. Sci., 368 (2011) 124-133.

[47] L. Mo, X. Huang, Fouling characteristics and cleaning strategies in a coagulation-microfiltration combination process for water purification Desalination, 159 (2003) 1-9.

[48] S. Kang, K. Choo, Use of submerged microfiltration membranes for glass industry wastewater reclamation: pilot-scale testing and membrane cleaning, Desalination, 189 (2006) 170-180.

[49] A Maskooki, T. Kobayashi, S.A. Mortazavi, A. Maskooki, Effect of low frequencies and mixed wave of ultrasound and EDTA on flux recovery and cleaning of microfiltration membranes, Sep. Purif. Technol., 59 (2008) 67-73.

[50] T. Koo, Y.J. Lee, R. Sheikholeslami, Silica fouling and cleaning of reverse osmosis membranes Desalination, 139 (2001) 43-56.

[51] G. Braun, W. Hater, C. zum Kolk, C. Dupoiron, T. Harrer, T. Götz, Investigations of silica scaling on reverse osmosis membranes, Desalination, 250 (2010) 982-984.

[52] R. Sheikholeslami, I.S. Al-Mutaz, S. Tan, S.D. Tan, Some aspects of silica polymerization and fouling and its pretreatment by sodium aluminate, lime and soda ash, Desalination, 150 (2002) 85-92.

[53] M. Gryta, Desalination of thermally softened water by membrane distillation process, Desalination, 257 (2010) 30-35.

[54] M. Gryta, Fouling in direct contact membrane distillation process, J. Membr. Sci., 325 (2008) 383-394.

[55] M. Gryta, Long-term performance of membrane distillation process, J. Membr.Sci., 265 (2005) 153-159.

[56] C.R. Martinetti, A.E. Childress, T.Y. Cath, High recovery of concentrated RO brines using forward osmosis and membrane distillation, J. Membr. Sci., 331 (2009) 31-39.

[57] F. He, J. Gilron, H. Lee, L. Song, K.K. Sirkar, Potential for scaling by sparingly soluble salts in crossflow DCMD, J. Membr. Sci., 311 (2008) 68-80.

[58] M.H.Kutner, C.J.Nachtsheim, J. Neter, Applied Linear Regression Models 4th ed., McGraw-Hill/Irwin, New York, U.S.A, 2004.

[59] F. Meng, H. Zhang, F. Yang, S. Zhang, Y. Li, X. Zhang, Identification of activated sludge properties affecting membrane fouling in submerged membrane bioreactors, Sep. Purif. Technol., 51 (2006) 95-103.

[60] V.D. Alves, I.M. Coelhoso, Effect of membrane characteristics on mass and heat transfer in the osmotic evaporation process, J. Membr. Sci., 228 (2004) 159-167.

[61] J. Zhang, J. D. Li, S. Gray, Effect of applied pressure on performance of PTFE membrane in DCMD J. Membr. Sci., 369 (2011) 514-525.

[62] J. A. Ruskowitz, A.E. Childress, Salt-Gradient Solar Pond and Membrane Distillation System for Water Desalination Powered by Renewable Energy, in: Thesis, University of Nevada, Reno, Reno, Nevada, 2012.

[63] E. Repo, T.A. Kurniawan, J.K. Warchol, M.E.T. Sillanpää, Removal of Co(II) and Ni(II) ions from contaminated water using silica gel functionalized with EDTA and/or DTPA as chelating agents, J. Hazard. Mater., 171 (2009) 1071-1080.

[64] D. Qu, J. Wang, B. Fan, Z. Luan, D. Hou, Study on concentrating primary reverse osmosis retentate by direct contact membrane distillation, Desalination, 247 (2009) 540-550.

[65] M. Gryta, Pretreatment of feed water for membrane distillation, Chemical Papers, 62 (2008) 100-105.

[66] K.L. Hickenbottom, T.Y. Cath, Sustainable operation of membrane distillation for enhancement of mineral recovery from hypersaline solutions, J.M.Sci, 454 (2014) 426-435.

Chapter 2

2 SIMPLIFIED FLUX PREDICTION IN DIECT-CONTACT MEMBRANE DISTILLATION USING A MEMBRANE STRUCTURAL PARAMETER

Abstract

A priori water flux prediction is desirable when conducting membrane distillation (MD) studies, however existing models are complicated with inconsistent mass transfer mechanism assumptions. To develop a simplified model that can be used to predict the relative magnitudes of water fluxes for a group of MD membranes, correlation analyses were performed between water flux and 28 structural parameters. Four parameters were found to be highly correlated with water flux: ε/δ, $\varepsilon/\tau\delta$, $1/\tau\delta$, and C_m. C_m is a newly introduced structural parameter that contains non-coupled membrane properties but still carries the physical meaning of a relationship between δ and ε, and is determined by simple and reliable measurements using inexpensive analytical equipment. The correlation result between water flux and C_m suggests C_m is a good structural parameter for MD flux prediction. The flux prediction errors for membranes with pore sizes from 0.1 to 0.9 μm were generally smaller for the model developed with C_m than for the dusty gas model. In addition to the new structural parameter and model, this study also makes available to the literature a detailed collection of MD membrane properties and their water flux values that will assist others in membrane selection, development, and application.

Keyword: Membrane distillation; Membrane structural parameter; Flux prediction model; Membrane characterization

2.1. Introduction

2.1.1. Membrane distillation

Membrane distillation (MD) is a thermally-driven process in which separation occurs through a phase change to produce clean water. The driving force in MD is the vapor pressure gradient, resulting from the temperature difference across the membrane. Among all types of MD, direct-contact MD (DCMD) is the most commonly used configuration in lab-scale research [1]. In DCMD, two solutions at different bulk temperatures are circulated on either side of a hydrophobic microporous membrane. Temperatures of the feed solution can range from 30-90 ^{o}C [2, 3], which makes it feasible to be combined with low-grade heat sources. DCMD has been used to treat feed waters with high fouling and scaling potentials, such as industrial wastewater [4, 5], water from salt lakes[6], RO brines[7, 8], and produced water from the oil and gas industry [9-11], because the driving force of DCMD does not decrease significantly with increasing water salinity. DCMD is also well suited to treat feed waters with low fouling and scaling potentials where targeted removal or polishing is desired because DCMD achieves near 100% salt and organic rejection [12, 13]. Examples include impaired water containing endocrine disrupting compounds [14]; brackish water contaminated with fluoride [15]; groundwater with heavy metals [16]; and feed waters with urine and hygiene wastewater [17]. In some DCMD applications (particularly with low fouling and scaling feedwaters) obtaining high water flux is desirable while in other applications (with high fouling and scaling feedwaters) it is not, thus *a priori* water flux prediction is desirable for membrane selection. Because MD water flux is affected by membrane properties, feed water properties, and operating conditions [18], if a group of MD membranes is operated on the

same feedwater at specific operating conditions, only the membrane properties will affect the relative magnitude of water flux.

2.1.2. Existing mass transfer models for flux prediction in MD

Water flux (N_i) through an MD membrane is given as:

$$N_i = B\Delta P_i \tag{1}$$

where B is the membrane mass transfer coefficient and ΔP_i is the water vapor pressure gradient across the membrane. Here, subscript i is used to represent water vapor and subscript j is used to represent air. Water vapor pressure (P_i) for both the feed stream and the distillate stream is expressed using the Antoine equation [19, 20]:

$$P_i = \exp(23.328 - \frac{3841}{T - 45}) \tag{2}$$

where T is the temperature of the respective stream. The dusty gas model is often used to estimate water flux in MD, where four mass transfer mechanisms (surface diffusion, Knudsen diffusion, molecular diffusion, and viscous flow) may occur; the thermal circuit representation is given in Fig. 2.1. The complete expression of the dusty gas model is complex, thus surface diffusion, which only occurs when membrane pore sizes are smaller than 0.02 μm [21], is typically not included so as to simplify MD flux prediction [2, 22]. MD water flux without consideration of surface diffusion is given as:

$$N_i = N_i^D + N_i^V \tag{3}$$

where N_i^D and N_i^V are the diffusive (combined Knudsen and molecular) flux and viscous flux of water vapor, respectively. In its most general form, the dusty gas model applicable to MD is given by two equations [2]:

$$\frac{N_i^D}{\frac{2r\varepsilon}{3\tau\delta}\left(\frac{8RT_m}{\pi M_i}\right)^{0.5}} + \sum_{j=1\neq i}^{n} \frac{P_j N_i^D - P_i N_j^D}{\frac{\varepsilon}{\tau\delta} PD_{ij}} = \frac{1}{RT}\Delta P_i \tag{4}$$

$$N_i^V = \frac{P_i}{8RT_m\mu}\frac{r^2\varepsilon}{\tau\delta}\Delta P \tag{5}$$

where r, ε, τ, and δ are the membrane pore radius, porosity, tortuosity, and thickness, respectively; R is the universal gas constant; T_m is the average temperature of the membrane; M_i is the molecular weight of water vapor; P_j is the air pressure inside the membrane pores; N_j^D is the diffusive flux of air; P is the total pressure; D_{ij} is the ordinary diffusion coefficient; μ is the fluid viscosity; and ΔP is the transmembrane pressure. Two equations for PD_{ij} are given in the literature [2, 12, 23]:

$$PD_{ij}\,(kPa\ m^2/s) = 4.46 \times 10^{-9} \times T_m^{2.334} \tag{6}$$

and [22, 24]:

$$PD_{ij}\ (kPa\ m^2/s) = 1.895 \times 10^{-8} \times T_m^{2.072} \tag{7}$$

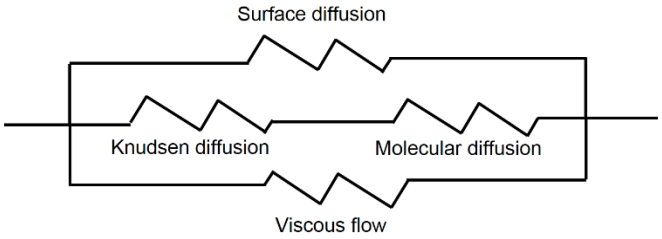

Figure 2.1 Thermal circuit of the dusty gas model [2].

Because of temperature polarization, the temperatures at the membrane surfaces (feed and distillate sides) are different from the bulk temperatures, thus the dynamic conditions inside the membrane module have to be considered (with hydraulic pressures, salinities, heat capacities, viscosities, and flow rates on both the feed and distillate sides, spacer properties if spacers are used, and membrane module dimensions) when determining the average membrane temperature (T_m) [19, 25-27]. Also, because hydraulic pressures always exist in flowing streams, membrane compaction may occur during MD testing, resulting in modified membrane properties (r, ε, τ, and δ) [28, 29]. Both temperature polarization and membrane compaction complicate the mass transfer equations. In seeking simplification of flux prediction, some investigations have assumed that viscous flow is negligible in DCMD due to the lack of a hydraulic pressure gradient [12, 22]; in these cases, only Eq. 4 is used to predict water flux. Other investigations assert that viscous flow cannot be neglected, especially for membranes with large (e.g., > 0.3 μm) pore sizes where the mean free path of water vapor in air is much greater than the membrane pore size [19, 30]. In these cases, a membrane pore size distribution instead of the average pore size has been used for mass transfer modeling [22, 31, 32].

The complicated model expressions and contradictory assumptions from the literature for the mass transfer mechanisms make prediction of water flux using the simplified dusty gas model cumbersome and ambiguous.

2.1.3. Existing membrane property parameters

If experimental operating conditions and solution chemistries are kept constant, then only the membrane properties will affect water flux. Considering this, further simplifications of the dusty gas model in the literature have used membrane property parameters (also referred to as membrane morphology parameters) to qualitatively analyze water flux. From Eqs. 4 and 5, membrane property parameters affecting water flux are $\varepsilon/\tau\delta$, $r\varepsilon/\tau\delta$, or $r^2\varepsilon/\tau\delta$ for molecular diffusion, Knudsen diffusion, and viscous flow, respectively. It is expected that membranes with greater $\varepsilon/\tau\delta$, $r\varepsilon/\tau\delta$, or $r^2\varepsilon/\tau\delta$ will have higher water fluxes [2, 24, 33-36]. It is also generally agreed that higher water fluxes occur for MD membranes with higher porosity [33, 37, 38] or lower tortuosity [23, 39].

It is unclear to what extent membrane pore size affects water flux since the role of membrane pore size is not the same in $\varepsilon/\tau\delta$, $r\varepsilon/\tau\delta$, and $r^2\varepsilon/\tau\delta$. Lawson et al. [37] found that water flux increased with increasing pore size. Mericq et al. [40] found that the Knudsen permeability ($B \propto r\varepsilon/\tau\delta$; r included) of the membrane strongly affected water flux. However, in a couple of observations, water flux was found to be highly sensitive to the characteristic parameter $\varepsilon/\tau\delta$ [27, 34] and only slightly sensitive to pore size [27]. Ali

et al. [36] also observed no dramatic increase of the water flux with increasing pore size, especially when the pore size was smaller than 0.3 μm.

Although thickness is generally included in the membrane property parameters, some studies discounted its role and utilized ε/τ, $r\varepsilon/\tau$, and $r^2\varepsilon/\tau$. Lawson et al. [37] found that flux increased as the membrane parameter $\tau\delta$ increased. Bonyadi et al. [33] and El-Bourawi et al. [38] found that thickness was important because thinner membranes have reduced mass transfer resistance but they also found that flux did not monotonically increase with thickness reduction because of increased conductive heat loss through the membrane.

Although several membrane property parameters have been analyzed in the literature, there are contradictory observations about their effects on water flux (with the exception of porosity and tortuosity). Furthermore, only qualitative analyses between water flux and membrane property parameters were given; these enable the evaluation of trends but not the prediction of specific values of flux. Uniform terminology for the combinations of membrane property parameters also does not exist: membrane constant, membrane parameter, model parameter, structural parameter, morphology parameter, membrane factor, and characteristic parameter have all been used in the literature. The term membrane structural parameter will be used in this work and will refer to a single membrane-specific property or a combination of properties.

2.1.4. Concern of coupled membrane properties in structural parameters

Often, membrane structural parameters given in the literature ($\varepsilon/\tau\delta$, $r\varepsilon/\tau\delta$, $r^2\varepsilon/\tau\delta$, $r\varepsilon/\tau$, $r^2\varepsilon/\tau$, ε/τ, and $\tau\delta$) may have coupled membrane properties. For example, porosity

may be calculated as a function of thickness [35, 37, 41, 42] and tortuosity is frequently calculated as a function of porosity [34, 35, 39, 43]. Thus, errors in the thickness measurement will be propagated into the porosity determination and then into the tortuosity determination. The presence of errors in measurements as straightforward as thickness measurements can be seen by comparing membrane thickness values for the same membrane from different sources (e.g., from [44, 47] for the GVHP and HVHP membranes). Although membrane structural parameters may be decoupled by evaluating more of the membrane properties experimentally, as has been done in some investigations (e.g., [33, 48, 49]), this comes with additional cost of time, effort, and equipment. Therefore, a membrane structural parameter that requires few laboratory measurements and does not include coupled membrane properties would be very useful to make a priori flux predictions.

2.1.5. Objective

Because low water flux is preferred when treating feedwaters with high fouling and scaling potentials and high water flux is preferred when treating less challenging feedwaters (Section 2.1.1), a simplified model that can predict the relative magnitudes of water fluxes for a group of MD membranes would be useful. Membrane structural parameters have been used to simplify mass transfer modeling in MD, however, no flux predictions with either absolute or relative magnitudes have been made using these parameters, and also, these parameters may contain coupled properties. In this work, a new membrane structural parameter is introduced to provide a priori assessment of the relative magnitude of water flux. First, a membrane structural parameter with no coupled

parameters and requiring simple and reliable laboratory measurements was identified. Second, an empirical model based on the new structural parameter was developed to predict water flux for single-layer membranes and composite membranes. Predictions from this model were compared with flux predictions of existing mass transfer models. Third, flux predictions from this model were correlated with water fluxes for membranes with a range of pore sizes. This study also makes available to the literature a detailed collection of MD membrane properties and their water flux values that will assist others in membrane selection, development, and application.

2.2. Materials and methods

2.2.1. MD membrane water flux test

Membrane water flux was evaluated using a bench-scale DCMD configuration (Fig. 2.2). Four liters of double-distilled water were added to both the feed and distillate reservoirs. The feed stream was maintained at 60 ºC using a flow-through heater (STFT-1500-120, TruHeat, Allegan, MI). The distillate stream was held at 20 ºC using a recirculating chiller (NESLAB ThermoFlex 1400, Thermo Fisher Scientific, Newington, NH). Temperatures were monitored using four resistance temperature detectors (PRTF-10, Omega, Stamford, CT) coupled to a 4-channel analog input module (NI 9217, National Instruments, Austin, TX) at the inlet and outlet of the feed and distillate loops of the membrane module. The membrane module utilized a flat-sheet membrane with 118 cm^2 of effective membrane surface area. Two spacers were used, one on the feed side and one on the distillate side of the membrane, to generate turbulence and reduce polarization effects. The feed and distillate streams were circulated counter-currently on their

respective sides of the membrane at 1.5 L/min. As water evaporated through the membrane, the excess water from the distillate reservoir overflowed into a beaker on an analytical balance and the overflow rate was used to calculate water flux. For each membrane, water fluxes of three membrane samples were measured and the average water flux was calculated.

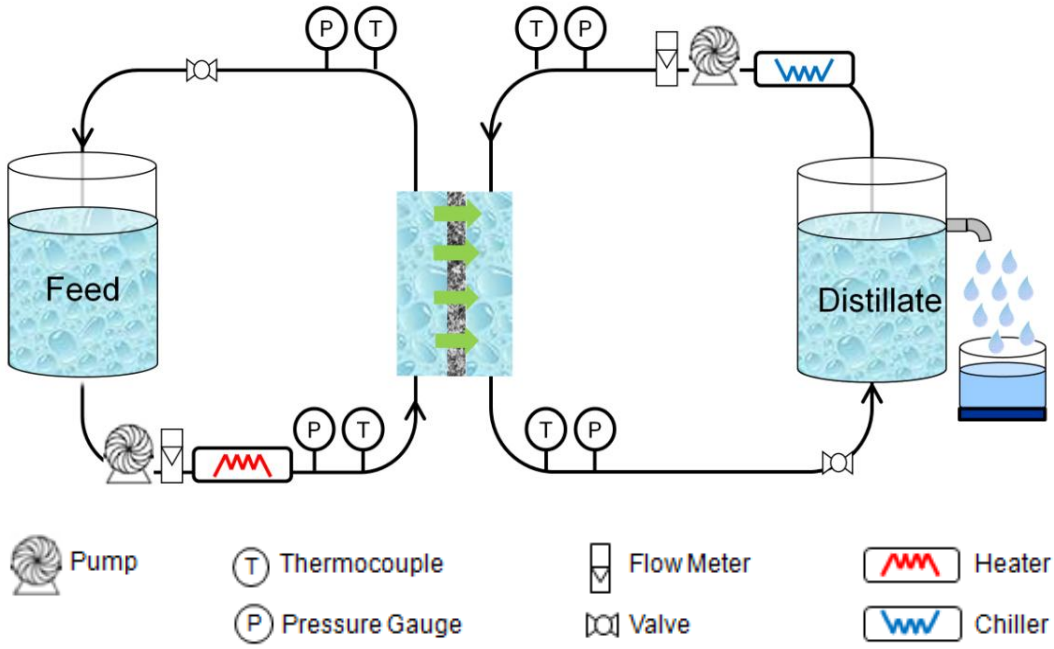

Figure 2.2 Schematic drawing of bench-scale DCMD system. The arrows in the membrane module indicate the direction of water vapor passing through the membrane.

2.2.2. Membrane characterization

A total of 19 flat-sheet membranes (10 single-layer, 9 composite) were tested. The membrane properties provided by the manufacturers are listed in Table 2.1 and the additional measurements performed to provide further membrane characterization are described below. The single-layer membranes were used directly for all characterization

measurements. The composite membranes were used intact for all measurements except porosity, which required peeling of the active layer off the support layer. Care was taken to ensure as minimal disruption as possible to the peeled active and support layers.

Table 2.1 Membrane properties as reported by manufacturers. PTFE - polytetrafluorethylene; PP - polypropylene; PVDF - polyvinylidene fluoride.

Membrane	Nominal pore size (μm)	Thickness[a] (μm)	Porosity (%)	Active layer material	Support layer material
A	0.20	79	70	PTFE	--
B	0.22	--	--	PTFE	--
C	0.22	--	--	PP	--
D	0.80	75	76	PTFE	--
E	0.20	80	74	PTFE	--
F	0.10	76-154	--	PTFE	--
G	0.10	--	--	PTFE	--
H	0.50	75	78	PTFE	--
I	0.10	70	68	PTFE	--
J	0.45	--	83	PVDF	--
K	0.45	--	--	PTFE	PP
L	0.45	195	--	PTFE	PP
M	0.20	192	--	PTFE	PP
N	0.45	279	--	PTFE	PP
O	0.20	--	--	PTFE	PP
P	0.20	--	--	PTFE	PP
Q	0.20	130	72[b]	PTFE	PP
R	0.50	120	74[b]	PTFE	PP
S	0.45	190	--	PTFE	PP

[a] sum of the active layer thickness and support layer thickness for composite membranes

[b] refers to the percent open area of the membrane

Average pore size measurement

Intact membranes were used to determine the average pore size of the single-layer membranes and the active layers of the composite membranes using the gas permeation

test with compressed air [50, 51]. The permeation flux of air through the dried membrane was measured at room temperature using transmembrane pressures from 10 to 100 kPa. Pore diameter (d) was then calculated as:

$$d = \frac{16}{3}\left(\frac{B_o}{K}\right)\left(\frac{2RT}{\pi M_j}\right)^{0.5} \quad (8)$$

where B_o is the geometric factor of a membrane; K is the permeability coefficient; and M_j is the molecular weight of air [52].

Porosity and tortuosity measurements

The porosity (ε) of the single-layer membranes and peeled active and support layers of the composite membranes was determined by:

$$\varepsilon = 1 - \frac{\rho_m}{\rho_p} \quad (9)$$

where ρ_m is the density of the membrane sample and ρ_p is the reported density of the polymer material [35]. The membrane sample density, ρ_m, for the single-layer membrane was calculated directly from the mass and dimensions of a membrane sample, excluding the pore space in the material. Values of ρ_p used were 2200 kg/m^3 for polytetrafluoroethylene (PTFE) [49, 53], 900 kg/m^3 for polypropylene (PP) [53], and 1780 kg/m^3 for polyvinylidene fluoride (PVDF) [54]. Although additives may be included during the membrane manufacturing proces [55], and could cause the actual density of the membrane material to be different from the reported polymer density, the difference is assumed negligible due to the very small additive amounts. Zhang et al. [35] used the reported polymer density in their porosity calculation and claimed a density

error of less than 3%. Ruskowitz et al. [56] used energy dispersive spectrometry (EDS) surface analysis (0.3-0.5 wt% detection limit) on a virgin PTFE sample (Membrane D, Table 2.1), and detected only carbon and fluorine on the membrane sample.

The tortuosity (τ) of each single-layer membrane was calculated by [23, 57]:

$$\tau = \frac{(2-\varepsilon)^2}{\varepsilon} \tag{10}$$

and the tortuosity of the active layer (τ_a) of the composite membrane was calculated by:

$$\tau_a = \frac{(2-\varepsilon_a)^2}{\varepsilon_a} \tag{11}$$

where ε_a is the porosity of the active layer. Tortuosity of the non-woven support layer (τ_s) of the composite membrane was calculated by [43, 58]:

$$\tau_s = \frac{1}{\varepsilon_s} \tag{12}$$

where ε_s is the porosity of the composite membrane support layer. The porosity-tortuosity relationship in Eq. 12 is different from Eqs. 10 and 11 because non-woven support layers are loosely packed, with structures similar to random spheres or clusters; while single-layer membranes and active layers of composite membranes are spongy, with structures similar to the interstices between closely packed spheres [43, 58]. Tortuosity of the scrim support layer of the composite membrane was assumed to be 1[59].

Membrane thickness measurement

The thickness (δ) of the single-layer membranes and the active layer and support layer of the composite membranes were measured from scanning electron micrographs of

membrane cross-sections. Prior to measurement, the intact membranes were immersed in liquid nitrogen and cut with a razor blade. The thicknesses of the active layer and the support layer of the composite membranes were measured separately on the same scanning electron micrograph (no peeling was necessary). Each thickness was measured on three different sections of the membrane and the average thickness was calculated

Contact angle measurement

Contact angle (θ) was measured as an indication of membrane hydrophobicity. A commercial goniometer (Ramé-Hart, Mountain Lakes, NJ) was used to perform captive-bubble measurements on intact membranes to determine the contact angle of the single-layer membranes and composite membrane active layers. By immersing the membrane sample into a water solution and completely hydrating it, the contact angle measurement is less influenced by pores and swelling [60]. For each membrane, triplicate contact angles were measured on three samples, resulting in nine contact angles measured per membrane, and the average contact angle was calculated.

Liquid-entry pressure measurement

Liquid-entry pressure (LEP) is the pressure that must be applied to a water solution to penetrate into dry membrane pores. It is a function of the membrane properties and the liquid properties. The expression for LEP is:

$$P_l - P_j = \frac{2B_o\gamma_l \cos\theta}{r_{\max}} < LEP \qquad (13)$$

where P_l is the pressure of the liquid on the membrane surface; γ_l is the liquid surface tension; and r_{max} is the largest membrane pore radius [61]. The experimental apparatus reported by Smolders et al. [48] was used to perform LEP measurements on intact membranes to determine the LEP of single-layer membranes and composite membrane active layers. Each membrane was placed in a static stainless-steel cell filled with double-distilled water. The water pressure was increased in increments of 5 kPa and maintained for one minute at each pressure; the pressure at which continuous flow was observed on the distillate side was considered to be the membrane LEP.

Percent of open surface area of the support layer measurement

Scanning electron micrographs with 35x magnification were used to determine the percent of open surface area (POSA) of the support layers. The scrim support layer had a uniform pore structure (Fig. 2.3a), thus the POSA was calculated by dividing the total pore area (function of pore area and pore number) by the whole membrane sample area [34]. Because of the non-uniform pore structure of the non-woven support layer (Fig. 2.3b), the POSA was determined using the grid method with the scanning electron micrographs.

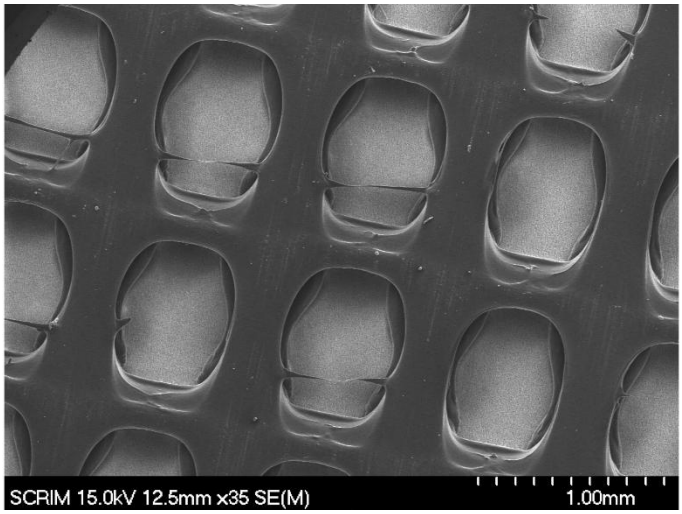

(a)

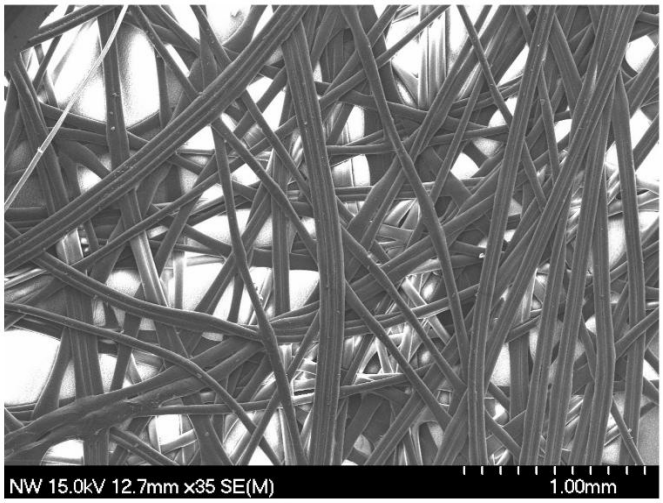

(b)

Figure 2.3 SEM images of (a) scrim support layer and (b) non-woven support layer.

2.2.3. Model development and validation for water flux prediction

Scatterplots and correlation matrices between water flux and the membrane structural parameters were developed and analyzed using Minitab® 15.1.0.0 with the goal of identifying the structural parameters with the strongest correlation with water flux. For selected structural parameters, a linear regression analysis was performed between water flux and the structural parameter to develop a water flux prediction model. To ensure the robustness of the model, the process was performed three times in total with membranes from Table 2.1 randomly selected each time for the linear regression. The single-layer membranes and the composite membranes were tested separately from each other.

The models developed above were validated both internally and externally. For internal validation, the sum of the estimated standard deviations of the regression coefficients (s{b_0} and s{b_1}), squared errors (SSE), mean squared error (MSE), adjusted R^2, and predicted residual sums of squares (PRESS) criteria were used[62]. All criteria were obtained from the Minitab® regression output. Typically, a model with small s{b_0}, s{b_1}, SSE, MSE, PRESS, and high adjusted R^2 will fit well and result in small errors between the predicted water flux and the measured water flux for the membranes used to develop the model. For external validation, the mean squared prediction error (MSPR) was used. If the MSPR to MSE ratio of a model is smaller than the critical F-test value ($p < 0.05$), the model is valid, and vice versa [63]. For a valid model, if the MSPR is much smaller than or fairly close to the MSE, the MSE will give an appropriate measure of the predictive capability of the model. If the MSPR is much greater than the MSE, then the MSPR should be used as an indicator of the predictive capability of the model [64]. A

model with a smaller MSPR or MSE (depending on which one is used) is expected to have a better predictive capability [64].

2.3. Results and discussions

2.3.1. Membrane property characterization and flux test results

The properties of the single-layer membranes and the active layers of the composite membranes, along with the intact membrane water fluxes are given in Table 2.2. The average pore sizes of the single-layer membranes (0.1-0.5 μm excluding membrane D) and the composite membrane active layers (0.2-0.6 μm) are comparable and generally within the range reported in the literature (0.2-1 μm) [1, 35, 36]. Membrane porosities for the single-layer membranes (37-85%) and the composite membrane active layers (47-90%) are also comparable and generally within the range reported in the literature (30-85%) [38, 39]. It follows from Eq. 10 that the tortuosities are also comparable (1.58-4.02 for the single-layer membranes except Membrane I and 1.59-5.05 for the active layers of the composite membranes) and consistent with the literature (1.21-6.84) [43]. The thicknesses of the single-layer membranes (39 to 205 μm) are similar to those reported in the literature (40 to 250 μm) [1]; they span a broader range than the thicknesses of the composite membrane active layers (27-59 μm). This is because single-layer membranes must be thick enough to be mechanically strong and to minimize conductive heat loss but thin enough to minimize the mass transfer resistance, while composite membranes must have thin active layers to reduce the mass transfer resistance and the support layers will provide mechanical strength and reduce conductive heat loss.

The contact angles of the single-layer membranes (109-131^{o}) and the composite membrane active layers (106-128 ^{o}) are similar and are comparable with what has been reported in the literature (110-165^{o} [58, 66]). The LEP values of the single-layer membranes (141-430 kPa) and the composite membrane active layers (95-438 kPa) are comparable and generally within the reported range (48-463 kPa) [39].

The single-layer membrane water fluxes (11-35 L/m^2 h) are within the reported flux range (4-42 L/m^2 h at feed-side temperatures near 40 ^{o}C and flow rates from 0.02 to 0.23 m/s for DCMD [39]); it should be noted that other experimental conditions including the distillate-side temperature and type of membrane spacers will also affect water flux. The lowest water flux occurs for Membrane I, which has the lowest porosity (37%) (hence, highest tortuosity (7.07)) and the smallest average pore size (0.1 μm). Membrane G has similar pore size (0.11 μm) as Membrane I, but the water flux is 54% higher than that of Membrane I, which is likely due to the much greater porosity (84%; hence, much lower tortuosity (1.60)). The composite membrane water fluxes fall within a more narrow range (22-28 L/m^2 h) with all but two membranes having a water flux above 25 L/m^2 h. The wide range of membrane properties and experimental water fluxes of the single-layer membranes is beneficial in developing the model to predict water fluxes.

Table 2.3 provides the characterization results of the composite membrane support layers. The thicknesses of the non-woven structural support layers (133-283 μm) are greater than the thicknesses of the scrim structural support layers (50-77 μm except Membrane O with a thickness of 255 μm). The porosities of the non-woven structural support layers (66-81%) are higher than the porosities of the scrim structural support layers (31-59%), while the POSA are generally an order of magnitude lower for the non-

woven structural support layers than the scrim structural support layers. This phenomena has been reported previously [58]. Because the larger POSA of the scrim structure benefits the mass transfer while the lower porosity limits the mass transfer, the effect of these on flux is not obvious.

Table 2.2 Properties of the single-layer membrane and composite membrane active layer.

Membrane	Pore size (μm)	Porosity [b] (%)	Tortuosity [b]	Thickness (μm)	Contact angle (^{o})	Liquid entry pressure (kPa)	Flux[c] (L/m^2 h)
A	0.22±0.11	53.4	4.02	39±5	125±2	380±4	28.7±0.9
B	0.25±0.06	84.5	1.58	119±11	128±3	430±5	25.8±0.5
C	0.24±0.13	82.6	1.67	205±4	126±1	375±3	21.3±0.7
D	0.90±0.09	78.8	1.86	78±2	121±2	141±5	26.8±1.5
E	0.25±0.06	67.4	2.61	95±3	114±3	258±5	18.3±1.1
F	0.18±0.02	80.1	1.79	67±17	131±3	385±3	34.5±1.2
G	0.11±0.05	84.1	1.60	111±4	124±3	358±6	17.5±0.3
H	0.36±0.04	61.2	3.15	56±4	109±4	183±5	21.9±1.2
I	0.10±0.01	37.4	7.07	63±4	114±2	400±10	11.4±3.0
J	0.51±0.04	65.2	2.79	109±6	118±3	154±6	24.3±1.1
K[a]	0.34±0.19	56.1	3.68	31±5	120±5	415±10	28.1±0.3
L[a]	0.52±0.08	84.2	1.59	27±2	118±5	190±5	26.0±1.1
M[a]	0.19±0.11	46.6	5.05	31±4	106±6	290±5	25.3±1.2
N[a]	0.57±0.26	90.3	1.33	59±3	126±1	95±6	26.3±0.6
O[a]	0.23±0.04	81.1	1.74	58±18	125±2	380±5	24.5±1.0
P[a]	0.25±0.01	79.6	1.82	50±11	125±3	395±10	24.0±0.9
Q[a]	0.21±0.04	64.4	2.85	31±10	128±2	390±15	25.7±1.1
R[a]	0.50±0.15	71.3	2.32	47±4	120±2	438±5	25.8±0.2
S[a]	0.44±0.13	77.5	1.94	21±3	109±2	238±15	22.2±3.5

[a] active layer of the composite membrane

[b] calculated using the average membrane properties

[c] refers to the intact membrane flux

Table 2.3 Composite membrane support layer properties. A tortuosity of 1 is assumed for the scrim support layers [59].

Membrane	Membrane structure	Porosity[a] (%)	Tortuosity[a]	Thickness (μm)	POSA (%)
K^s	Scrim	58.6	1	77±14	43.2
L^s	Non-woven	72.8	1.37	283±9	3.76
M^s	Non-woven	80.9	1.20	171±8	4.09
N^s	Non-woven	70.6	1.42	230±10	3.97
O^s	Scrim	52.0	1	255±14	44.6
P^s	Non-woven	72.3	1.38	194±13	11.4
Q^s	Scrim	39.4	1	54±7	35.4
R^s	Scrim	30.5	1	50±6	37.4
S^s	Non-woven	65.5	1.53	133±11	3.21

[s] support layer of the composite membrane

[a] calculated using the average membrane properties

2.3.2. Model development and validation for single-layer membranes

Identification of structural parameters that have high correlations with water flux

As discussed in Section 2.1.3, pore size, porosity, tortuosity, and thickness may each affect water flux in MD. In this work, four characteristics (r, ε, $1/\tau$, $1/\delta$) were considered in various combinations ($r^n\varepsilon/\tau\delta$, $r^n\varepsilon/\delta$, $r^n\varepsilon/\tau$, $r^n/\tau\delta$, $r^n\varepsilon$, r^n/τ, r^n/δ, and r^n), where n is 0, 1, or 2. Additional membrane properties, including θ, 1/LEP, 1/thermal conductivity ($1/k_m$), and 1/heat transfer coefficient ($1/h_m$) were also investigated to ensure a comprehensive analysis of possible structural parameters (28 total parameter combinations were tested). Calculations of k_m and h_m were performed as reported in the literature [2, 12, 45]. Overall, the structural parameters were classified into three groups: 1) those already reported in the literature: $\varepsilon/\tau\delta$, $r\varepsilon/\tau\delta$, $r^2\varepsilon/\tau\delta$, ε/τ, $r\varepsilon/\tau$, $r^2\varepsilon/\tau$, $1/\tau\delta$. r, ε, and $1/\delta$; 2) basic membrane properties and their reciprocals that were not included in the first

group: $1/\tau$, 1/LEP, $1/k_m$, and $1/h_m$; and 3) others: $r\varepsilon/\delta$, $r^2\varepsilon/\delta$, ε/δ, $r^2\varepsilon$, $r\varepsilon$, r^2/δ, r/δ, $r/\tau\delta$, $r^2/\tau\delta$, r/τ, r^2/τ, and r^2. Membrane contact angle, θ, was eventually removed from consideration as a structural parameter to predict water flux in this investigation because there was little range in the contact angle of the single-layer membranes (Table 2.2).

To identify the structural parameters that correlate well with water flux, a correlation analysis between water flux and each structural parameter was first performed for the ten single-layer membranes. Although investigations of the effects of membrane pore size, porosity, and inverse thickness on water flux have been discussed in the literature (Section 2.1.3), the correlation results in Table 2.4 (correlation coefficient, β, from 0.243 to 0.428) suggest that none of the parameters alone can be used to adequately estimate water flux. The structural parameters ε/δ, $\varepsilon/\tau\delta$, and $1/\tau\delta$ all correlate well with water flux (β from 0.638 to 0.781), and those correlation observations are also supported by the scatterplots in Appendix A; thus, these structural parameters may be used to predict water flux. Care should be taken, however, because the three structural parameters include membrane properties that may be coupled, which can lead to error propagation as discussed in Section 2.1.4.

Table 2.4 Correlation results between water flux and membrane structural parameters for single-layer membranes. Bold numbers indicate the structural parameters having the highest correlations with water flux.

	Structural parameter	Correlation coefficient
Structural parameters reported in literature	$\varepsilon/\tau\delta$	**0.731**
	$r\varepsilon/\tau\delta$	0.399
	$r^2\varepsilon/\tau\delta$	0.251
	ε/τ	0.326
	$r\varepsilon/\tau$	0.336
	$r^2\varepsilon/\tau$	0.243
	$1/\tau\delta$	**0.781**
	r	0.303
	ε	0.428
	$1/\delta$	0.243
Basic membrane properties	$1/\tau$	0.357
	1/LEP	0.111
	$1/k_m$	0.168
	$1/h_m$	-0.080
Other structural parameters	$r\varepsilon/\delta$	0.402
	$r^2\varepsilon/\delta$	0.257
	ε/δ	**0.638**
	$r^2\varepsilon$	0.244
	$r\varepsilon$	0.329
	r^2/δ	0.261
	r/δ	0.376
	$r/\tau\delta$	0.405
	$r^2/\tau\delta$	0.253
	r/τ	0.336
	r^2/τ	0.244
	r^2	0.243
New structural parameter	C_m	**0.714**

To avoid the use of coupled membrane properties, a structural parameter that can be measured independently but maintains the physical meaning of those membrane properties that may affect water flux (e.g., thickness and porosity) is preferred. In this regard, membrane porosity (Eq. 9) can be expressed as [35]:

$$\varepsilon = 1 - \frac{m}{\rho_p \times l \times w \times \delta} \tag{14}$$

*w*here *m*, *l*, and *w* are the mass, length, and width, respectively, of the membrane sample. Eq. 14 can be used to decouple porosity and thickness by incorporating the constant membrane properties (*m*, *l*, *w*, and ρ_p) into a new structural parameter termed the membrane constant (C_m):

$$C_m = \frac{\rho_p \times l \times w}{m} \tag{15}$$

The physical relationship between the membrane constant, porosity, and thickness can be seen by combining Eqs. 14 and 15:

$$C_m = \frac{1}{\delta(1-\varepsilon)} \tag{16}$$

The correlation analysis between water flux and Cm for the 10 single-layer membranes was performed and a correlation of $\beta = 0.714$ was observed (last row of Table 2.4), suggesting it was a good structural parameter for flux prediction.

Because C_m is not based on thickness or porosity measurements (Eq. 15), constant flux will be predicted during membrane compaction periods. To experimentally validate this, four randomly selected membranes were compacted under feed-side pressures up to 100 kPa in DCMD. No flux change was observed for the four membranes; similar

phenomena have also been reported by Cath et al. [28]. Although membrane compaction may occur, it may not be significant enough to measurably decrease flux. If the membrane were to be highly compacted, flux decline would likely occur and would not be predicted by C_m, thus using C_m to estimate water flux does have practical limitations. It should also be noted that C_m can only be used to estimate the steady-state water flux and not dynamic water flux behavior such as that frequently observed in the initial stages of an MD flux test [67-69].

Model development and validation using the membrane constant

A simple linear regression model using C_m was used to predict water flux under the given experimental conditions. The model was expressed as:

$$\hat{N}_i = b_0 + b_1 C_m \tag{17}$$

where $\hat{N}_i$ is the predicted water flux and b_0 and b_1 are the regression constants. Because the pore sizes of a typical MD membrane range from 0.2 to 1.0 μm [1, 35, 65] and are recommended to be smaller than 0.6 μm to prevent wetting [39, 67, 70], only the seven single-layer membranes with pore sizes from 0.18 to 0.51 μm were used during model development. Three independent test sets were performed; each test set used five membranes randomly selected for model development and the remaining two for model validation. In Test Set 1, Membranes B and E were used to validate the model; in Test Set 2, Membranes H and J were used; and in Test Set 3, Membranes A and C were used. The linear regression model was also used to predict water flux based on the other three well correlated structural parameters ($\varepsilon/\tau\delta$, $1/\tau\delta$, and ε/δ) simply by replacing C_m in Eq.

17 with $\varepsilon/\tau\delta$, $1/\tau\delta$ and ε/δ, respectively. Results using ε/δ revealed a nonlinear relationship with water flux for all three tests ($p > 0.14$; results not shown) and was thus dropped from further model development. The linear regression results for C_m, $\varepsilon/\tau\delta$, and $1/\tau\delta$ are given in Table 2.5. Linear relationships are observed ($p \leq 0.1$) for all three. The residual plots (Appendix 2.B) for each structural parameter suggest that it is reasonable to use the linear regression analysis.

In Table 2.5, the calculated MSPR to MSE ratios are smaller than the critical $F_{0.05}$ value (5.786) for all tests, thus the developed models are valid to predict water flux for the membranes in the model validation group. In Test Set 1, no single structural parameter is consistently better than the others for the model development considering all model criteria (i.e., none has a consistently lower s{b_0}, s{b_1}, SSE, PRESS, and MSE and a higher adjusted R^2); however, the model developed using C_m has a better predictive capability due to the smaller MSE. The MSE criterion was used because the MSPR was similar to the MSE for each structural parameter. In Test Set 2, the model developed using C_m has lower s{b_0}, s{b_1}, SSE, PRESS, and MSE and a higher adjusted R^2 than the models developed using $\varepsilon/\tau\delta$ and $1/\tau\delta$, indicating that C_m is a better structural parameter for the model development. It should be noted however, that the predictive capability of this model (MSPR of 20.71) is not as good as the one developed using $\varepsilon/\tau\delta$ (MSE of 12.58). The MSPR criterion was used for C_m because the MSPR was much greater than the MSE; while the MSE criterion was used for $\varepsilon/\tau\delta$ because the MSE was close to the MSPR. In Test Set 3, the structural parameter $\varepsilon/\tau\delta$ is identified as a better structural parameter for the model development (lower s{b_0}, s{b_1}, SSE, PRESS, and

MSE and a higher adjusted R^2) and the model has a better predictive capability due to the smaller MSE. The MSE criterion was used because the MSE was close to or much larger than the MSPR for each structural parameter. Overall, the models developed using C_m and $\varepsilon/\tau\delta$ have better flux prediction performance than the model developed using $1/\tau\delta$. Because the characterization of the membrane constant requires only basic and independent measurements (mass, length, and width of the membrane sample) that can be obtained with inexpensive analytical equipment (a ruler and a balance), less cost is associated with the measurement as compared to $\varepsilon/\tau\delta$, where the thickness measurement must be determined using scanning electron micrographs. Additionally, the problem of coupled parameters may exist between porosity, tortuosity, and thickness with $\varepsilon/\tau\delta$. Comparing the results of the three test sets using C_m, the model developed in Test Set 1 has the smallest MSE or MSPR (depending on which one is used) compared to the models developed in Test Sets 2 and 3. Therefore, this model has the smallest flux prediction errors for the membranes used in the model validation process. The model developed in Test Set 2 has the lowest $s\{b_0\}$, $s\{b_1\}$, SSE, PRESS, and MSE and the highest adjusted R^2 compared to the models developed in Test Sets 1 and 3, thus it has the smallest flux prediction errors for the membranes used in the model development process. Because five out of the seven membranes had better flux predictions using the model developed in Test Set 2, this model was taken as the final model for flux prediction under the current experimental conditions. The model is expressed as:

$$\hat{N}_i = 10.1 + 318 \times C_m \tag{18}$$

where the units of $\hat{N}_i$ and C_m are L/m^2 h and μm^{-1}, respectively.

Table 2.5 Regression results for candidate models based on the model development and validation data sets. The structural parameters all have units of 1/μm.

Statistics	Test 1			Test 2			Test 3		
	C_m $\times 10^3$	$\varepsilon/\tau\delta$ $\times 10^4$	$1/\tau\delta$ $\times 10^4$	C_m $\times 10^3$	$\varepsilon/\tau\delta \times 10^4$	$1/\tau\delta$ $\times 10^4$	C_m $\times 10^3$	$\varepsilon/\tau\delta$ $\times 10^4$	$1/\tau\delta$ $\times 10^4$
p	0.053	0.062	0.073	0.010	0.052	0.019	0.079	0.058	0.102
b_0	15.13	16.60	15.10	10.10	13.04	10.41	12.67	13.46	11.53
$s\{b_0\}$[a]	3.802	3.593	4.348	2.863	4.363	3.513	4.991	4.147	6.054
b_1	0.239	0.263	0.208	0.318	0.323	0.285	0.262	0.295	0.252
$s\{b_1\}$[b]	0.077	0.091	0.077	0.006	0.103	0.061	0.100	0.099	0.108
SSE	28.87	31.96	35.27	13.36	37.75	19.83	44.50	36.76	52.13
PRESS	81.69	73.41	92.87	39.92	69.61	62.18	183.8	145.9	227.7
MSE	9.622	10.65	11.76	4.450	12.58	6.610	14.83	12.25	17.38
MSPR	13.01	18.57	13.60	20.71	12.16	21.19	2.031	13.83	3.450
MSPR:MSE	1.352	1.744	1.156	4.654	0.967	3.206	0.137	1.129	0.198
Adjusted R^2	68.4%	65.0%	61.4%	89.0%	68.8%	83.6%	59.5%	66.5%	52.5%

[a] estimated standard deviation of the regression coefficient b_0

[b] estimated standard deviation of the regression coefficient b_1

Flux prediction for membranes with pore sizes outside the typical range

The model (Eq. 18) was also used to predict water flux for membranes with pore sizes outside the range used for the model development (d < 0.18 or > 0.51 μm). The flux prediction errors, along with the errors for the membranes used to develop and validate the model, are given in Table 2.6. As expected, the water flux prediction errors for membranes used to develop the model are relatively small (≤ 11.5%). However, a relatively large flux prediction error (-23.9%) for one of the membranes used to validate the model (Membrane A) was observed. This is likely because of the relatively low porosity of this membrane (Table 2.2). As stated in Section 2.3.2., flux decline would likely occur for a highly compacted membrane and would not be predicted by C_m.

Because a membrane with a low porosity is expected to be structurally similar to a highly compacted membrane, it follows that the flux prediction error using C_m for the low porosity membrane is also larger. This suggests the practical limitations of using C_m for flux prediction. The model predicts water flux well for the membrane with a large pore size (Membrane D; 0.9 μm) and one of the two membranes with very small pore size (Membrane G; ~ 0.1 μm). The error in flux prediction for Membrane I, which also has a very small pore size (0.1 μm), is nearly 60%. It is unclear whether the low porosity (37.4%) or the large variation of the experimental water flux (±3 L/m^2 h, twice the variation observed for other membranes) led to the large predicted flux error for Membrane I. Overall, it appears that the developed model can be used to predict the water flux of membranes with pore sizes from 0.10 to 0.9 μm, but may not be appropriate for membranes with very low porosities (e.g., Membrane I).

Table 2.6 Flux prediction error (%) between the measured water fluxes and the predicted water fluxes.

	Membrane	Current model[a] (%)	Dusty gas model v.1[b] (%)	Dusty gas model v.2[c] (%)
Model development	B	5.97	48.2	42.8
	C	-10.6	-2.61	-6.13
	E	11.5	28.0	23.4
	F	-1.59	36.9	32.5
	J	-3.84	-7.05	-11.2
Model validation	A	-23.9	-2.50	-5.86
	H	12.6	50.9	44.6
Pore size near 0.1μm	G	16.4	61.3	57.3
	I	59.3	-59.7	-60.7
Pore size of 0.9 μm	D	9.36	138	126

[a] Eq. 18

[b] Eq. 6 was used for PD_{ij} in Eq. 4 for flux prediction

[c] Eq. 7 was used for PD_{ij} in Eq. 4 for flux prediction

Performance comparison between the developed model and the simplified dusty gas model

The flux prediction performance using the simplified dusty gas model with two different PD_{ij} equations is also given in Table 2.6. Both PD_{ij} equations resulted in similar flux prediction. The simplified dusty gas model (Eq. 4) does not predict flux well for membranes with extremely small pore sizes (Membranes G and I) or large pore sizes (Membrane D). Because the dusty gas model neglects both surface diffusion and viscous flow when applied to DCMD, only Knudsen diffusion and molecular diffusion are considered as the mass transfer mechanisms. When the membrane pore size is comparable with the mean free path of water vapor in air (0.11 μm [22]), Knudsen diffusion is the dominant mass transfer mechanism. The addition of a molecular diffusion

term may result in either over- or under-estimation of water flux depending on membrane properties and experimental conditions (Eq.4). When the membrane pore size is much greater than the mean free path of water vapor in air, molecular diffusion is the dominant mass transfer mechanism. The addition of a Knudsen diffusion term likely led to the over-estimation of water flux for Membrane D (0.9 μm). Overall, the model developed using C_m has better flux prediction than the dusty gas model and can be used for membranes with a wider range of pore sizes.

2.3.3. Model development for the composite membranes

To investigate whether the membrane constant can be used to predict water flux for composite membranes, nine composite membranes were characterized and studied (Tables 2.2 and 2.3). The active layer membrane constant (C_{ma}) was used to represent the active layer properties since the membrane constant was already validated for single-layer membranes. The support layer properties investigated include support layer membrane constant (C_{ms}), thickness (δ_s), tortuosity (τ_s), porosity (ε_s), and POSA. Correlation results between composite membrane water flux and the membrane properties are given in Table 2.7, and it can be seen that none of the membrane properties alone correlate strongly with water flux. Although C_{ms} does not have the highest correlation coefficient with water flux, it's applicability for use with composite membranes alone and in conjunction with C_{ma} is evaluated here. Two linear regression models were tested based on: 1) a single composite membrane property (C_{ma} or C_{ms}), where the model was expressed the same as Eq. 17; and 2) the mass transfer in series theory, where the model was expressed as:

$$\frac{1}{\hat{N}_i} = b_0 + b_1 \frac{1}{C_{ma}} + b_2 \frac{1}{C_{ms}} \quad (19)$$

Linear regression tests were performed for both models and the absolute *p* values were found to be much greater than 0.316. Therefore, a nonlinear relationship exists between water flux and the membrane constant for the composite membranes. One possible reason is the narrow range of experimental water flux; membranes with a wider range of water flux should be tested to continue the model development for the composite membranes.

Table 2.7 Correlation results between water flux and membrane structural parameters for composite membranes.

Membrane property	Correlation coefficient
C_{ma}	-0.316
$1/\delta_s$	0.309
ε_s	-0.165
$1/\tau_s$	0.496
C_{ms}	0.318
POSA	0.448

2.4. Conclusions

A simplified water flux prediction model was developed to predict the water flux of DCMD membranes. The model uses a newly introduced structural parameter that does not contain coupled properties and can be measured independently while still carrying the physical meaning of a relationship with those membrane properties that may affect water flux (thickness and porosity). Compared to the simplified dusty gas model, the empirical model developed in the current investigation using C_m has the following advantages: 1) it

can quantitatively analyze water flux with a less complicated expression using uncoupled membrane properties; 2) it has better flux prediction and can be used for membranes with a wide range of pore sizes (0.1-0.9 μm); and 3) C_m characterization can be carried out through simple and reliable measurements using inexpensive analytical equipment. However, using C_m for flux prediction does have limitations. It may not be valid for membranes with low porosities and it cannot adequately predict water flux for composite membranes when using the linear regression approach. Future efforts should be made to develop a non-linear prediction model for composite membranes.

Acknowledgments

The authors would like to thank the U.S. Department of Energy Geothermal Technologies Program (Grant No. DE-EE00003231) for the financial support of this work.

Nomenclature and units

$b_{(0,1,2)}$ Constants in the regression equation

B Membrane mass transfer coefficient (L/m^2 Pa h)

B_o Membrane geometric factor

C_m Membrane constant (m^{-1})

$C_{m(a,s)}$ Membrane constant of the active layer (a) or support layer (s) (m^{-1})

d Membrane pore size (m)

D_{ij} Ordinary diffusion coefficient (m^2/s)

h_m Heat transfer coefficient of the membrane (W/m^2 K)

k_m Thermal conductivity of the membrane (W/m K)

K Knudsen permeability coefficient (L/m^2 Pa h)

l Membrane length (m)

m Membrane mass (kg)

$M_{(i,j)}$ Molecular weight of vapor (i) or air (j) (kg/kmol)

n Exponent of membrane pore size

N_i Overall water flux (L/m^2 h)

$N_{(i,j)}^D$ Diffusive flux of vapor (i) or air (j) (L/m^2 h)

N_i^V Viscous flux of vapor (L/m^2 h)

$\widehat{N}_i$ Predicted water flux (L/m^2 h)

p Probability of obtaining a test statistic

P Total pressure (Pa)

$P_{(i,j,l)}$ Pressure of vapor, air inside membrane pores, or liquid on membrane surface (Pa)

r Membrane pore radius (m)

r_{max} Largest membrane pore radius (m)

R Universal gas constant (J/mol K)

T Temperature (K)

T_m Membrane temperature (K)

w Membrane width (m)

β Correlation coefficient

γ_l Liquid surface tension (Pa m)

δ Membrane thickness (m)

δ_s Support layer thickness (m)

ΔP Total pressure gradient (Pa)

ΔP_i Vapor pressure gradient (Pa)

ε Membrane porosity

$\varepsilon_{(a,s)}$ Porosity of the membrane active layer (*a*) or support layer (*s*)

θ Contact angle (^{o})

μ Fluid viscosity (kg/m s)

$\rho_{(m,p)}$ Density of the membrane (*m*) or membrane polymer (*p*) (kg/m^3)

τ Membrane tortuosity

$\tau_{(a,s)}$ Tortuosity of the membrane active layer (*a*) or support layer (*s*)

Reference

[1] L.M. Camacho, L. Dumée, J. Zhang, J. Li, M. Duke, J. Gomez, S. Gray, Review: Advances in Membrane Distillation for Water Desalination and Purification Applications, Water, 5 (2013) 94-196.

[2] K.W. Lawson, D.R. Lloyd, Review: Membrane distillation, J. Membr. Sci. , 124 (1997) 1-25.

[3] A.M. Alklaibi, N. Lior, Transport analysis of air-gap membrane distillation, J. Membr. Sci. 255 (2005) 239-253.

[4] M. Gryta, Concentration of saline wastewater from the production of heparin, Desalination 129, (2000) 35-44.

[5] A. El-Abbassi, A. Hafidi, M.C. García-Payo, M. Khayet, Concentration of olive mill wastewater by membrane distillation for polyphenols recovery, Desalination 245, (2009) 670-674.

[6] P.P. Zolotarev, V.V. Ugrozov, I. B. Volkina, V.M. Nikulin, Treatment of waste water for removing heavy metals by membrane distillation, J. Hazard. Mater, 37 (1994) 77-82.
[7] C.R. Martinetti, A.E. Childress, T.Y. Cath, High recovery of concentrated RO brines using forward osmosis and membrane distillation, J. Membr. Sci., 331 (2009) 31-39.
[8] F. Edwie, T.S. Chung, Development of hollow fiber membranes for water and salt recovery from highly concentrated brine via direct contact membrane distillation and crystallization, J. Membr. Sci., 421-422 (2012) 111-123.
[9] C. M. Tun, A. G. Fane, J.T. Matheickal, R. Sheikholeslami, Membrane distillation crystallization of concentrated salts-flux and crystal formation, J. Membr. Sci., 257 (2005) 144-155.
[10] D. Singh, K.K. Sirkar, Desalination of brine and produced water by direct contact membrane distillation at high temperatures and pressures, J. Membr. Sci., 389 (2012) 380-388.
[11] A. Alkhudhiri, N. Darwish, N. Hilal, Produced water treatment: Application of Air Gap Membrane Distillation, Desalination 309, (2013) 46-51.
[12] K.W. Lawson, D.R. Lloyd, Membrane Distillation. II. Direct contact MD, J. Membr.Sci. , 120 (1996) 123-133.
[13] K. W. Lawson, D.R. Lloyd, Review: Membrane distillation, J. Membr. Sci. , 124 (1997) 1-25.
[14] J.L. Cartinella, T.Y. Cath, M.T. Flynn, G.C. Miller, K.W. Hunter, A.E. Childress, Removal of natural steroid hormones from wastewater using membrane contactor processes, Environ. Sci. Technol., 40 (2006) 7381-7386.
[15] J.W. D. Hou, C. Zhao, B. Wang, Z. Luan and X. Sun, Fluoride removal from brackish groundwater by direct contact membrane distillation, J. Environ. Sci., 22 (2010) 1860-1867.
[16] S. Yarlagadda, V.G. Gude, L.M. Camacho, S. Pinappu, S. Deng, Potable water recovery from As, U, and F contaminated ground waters by direct contact membrane distillation process, J. Hazard. Mater, 192 (2011) 1388-1394.
[17] T.Y. Cath, V.D. Adams, A.E. Childress, Membrane contactor processes for wastewater reclamation in space. II. Combined direct osmosis, osmotic distillation, and

membrane distillation for treatment of metabolic wastewater, J. Membr. Sci., 257 (2005) 111-119.
[18] A.O. Imdakm, T. Matsuura, Simulation of heat and mass transfer in direct contact membrane distillation (MD): The effect of membrane physical properties, Journal of Membrane Science 262 (2005) 117-128.
[19] R.W. Schofield, A.G. Fane, C.J.D. Fell, Heat and mass transfer in membrane distillation, J. Membr. Sci., 33 (1987) 299-313.
[20] L. Mart´ınez-D´ıez, M.I. Vázquez-González, A method to evaluate coefficients affecting flux in membrane distillation, Journal of Membrane Science, 173 (2000) 225–234.
[21] A.O. Imdakm, T. Matsuura, A Monte Carlo simulation model for membrane distillation processes: direct contact (MD), J. Membr. Sci., 237 (2004) 51-59.
[22] J. Phattaranawik, R. Jiraratananon, A.G. Fane, Effect of pore size distribution and air flux on mass transport in direct contact membrane distillation, J. Membr. Sci., 215 (2003) 75-85.
[23] S. Srisurichan, R. Jiraratananon, A.G. Fane, Mass transfer mechanisms and transport resistances in direct contact membrane distillation process, J. Membr. Sci., 277 (2006) 186-194.
[24] M. Qtaishat, T. Matsuura, B. Kruczek, M. Khayet, Heat and mass transfer analysis in direct contact membrane distillation, Desalination 219, (2008) 272-292.
[25] A.R.D. Costa, A.G. Fane, D.E. Wiley, Spacer characterization and pressure drop modelling in spacer-filled channels for ultrafiltration, J. Membr. Sci., 87 (1994) 79-98.
[26] J. Phattaranawik, R. Jiraratananon, A.G. Fane, C. Halim, Mass flux enhancement using spacer filled channels in direct contact membrane distillation, J. Membr. Sci., 187 (2001) 193-201.
[27] L. Martínez, J.M. Rodríguez-Maroto, Characterization of membrane distillation modules and analysis of mass flux enhancement by channel spacers, J. Membr. Sci., 274 (2006) 123-137.

[28] T.Y. Cath, V.D. Adams, A.E. Childress, Experimental study of desalination using direct contact membrane distillation: a new approach to flux enhancement, J. Membr.Sci., 228 (2004) 5-16.
[29] J. Zhang, J. D. Li, S. Gray, Effect of applied pressure on performance of PTFE membrane in DCMD J. Membr. Sci., 369 (2011) 514-525.
[30] Z. Ding, R. Ma, A.G. Fane, A new model for mass transfer in direct contact membrane distillation, Desalination 151, (2002) 217-227.
[31] A. Hernfindez, J.I. Calvo, P. Prfidanos, F. Tejerina, Pore size distributions in microporous membranes: A critical analysis of the bubble point extended method, J. Membr. Sci., 112 (1996) 1-12.
[32] J. Woods, J. Pellegrino, J. Burch, Generalized guidance for considering pore-size distribution in membrane distillation, J. Membr. Sci., 368 (2011) 124-133.
[33] S. Bonyadi, T.S. Chung, Flux enhancement in membrane distillation by fabrication of dual layer hydrophilic–hydrophobic hollow fiber membranes, J. Membr. Sci., 306 (2007) 134–146.
[34] L. Martínez, J.M. Rodríguez-Maroto, Membrane thickness reduction effects on direct contact membrane distillation performance, J. Membr. Sci., 312 (2008) 143-156.
[35] J. Zhang, N. Dow, M. Duke, E. Ostarcevic, J. Li, S. Gray, Identification of material and physical features of membrane distillation membranes for high performance desalination, J. Membr. Sci. , 349 (2010) 295-303.
[36] M. I. Ali, E. K. Summers, H. A. Arafat, J.H. LienhardV, Effects of membrane properties on water production cost in small scale membrane distillation systems, Desalination 306, (2012) 60-71.
[37] K.W. Lawson, M.S. Hall, D.R. Lloyd, Compaction of microporous membranes used in membrane distillation. I. Effect on gas permeability, J. Membr. Sci., 101 (1995) 99-108.
[38] M.S. El-Bourawi, Z. Ding, R. Ma, M. Khayet, A framework for better understanding membrane distillation separation process, J. Membr. Sci., 285 (2006) 4-29.
[39] A. Alkhudhiri, N. Darwish, N. Hilal, Membrane distillation: A comprehensive review, Desalination 287, (2012) 2-18.

[40] J. Mericq, S. Laborie, C. Cabassud, Vacuum membrane distillation of seawater reverse osmosis brines, Water Res., 44 (2010) 5260-5273.
[41] D. Hou, G. Dai, J. Wang, H. Fan, L. Zhang, Z. Luan, Preparation and characterization of PVDF/nonwoven fabric flat-sheet composite membranes for desalination through direct contact membrane distillation, Sep. Purif. Technol. 101, (2012) 1-10.
[42] B.S. Lalia, E. Guillen-Burrieza, H.A. Arafat, R. Hashaikeh, Fabrication and characterization of polyvinylidenefluoride-co-hexafluoropropylene (PVDF-HFP) electrospun membranes for direct contact membrane distillation J. Membr. Sci. , 428 (2013) 104-115.
[43] S. B. Iversen, V. K. Bhatia, K .Dam-Johansen, G. Jonsson, Characterization of microporous membranes for use in membrane contactors, J. Membr. Sci., 130 (1997) 205-217.
[44] C. Fernández-Pineda, M.A. Izquierdo-Gil, M.C. Garcia-Payo, Gas permeation and direct contact membrane distillation experiments and their analysis using different models, J. Membr. Sci., 198 (2002) 33-49.
[45] J. Phattaranawik, R. Jiraratananon, A.G. Fane, Heat transport and membrane distillation coefficients in direct contact membrane distillation, J. Membr. Sci., 212 (2003) 177-193.
[46] M. Khayet, K.C. Khulbe, T. Matsuurab, Characterization of membranes for membrane distillation by atomic force microscopy and estimation of their water vapor transfer coefficients in vacuum membrane distillation process
J. Membr. Sci., 238 (2004) 199–211.
[47] M. Khayet, Membranes and theoretical modeling of membrane distillation: A review, Adv. Colloid Interface Sci., 164 (2011) 56-88.
[48] F.K. Smolders, Terminology for Membrane Distillation, Desalination 72, (1989) 249-262.
[49] Q. Huang, C. Xiao, X. Hu, X. Li, Study on the effects and properties of hydrophobic poly(tetrafluoroethylene) membrane, Desalination 277, (2011) 187-192.

[50] S. Nakao, Review: Determination of pore size and pore size distribution 3. Filtration membranes, J. Membr. Sci., 96 (1994) 131-165.
[51] M. Khayet, T. Matsuura, Determination of surface and bulk pore sizes of flat-sheet and hollow-fiber membranes by atomic force microscopy, gas permeation and solute transport methods, Desalination 158, (2003) 57-64.
[52] H.Yasuda, J.T.Tsai, Pore size of microporous polymer membranes, J. Appl. Polym. Sci., 18 (1974) 805-819.
[53] R. Mishra, S.P. Tripathy, D. Sinha, K.K. Dwivedi, S. Ghosh, D.T. Khathing, M. Muller, D. Fink, W.H. Chung, Optical and electrical properties of some electron and proton irradiated polymers, Nucl. Instrum. Methods Phys. Res., Sect. B 168, (2000) 59-64.
[54] Y. Luo, Y. Liu, Q. Yu, Influence of glow discharge plasma treatment on vapor-induced response of poly(vinylidene fluoride)-carbon black composite thin films, Thin Solid Films 515, (2007) 4016-4023.
[55] M. Mulder, Basic principles of membrane technology, Kluver Academic Publishers, Dordrecht, Netherlands, 1991.
[56] J. A. Ruskowitz, A.E. Childress, Salt-Gradient Solar Pond and Membrane Distillation System for Water Desalination Powered by Renewable Energy, in: Thesis, University of Nevada, Reno, Reno, Nevada, 2012.
[57] V.D. Alves, I.M. Coelhoso, Effect of membrane characteristics on mass and heat transfer in the osmotic evaporation process, J. Membr. Sci., 228 (2004) 159-167.
[58] S. Adnan, M. Hoang, H. Wang, Z. Xie, Commercial PTFE membranes for membrane distillation application: Effect of microstructure and support material, Desalination 284, (2012) 297-308.
[59] F. Meng, H. Zhang, F. Yang, S. Zhang, Y. Li, X. Zhang, Identification of activated sludge properties affecting membrane fouling in submerged membrane bioreactors, Sep. Purif. Technol., 51 (2006) 95-103.
[60] J.A. Brant, A.E. Childress, Assessing short-range membrane-colloid interactions using surface energetics, J. Membr. Sci., 203 (2002) 257-273.

[61] P.C. Carman, Flow of Gases Through Porous Media, Butterworth Scientific Publications, London, UK, 1956.
[62] M.H.Kutner, C.J.Nachtsheim, J. Neter, Applied Linear Regression Models 4th ed., McGraw-Hill/Irwin, New York, U.S.A, 2004.
[63] J. W. Stephens, J. A. Unruh, M. E. Dikeman, M. C. Hunt, T. E. Lawrence, T. M.Loughin, Mechanical probes can predict tenderness of cooked beef longissimus using uncooked measurements, J. Anim. Sci., 82 (2004) 2077-2086.
[64] R.L. Ott, M. Longnecker, An introduction to statistical methods and data analysis, fifth ed., Duxbury, California, 2001.
[65] A.M. Alklaibi, N. Lior, Membrane-distillation desalination: status and potential, Desalination, 171 (2004) 111-131.
[66] M. C. Garc ía-Payo, M. A. Izquierdo-Gil, C.F. ández-Pineda, Wetting Study of Hydrophobic Membranes via Liquid Entry Pressure Measurements with Aqueous Alcohol Solutions, J. Colloid Interface Sci., 230 (2000) 420-431.
[67] F. A. Banat, J. Simandl, Theoretical and experimental study in membrane distillation, Desalination 95, (1994) 39-52.
[68] A.M. Barbe, P.A. Hogan, R.A. Johnson, Surface morphology changes during initial usage of hydrophobic, microporous polypropylene membranes, J. Membr.Sci. , 172 (2000) 149-156.
[69] M. Gryta, Long-term performance of membrane distillation process, J. Membr.Sci., 265 (2005) 153-159.
[70] S. K, W. Hölz, R. Wollbeck, Membranes and modules for transmembrane distillation, J. Membr. Sci., 39(1) (1988) 25–42.

Appendix 2.A Scatterplots of water flux vs. membrane structural parameters for single-layer membranes used to identify the structural parameters that correlate well with water flux.

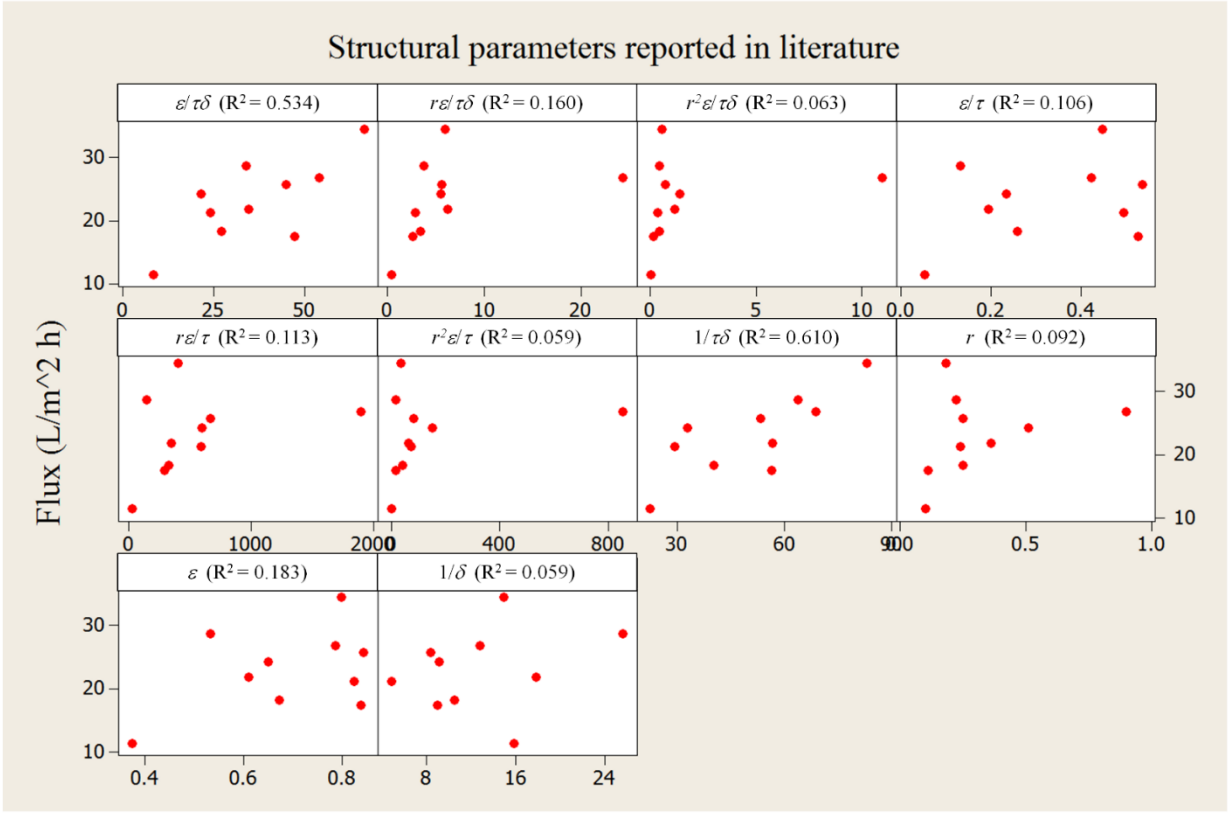

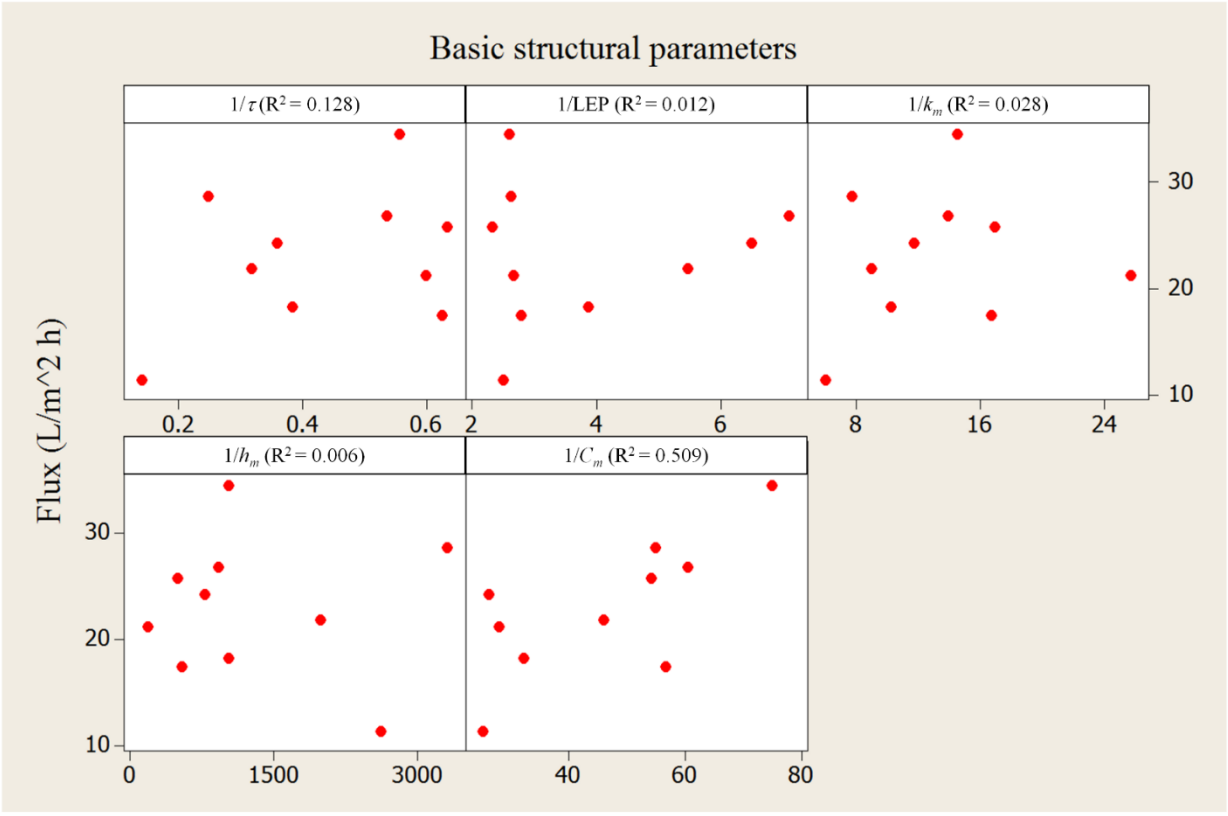
Basic structural parameters
1/τ (R² = 0.128)
1/LEP (R² = 0.012)
1/k_m (R² = 0.028)
1/h_m (R² = 0.006)
1/C_m (R² = 0.509)
Flux (L/m^2 h)

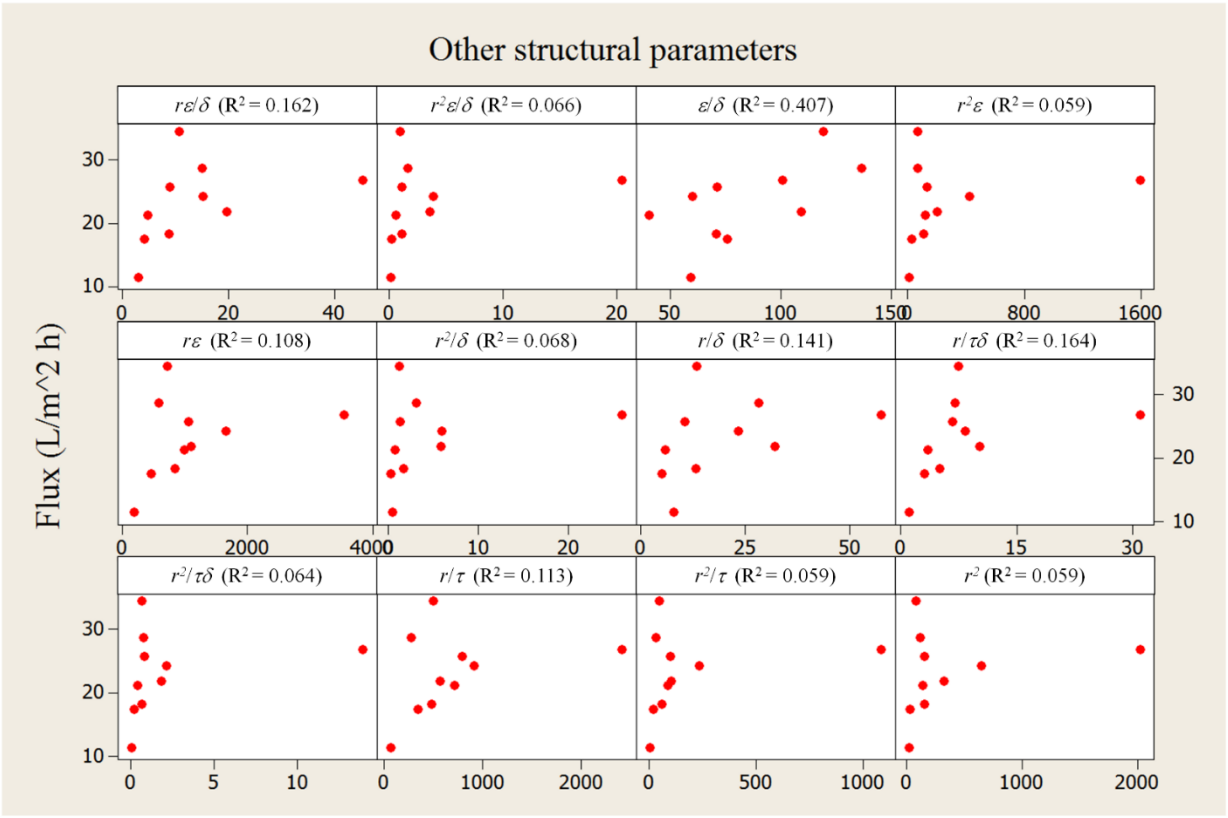
Other structural parameters
rε/δ (R² = 0.162)
r²ε/δ (R² = 0.066)
ε/δ (R² = 0.407)
r²ε (R² = 0.059)
rε (R² = 0.108)
r²/δ (R² = 0.068)
r/δ (R² = 0.141)
r/τδ (R² = 0.164)
r²/τδ (R² = 0.064)
r/τ (R² = 0.113)
r²/τ (R² = 0.059)
r² (R² = 0.059)
Flux (L/m^2 h)

Appendix 2. B Residual plots used to validate the assumptions of the linear regression analysis.

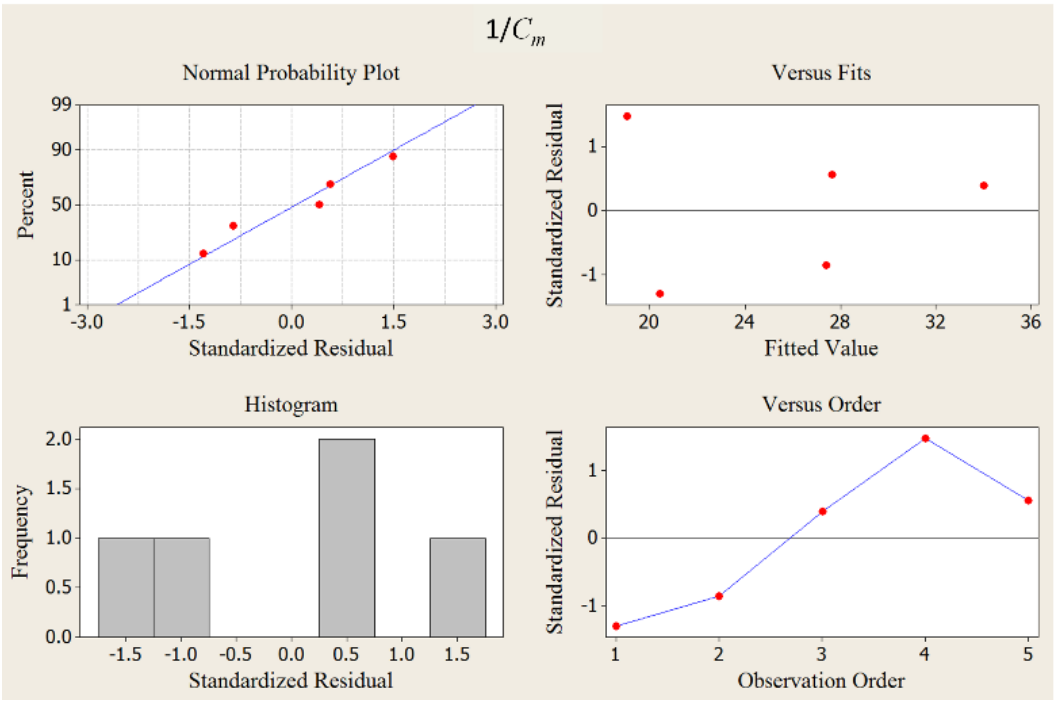

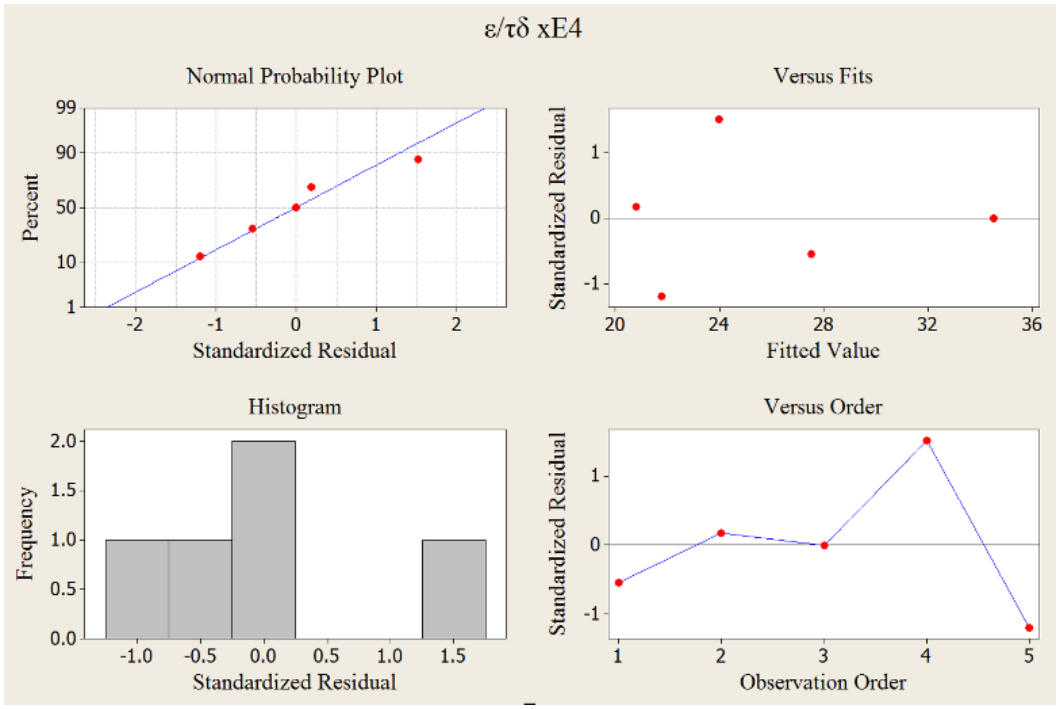

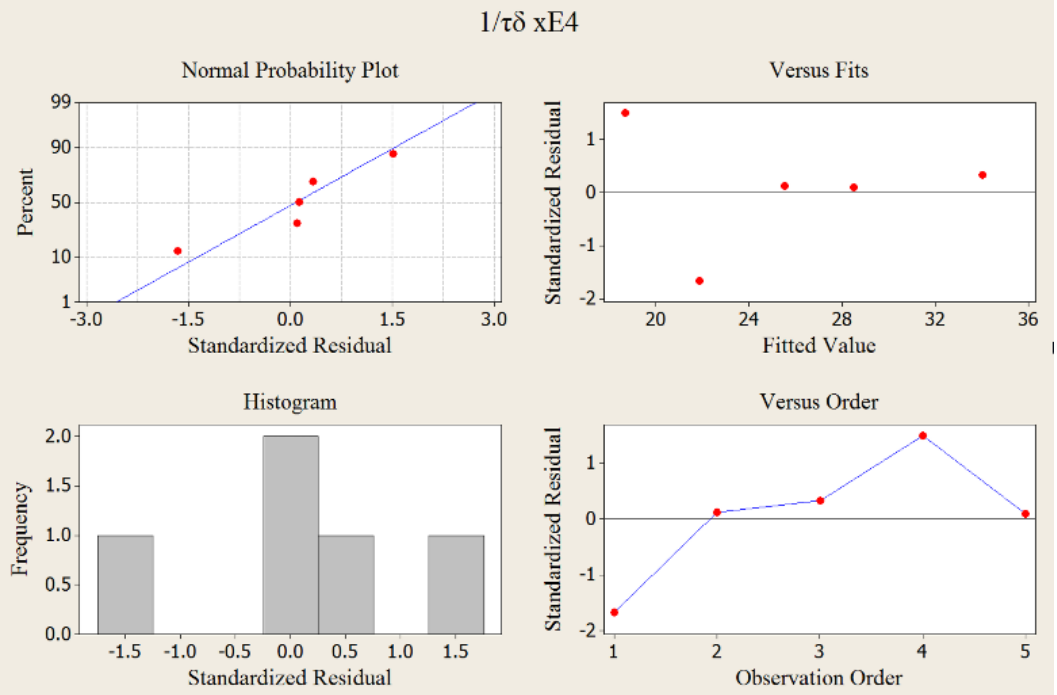
1/τδ xE4
Normal Probability Plot
Percent
99
90
50
10
1
-3.0
-1.5
0.0
1.5
3.0
Standardized Residual
Versus Fits
Standardized Residual
1
0
-1
-2
20
24
28
32
36
Fitted Value
Histogram
Frequency
2.0
1.5
1.0
0.5
0.0
-1.5
-1.0
-0.5
0.0
0.5
1.0
1.5
Standardized Residual
Versus Order
Standardized Residual
1
0
-1
-2
1
2
3
4
5
Observation Order

Chapter 3

3 FACTORS CONTRIBUTING TO IMPROVEMENT OF FLUX IN VACUUM- ENHANCED DIRECT CONTACT MEMBRANE DISTILLATION (VEDCMD)

Abstract

Low water flux in MD is one of the major factors limiting its full-scale application. In the past decades, attempts have been made to improve water flux of MD, and VEDCMD was found to be a very effective configuration to achieve this purpose. However, only qualitative investigations about the factors that may influence water flux have been reported in the literature. In this study, a mechanistic investigation of the factors attributing to higher water fluxes of VEDCMD was completed. DCMD and PEDCMD configurations were also compared. Severe membrane compaction was observed in PEDCMD followed by DCMD, while almost no compaction occurred in VEDCMD, resulting in higher water flux for VEDCMD. Air pressure inside the membrane pores was found to be the other dominant factor affecting water flux and the magnitude of the air pressure was estimated to be equal the distillate-side pressure in DCMD and PEDCMD and average of the feed and distillate pressures in VEDCMD. Pressure gradient, as is present in both PEDCMD and VEDCMD, was found to have a minimal affect on water flux.

Keywords: Vacuum-enhanced DCMD, Membrane compaction, Air pressure, Pressure gradient, Flux prediction

3.1. Introduction

3.1.1. Membrane distillation

Membrane distillation (MD) is a thermally-driven membrane process in which separation occurs through a phase change. The driving force in MD is the vapor pressure gradient resulting from the temperature difference across the membrane. Because of the high latent heat of evaporation for water, MD is an energy intensive process [1]. However, it can be combined with solar energy, geothermal energy, and waste industrial heat to reduce energy costs [2-8]. MD can achieve near 100% rejection of salts and non-volatile organics despite the fouling and scaling potential of the feed water [3]; therefore, it is well suited to remove low molecular weight contaminants such as endocrine disrupting compounds that may not be rejected well by reverse osmosis (RO) membranes [9].

3.1.2. Methods to improve water flux in DCMD

When treating feed waters with relatively low fouling and scaling potentials such as seawater, obtaining high water flux is desirable. Approaches to improve water flux have included developing novel membranes [10], deaerating feed waters [2, 11], and employing vacuums into membrane modules [12, 13]. Schofield et al. [11] and Cath et al. [12] employed vacuum of equal magnitude on the feed and distillate sides of the membrane, and flux improvement was observed in each study compared to the flux of traditional DCMD (without the use of hydraulic pressure or vacuum). The use of vacuum on the distillate side while maintaining atmospheric pressure on the feed side led to greater flux improvement [12]. Decreased air pressure inside the membrane pores, decreased membrane conductive

heat loss, decreased temperature polarization, and increased pressure gradient across the membrane have all been proposed as possible mechanisms for flux improvement when a vacuum was present in the system [12-14]. However, these mechanisms have not been systematically investigated and the dominant factors affecting water flux are unclear: it is possible that only one or two factors among air pressure inside the membrane pores, membrane conductive heat loss, temperature polarization and pressure gradient may dominate water flux. The magnitude of the air pressure inside the membrane pores is also unclear. Zhang et al. [13] assumed the pore pressure (sum of air pressure and water vapor pressure inside the pores [15, 16]) to be equal to the vacuum pressure of the liquid stream when vacuum was employed on the distillate side of the DCMD system. The same assumption was used when vacuum was employed on both the feed and distillate sides [11]. Because water vapor pressure is only a function of temperature (Antoine equation [17, 18]), it is doubtful to assume an air pressure with the same magnitude when the vacuum is only employed on the distillate side or on both the feed and distillate sides. Therefore, clarification of the dominant factor affecting water flux and the magnitude of air pressure are needed to assess and improve the water flux in DCMD.

Studies that used hydraulic pressures at equal magnitudes on the feed and distillate sides of the membrane observed a reduction in flux compared to the traditional DCMD system [19], and no obvious flux change occurred when only employing hydraulic pressure on the feed side [12]. Membrane compaction was thought to be a factor that increased water flux (other factors decreased water flux, leading to an unchanged or decreased overall water flux) [12]. However, a contradictory thought that membrane compaction reduced flux has been given by Zhang et al. [19], especially for membranes with low porosities [20].

3.1.3. Objectives

The overall objective of this study was to mechanistically evaluate the factors contributing to the improvement of water flux when vacuum was employed in DCMD. Because employing vacuum only on the distillate side of the membrane (VEDCMD) led to greater flux improvement than when employing vacuum on both sides of the membrane, VEDCMD is expected to be more popular in practice and will be the focus of this study. To achieve the overall objective, three sub-objectives were addressed. First, the dominant factors attributing to higher water flux in VEDCMD were evaluated theoretically. Second, the magnitude of air pressure inside the membrane pores in VEDCMD was quantified. Third, membrane compaction was measured and the effect of membrane compaction on water flux was evaluated. This study was designed to improve the understanding of the mass transfer mechanisms in VEDCMD, to facilitate the application of the mass transfer models for flux prediction in VEDCMD, and to promote its applications in low fouling and scaling MD applications.

3.2. Materials and methods

3.2.1. Experimental setup

Three DCMD configurations were evaluated: 1) traditional DCMD without hydraulic pressures or vacuums employed; 2) VEDCMD with vacuums employed on the distillate side; and 3) pressure-enhanced DCMD (PEDCMD) with hydraulic pressures employed on the feed side. The PEDCMD configuration was used for comparative purposes by creating the same pressure gradient as VEDCMD, because other factors besides pressure gradient may affect water flux (Section 3.1.2). A bench-scale system

with a modified acrylic SEPA-CF membrane cell (Osmonics, Minnetonka, MN) was used to study these configurations. DCMD and PEDCMD used the same setup (Fig. 3.1a) with a needle valve at the outlets of both the feed and distillate sides to adjust the pressure inside the membrane module. In VEDCMD (Fig. 3.1b), the distillate-side pump was located on the outlet of the membrane module to pull water from the module (rather than pushing into the module as is the case in DCMD and PEDCMD), creating a vacuum on the distillate side. The pressures on the feed and distillate sides were controlled at 20/20 (feed/distillate) kPa in DCMD; 60/20, 80/20, and 100/20 kPa in PEDCMD; and 20/-20, 20/-40, and 20/-60 kPa in VEDCMD. All pressures in the current study were reported as gauge pressures. All tests were performed using the same feed temperature (40 ^{o}C), distillate temperature (20 ^{o}C), and fluid flow rates (1 L/min) on both the feed and distillate sides. A 3.5% NaCl solution was used as the feed solution and double-distilled water was used on the distillate side; the feed solution and distillate-side water were re-circulated counter-currently on their respective sides of the membrane. As water evaporated through the membrane, excess water from the distillate reservoir overflowed into a beaker on an analytical balance. The overflow rate was used to calculate the water flux. The test was stopped when the flux was stable for 30 min. To create turbulent flow and reduce temperature polarization, spacers were placed in the flow channels on both the feed and distillate sides. Temperatures, pressures, and dissolved oxygen (DO) were monitored using dual-channel digital thermometers, pressure gauges, and DO meters at the inlet and outlet of the membrane cell. Average DO values at the inlet and outlet were calculated and used to investigate oxygen (i.e., air) transport across the membrane.

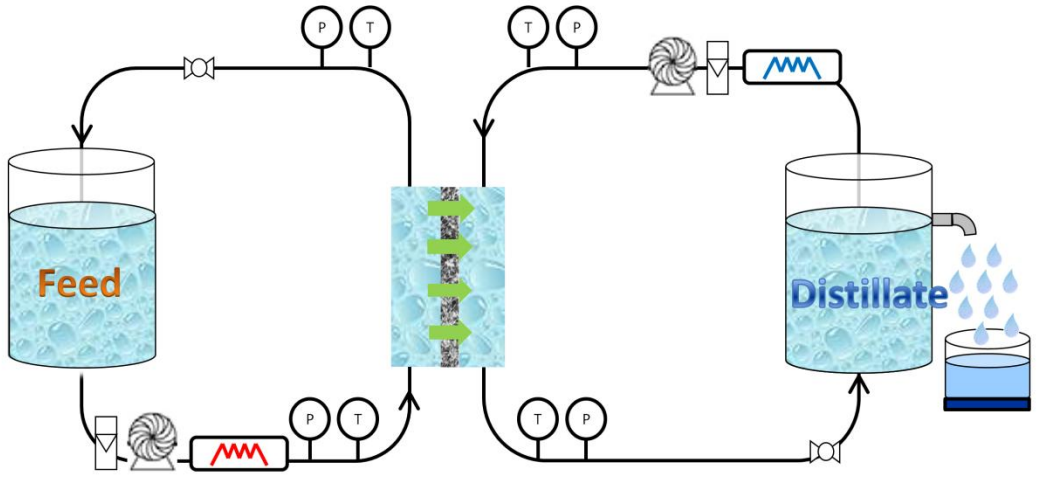

(a)

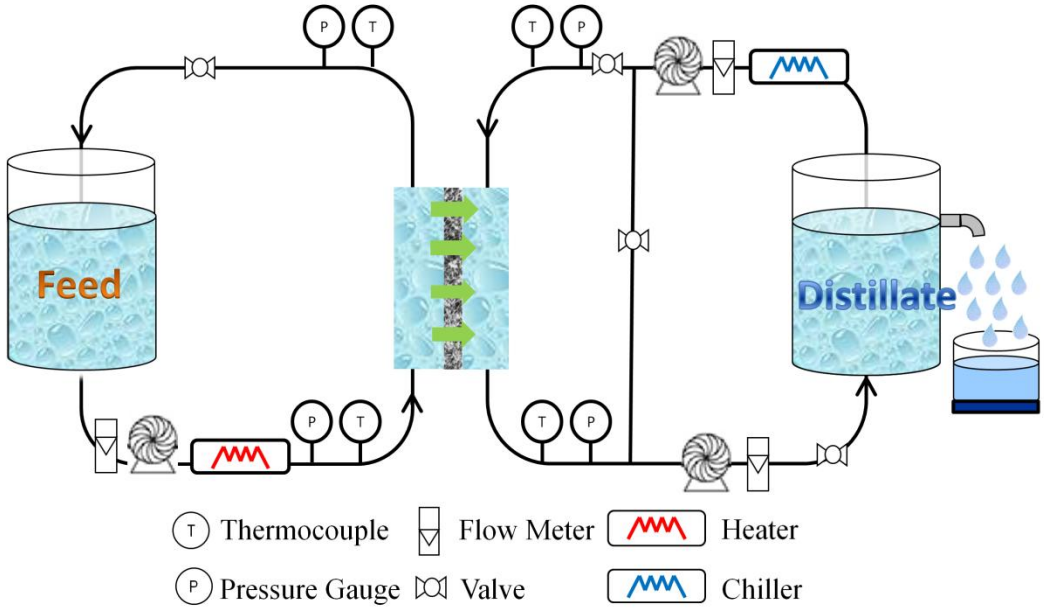

(b)

Figure 3.1 Schematic drawings of the bench-scale MD system configurations for (a) DCMD and PEDCMD and (b) VEDCMD.

3.2.2. Membrane characterization

A single-layer flat-sheet polytetrafluoroethylene membrane was used in this investigation. A new membrane coupon was used for each test. Membrane properties before and after testing in DCMD, PEDCMD, and VEDCMD were measured or calculated as described below.

Membrane thickness measurement

Membrane thickness (δ) was measured from scanning electron micrographs of membrane cross-sections. Before the measurement, the membranes were frozen in liquid nitrogen and cut with a blade. The thickness of each membrane was measured on three different sections and the average thickness was calculated.

Porosity and tortuosity measurements

Membrane porosity (ε) was determined by [21]:

$$\varepsilon = 1 - \frac{m}{\rho_p \times A \times \delta} \tag{15}$$

where m and A are the mass and surface area of the membrane sample and were assumed constant before and after flux testing; ρ_p is the reported density of the polymer material (2.2 g/cm^3 [22, 23]). Although additives may be included during the membrane manufacturing process which could cause ρ_p to be different from 2.2 g/cm^3, the effects were assumed negligible due to the very small amounts[24]. Energy dispersive spectrometry surface analysis (0.3-0.5 wt% detection limit) on the membrane surface revealed only carbon and fluorine [25]. Furthermore, Zhang et al. [21] used the midpoint

of the reported polymer densities in their porosity calculation and found an error less than 3%. Membrane tortuosity (τ) was calculated as [26, 27]:

$$\tau = \frac{(2-\varepsilon)^2}{\varepsilon} \tag{16}$$

Average pore size determination

The average pore size of the membrane (d; equals twice of the pore radius, r) was determined by the gas permeation test with compressed air [28, 29]. The permeation flux of air through the dried membrane was measured at room temperature using transmembrane pressures from 10 to 100 kPa. Pore diameter (d) was then calculated as:

$$d = 2r = 2 \times \left(\frac{8}{3}\left(\frac{B_o}{K}\right)\left(\frac{2RT}{\pi M_i}\right)^{0.5}\right) \tag{3}$$

where B_o is the geometric factor of the membrane; K is the permeability coefficient; and M_j is the molecular weight of air [30].

3.2.3. Flux prediction using mass transfer models

In DCMD, viscous flow where the air and vapor mixture behaves as a continuous fluid [31] can be neglected because no pressure gradient exists [32]. Because of this, both the Schofield model (Fig. 3.2a) and the simplified dusty-gas model (surface diffusion neglected; Fig. 3.2b) reach the same thermal circuit. In PEDCMD and VEDCMD, viscous flow must be included because a pressure gradient exists. Therefore, both the simplified dusty-gas model and the Schofield model are reasonable for mass transfer modeling. The fluxes attributed to Knudsen diffusion (N_k) were determined by [3]:

$$N_k = \frac{2}{3}\frac{r\varepsilon}{\tau\delta}\left(\frac{8M}{\pi RT_m}\right)^{0.5}\Delta P_i \quad (4)$$

where M is the vapor molecular weight (18 g/mol); R is the universal gas constant; T_m is the average temperature of the membrane surfaces on the feed (T_{mf}) and distillate (T_{md}) sides, respectively; and ΔP_i is the vapor pressure gradient across the membrane. P_i at a certain temperature (T) and salinity was determined using the Antoine equation [16, 17]:

$$P_i = \exp\left(23.328 - \frac{3841}{T-45}\right)(1 - x_{NaCl})(1 - 0.5x_{NaCl} - 10x_{NaCl}^2) \quad (5)$$

where x_{NaCl} is the molar fraction of NaCl inside the solution. T_{mf} was determined by [16, 17, 33]:

$$T_{mf} = T_f - \frac{Q}{h_f} \quad (6)$$

where T_f is the bulk temperature of the feed solution; h_f is the heat transfer coefficient in the boundary layer on the feed side; and Q is the total heat input in the system, which was determined by:

$$Q = C_p\dot{m}(T_{dout} - T_{din}) \quad (7)$$

where C_p and $\dot{m}$ are the heat capacity and water flow rate of the distillate-side of the membrane, respectively; and T_{dout} and T_{din} are the temperatures on the distillate-side temperatures at the outlet and inlet of the membrane module, respectively. T_{md} was determined by [16, 17, 33]:

$$T_{md} = T_d + \frac{Q}{h_f} \quad (8)$$

where T_d is the bulk water temperature on the distillate-side and h_d is the heat transfer coefficient in the boundary layer on the distillate side. The heat transfer coefficient (h) was determined by:

$$h = \frac{Nuk_f}{d_h} \tag{9}$$

where k_f is the thermal conductivity of the fluid; d_h is the hydraulic diameter of the flow channel; and Nu is the Nusselt number. Nu for a spacer-filled channel was determined by [34]:

$$Nu = 0.664k_{dc}\,\mathrm{Re}^{0.5}\,\mathrm{Pr}^{0.33}\left(\frac{2d_h}{l_m}\right)^{0.5} \tag{10}$$

where Re is the Reynolds number; P_r is the Prandtl number; l_m is the mesh size of the spacer; and k_{dc} was determined by [34, 35]:

$$k_{dc} = 1.654\left(\frac{d_f}{H}\right)^{-0.039}\varepsilon_s^{0.75}\left(\sin\frac{\theta_s}{2}\right)^{0.086} \tag{11}$$

where d_f is the spacer filament size; H is the channel height; ε_s is the spacer porosity; and θ_s is the hydrodynamic angle of the spacer, which is the angle formed by the grids of the spacer.

The flux attributed to molecular diffusion (N_m) was determined by [3]:

$$N_m = \frac{\varepsilon}{\tau\delta}\frac{P_{pore}D}{RT_m}\frac{1}{\left|P_{air}\right|_{\ln}}\Delta P_i \tag{12}$$

where P_{air} is the air pressure inside the membrane pores; P_{pore} is the membrane pore pressure, which equals the sum of P_{air} and P_i; and D is the diffusion coefficient. $P_{pore}D$ was calculated as:

$$P_{pore}D = 1.895 \times 10^{-8} \times T_m^{2.072} \quad \text{[16, 36]}$$

(13)

The flux attributed to viscous flow (N_v) was determined by [3]:

$$N_i^V = \frac{P_i}{8RT_m\mu}\frac{r^2\varepsilon}{\tau\delta}\Delta P \quad (14)$$

where μ is the vapor dynamic viscosity and ΔP is the pressure gradient across the membrane.

According to the structure of the thermal circuits (Fig. 3.2), the overall flux (N) for the dusty-gas model (without surface diffusion) is [31]:

$$N = N_v + \frac{N_k N_m}{N_k + N_m} \quad (15)$$

and the overall flux for the Schofield model is[31]:

$$\frac{1}{N} = \frac{1}{N_k + N_v} + \frac{1}{N_m} \quad (16)$$

As can be seen, experimental conditions, feed water chemistry, and membrane properties will affect water flux. However, membrane compaction during the DCMD tests can influence pore size, porosity, tortuosity, and thickness of the membrane. Eqs. 1 and 2 suggest that membrane porosity and tortuosity in the mass transfer modeling can both be replaced by membrane thickness. Membrane pore size was also expressed as a function of thickness through the following steps:

First, membrane porosity was expressed as [19]:

$$\varepsilon = N_{pore}\frac{\pi r^2 \tau}{A} \quad (17)$$

where N_{pore} is the membrane pore number and was assumed constant. For an unused membrane, the above equation was also expressed as [19]:

$$\varepsilon_o = N_{pore}\frac{\pi r_o^2 \tau_o}{A} \tag{18}$$

where ε_o, r_o, and τ_o are the porosity, pore radius, and tortuosity of an unused membrane, respectively, which are constant and can be characterized using Eqs. 1 and 2 and the gas permeation method. Combining Eqs. 3 and 4 gives:

$$r = r_o\sqrt{\frac{\varepsilon\tau_o}{\varepsilon_o\tau}} \tag{19}$$

Second, by combining Eqs. 1, 2 and 19, *r* was expressed as:

$$r = r_o\left(\frac{\rho_p A\delta - m}{\rho_p A\delta + m}\right)\sqrt{\frac{\tau_o}{\varepsilon_o}} \tag{20}$$

In this way, only membrane thickness is needed for flux prediction in the mass transfer models and thickness can be easily measured if membrane compaction occurred during the test.

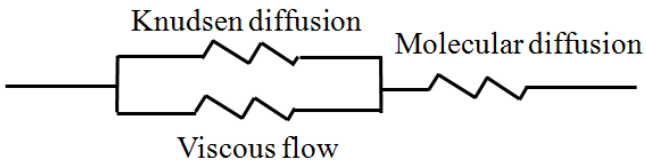

(a)

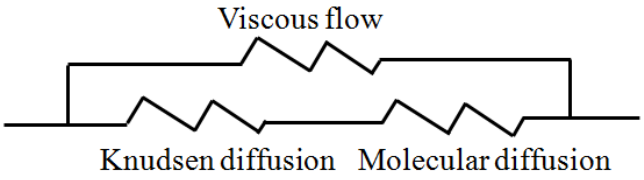

(b)

Figure 3.2 Thermal circuits of (a) the simplified dusty-gas model and (b) the Schofield model.

3.3. Results and discussion

3.3.1. Flux test results

Based on the results of flux testing for DCMD, PEDCMD, and VEDCMD (Table 3.1), two observations can be made. First, DCMD and PEDCMD had similar fluxes (12-13 L/m^2-hr) despite the ΔP that exists in PEDCMD. Second, VEDCMD had higher fluxes (16-21 L/m^2-hr) than PEDCMD (12-13 L/m^2-hr) although the same ΔP of 40, 60, and 80 kPa were used in both. Similar phenomena were also reported by Cath et al. [12]. The different flux results in the presence of the same ΔP suggested that the enhanced flux in VEDCMD could not simply be attributed to pressure gradient as will be discussed in the following sections.

Table 3.1 Flux test results for DCMD, PEDCMD, and VEDCMD (T_f: 40 ^{o}C, T_d: 20 ^{o}C, flow rate: 1 L/min).

Configuration	Feed/distillate pressure (kPa)	Pressure gradient (kPa)	Flux (L/m^2 h)
DCMD	20/20	0	12±0.63
PEDCMD	60/20	40	12±1.1
	80/20	60	12±1.1
	100/20	80	13±1.5
VEDCMD	20/-20	40	16±0.50
	20/-40	60	17±0.48
	20/-60	80	21±0.66

3.3.2. Membrane characterization results

Membrane properties before and after flux testing are given in Fig. 3.3. The unused membrane has a pore size of 0.18 μm, porosity of 80%, and thickness of 67 μm. By comparing the thickness data for the unused membrane with the membranes tested in VEDCMD, it can be seen that slight or no thickness reduction (thus membrane compaction) occurred in VEDCMD, which is consistent with what has been reported in the literature [11-13], where no compaction occurred regardless of which side (feed or distillate) the vacuum was employed on. Porosities and average pore sizes (determined from the gas permeation test) of the membranes after testing in VEDCMD were all comparable with the unused membrane. This was reasonable since minimal membrane compaction occurred in VEDCMD.

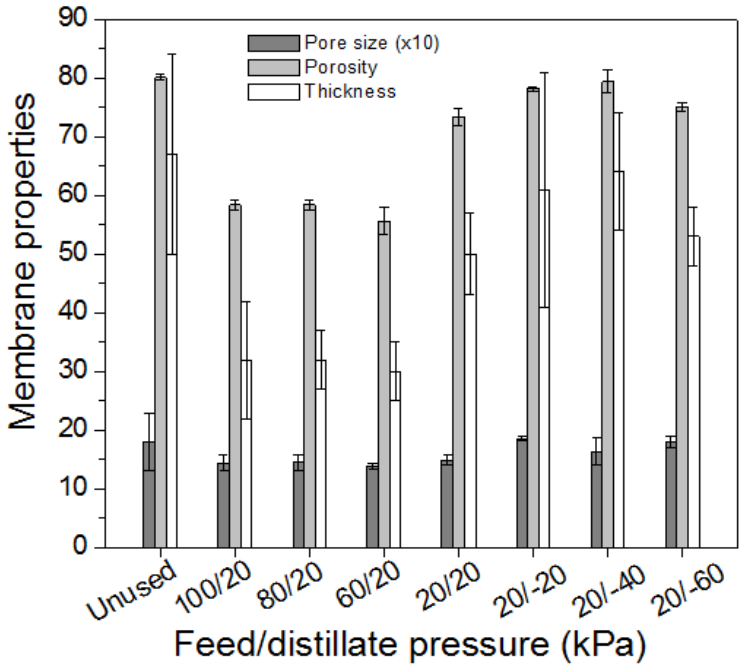

Figure 3.3 Membrane thicknesses, porosities, and pore sizes before and after testing in DCMD, PEDCMD, and VEDCMD.

By comparing the thickness data for the unused membrane with the membranes tested in DCMD and PEDCMD, respectively, a 25% thickness reduction (thus membrane compaction) was observed in DCMD and nearly 55% in PEDCMD with the feed-side pressure up to 100 kPa. For comparison, Zhang et al. [19] reported 10 to 33% thickness reductions when equal pressures on both membrane surfaces were employed (with zero ΔP, similar to DCMD) from 10 to 70 kPa. Lawson et al. [37] reported 13 to 20% membrane thickness reductions for different membranes when the upper membrane surface was pressurized to 35 kPa (similar to PEDCMD with a ΔP of 35 kPa). According to Eq. 1, the 25% thickness reduction in DCMD resulted in an 8% decrease in membrane porosity and the 55% thickness reduction in PEDCMD resulted in a 30% decrease in membrane porosity for this membrane. For comparison, Zhang et al. [19] reported nearly

a 30% porosity reduction with a 33% reduction in thickness. The decrease of porosity due to membrane compaction was also reported by Lawson et al. [20]. Similar to porosity, the average pore sizes of the membranes tested in DCMD and PEDCMD were expected to be smaller than the average pore size of the unused membrane (Eq. 5) due to membrane compaction; similar phenomena were observed for the measured average pore sizes through the gas permeation test. Based on the measured membrane properties caused by membrane compaction alone (Fig. 3.3), the DCMD flux was expected to be close to the VEDCMD flux and different from the PEDCMD flux, which was not what was observed experimentally (Table 3.1). Thus, it is likely that other factors besides membrane compaction alone influenced water flux. To identify these factors, the mass transfer models were studied and the effects of each variable on water flux were investigated as described in Section 3.3.3.

3.3.3. Theoretical identification of factors increasing fluxes in VEDCMD

According to the mass transfer mechanisms (Eqs. 7 through 9), factors that may affect membrane flux include temperature, feed concentration, fluid flow rate, ΔP, P_{air}, and membrane properties (which may be altered by membrane compaction). Because DCMD, PEDCMD, and VEDCMD were all tested under the same experimental conditions except the liquid pressures on the feed and distillate sides, P_{air}, the factor in addition to ΔP and any membrane property that changed due to membrane compaction, is the only factor that could affect water flux. The predicted variation of water flux as a function of ΔP (Fig. 3.4a) using the Schofield model and the simplified dusty-gas model both suggested that ΔP should have minimal effect on water flux, despite operating in

either PEDCMD or VEDCMD. As ΔP is the driving force for viscous flow, both the Schofield model and the simplified dusty-gas model had nearly the same predicted fluxes (results not given), thus only the Schofield model was used later.

According to Section 3.2.3, the predicted variation of water flux as a function of membrane thickness is given in Fig. 3.4b. Over the range shown, the water flux remained constant during the intial stages of membrane compaction (50-67 μm), until membrane thickness was reduced to a certain point (~50 μm), where the flux was predicted to drop significantly. The constant water flux at the initial stages of membrane compaction may be due to the fact that although the gas diffusion path was reduced, membrane porosity (Eq. 1) and average pore size (Eq. 5) were also reduced. Furthermore, the conductive heat loss of the membrane increased. Thus, the overall flux remained unchanged.

Because greater membrane compaction occurred in PEDCMD and DCMD than VEDCMD (Fig. 3.3), and the effect of ΔP on water flux was negligible, based on only membrane compaction and ΔP, VEDCMD was expected to have higher water fluxes. This was already consistent with the flux test results. Thus the effect of P_{air} on water flux may be insignificant at this stage of membrane compaction. However, the prediction of water flux as a function of P_{air} (Fig. 3.4c) suggested that the water flux decreased significantly from 20 to 8 L/m^2 h when P_{air} increased from -100 to 100 kPa. Thus P_{air} was thought to significantly influence water flux.

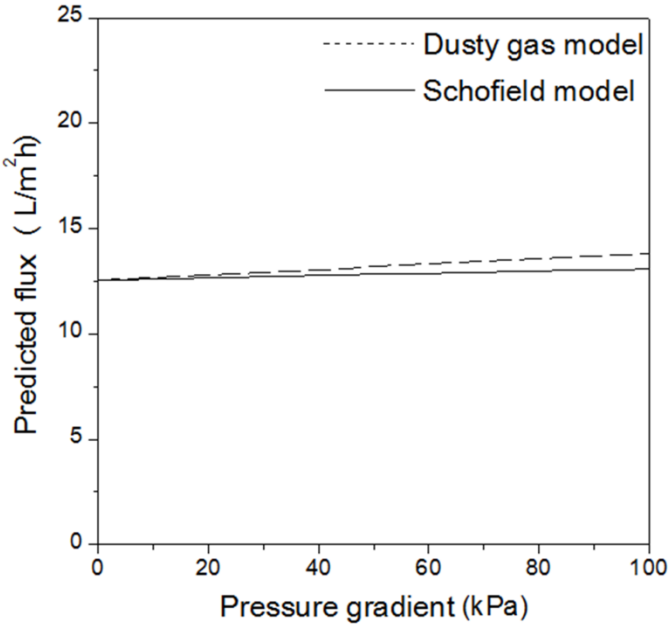
Dusty gas model
Schofield model
Predicted flux (L/m²h)
Pressure gradient (kPa)
0
5
10
15
20
25
0
20
40
60
80
100

(a)

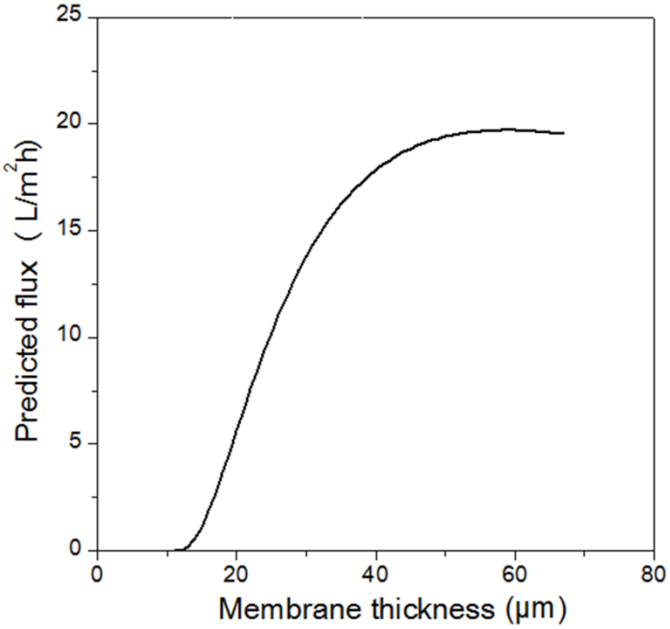
Predicted flux (L/m²h)
Membrane thickness (μm)
0
5
10
15
20
25
0
20
40
60
80

(b)

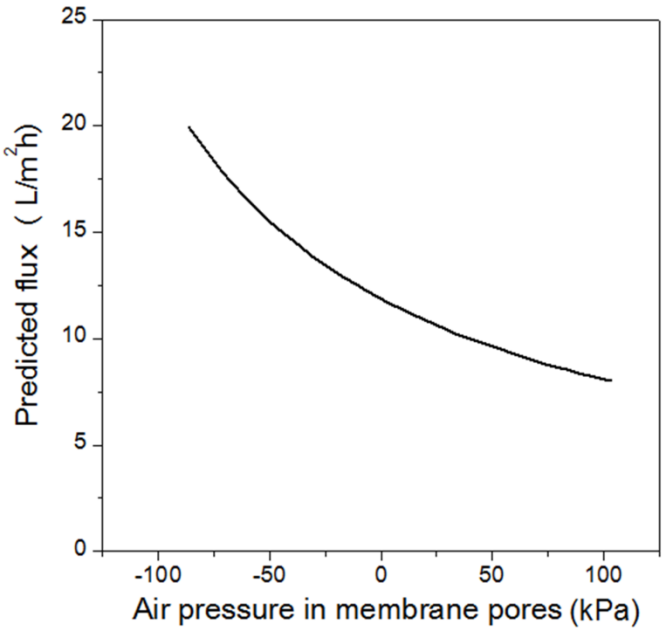

(c)

Figure 3.4 Predicted water flux as a function of: (a) ΔP (assumptions: constant thickness and P_{air}); (b) membrane thickness (assumptions: no ΔP; constant P_{air}); (c) P_{air} (assumptions: no ΔP; constant membrane thickness) when operated at T_f of 40°C, T_d of 20°C, and $\dot{m}$ of 1kg/min on both the feed and distillate sides.

3.3.4. Evaluation of reasonable P_{air} in DCMD, PEDCMD, and VEDCMD

Since P_{air} cannot be measured directly, the suggested magnitudes of P_{air} in research literature were used. In addition, the force balance at the membrane pore surface was also analyzed to estimate P_{air}.

Estimation of P_{air} using the ideal gas law assumption

Zhang et al. [19] used the ideal gas law to calculate P_{pore} (sum of P_{air} and P_i) by assuming that the air inside the membrane pores was stagnant. Because the DCMD,

PEDCMD, and VEDCMD configurations used in the current study were different from that reported in the literature [19], where equal magnitudes of hydraulic pressures were employed on both the feed and distillate sides of the membrane, the stagnant air assumption for the ideal gas law may not hold. To verify this, the DO concentrations of the feed and distillate streams were monitored (Fig. 3.5). The DO concentrations in DCMD and PEDCMD were relatively constant and at the same values over the investigated time period, but significant decreases were measured in VEDCMD on both the feed and distillate sides of the membrane. Because the vacuum pump was located at the outlet of the distillate side in VEDCMD to create a vacuum, it was likely that the pump was degassing the liquid and pulling air from the feed stream through the membrane and into the distillate stream. The accumulation of air bubbles observed in the distillate loop in VEDCMD but not in DCMD or PEDCMD also supported this. Therefore, the ideal gas law appears valid for estimating P_{air} for DCMD and PEDCMD, but not for VEDCMD. Modeled fluxes for DCMD and PEDCMD using this assumption are given in Fig. 3.6. Experimental data are for ΔP of 60 kPa. Comparing the tested water fluxes in PEDCMD to the predicted water fluxes at a thickness near 30 μm (membrane thickness after the PEDCMD test; Fig. 3.3), the flux predicted by the model had an error of approximately -44%. Comparing the tested water flux in DCMD to the predicted water flux at a thickness of 50 μm (membrane thickness after the DCMD test; Fig. 3.3), the flux predicted by the model had an error of 29%. In addition, the model predicted that fluxes in PEDCMD (at a thickness near 30 μm) were much lower than the flux in DCMD (at the thickness of 50 μm), which was not what were observed experimentally

(Table 3.1). Therefore, it may not be proper to use the ideal gas law to estimate P_{air} in DCMD or PEDCMD.

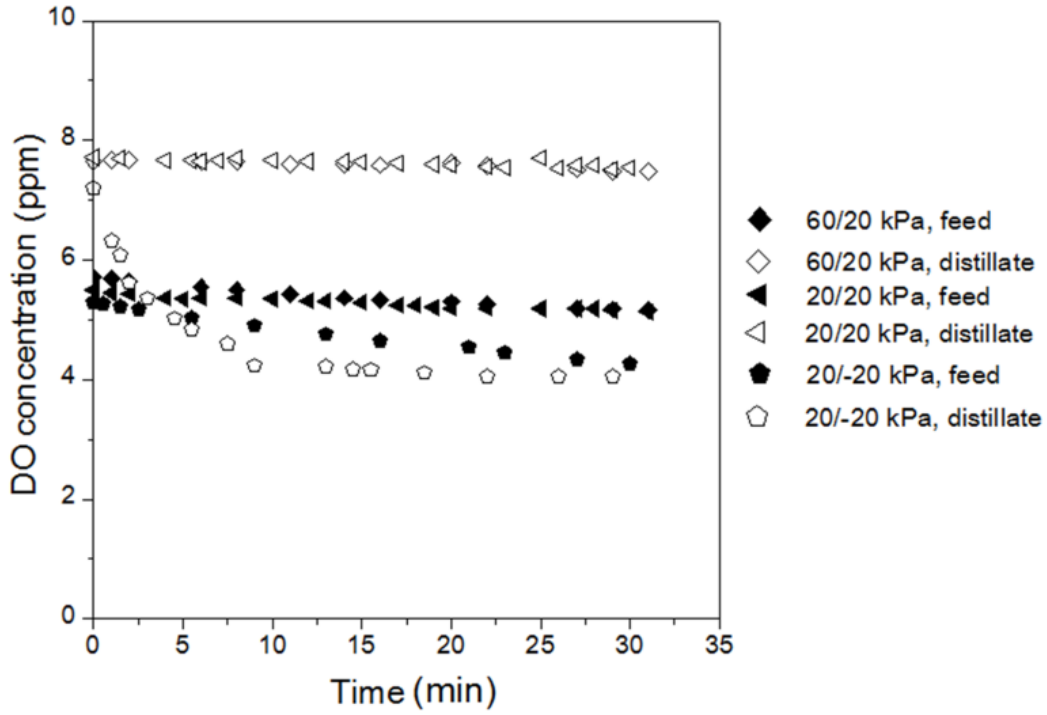

Figure 3.5 Dissolved oxygen concentration inside the feed and distillate streams in DCMD, PEDCMD, and VEDCMD.

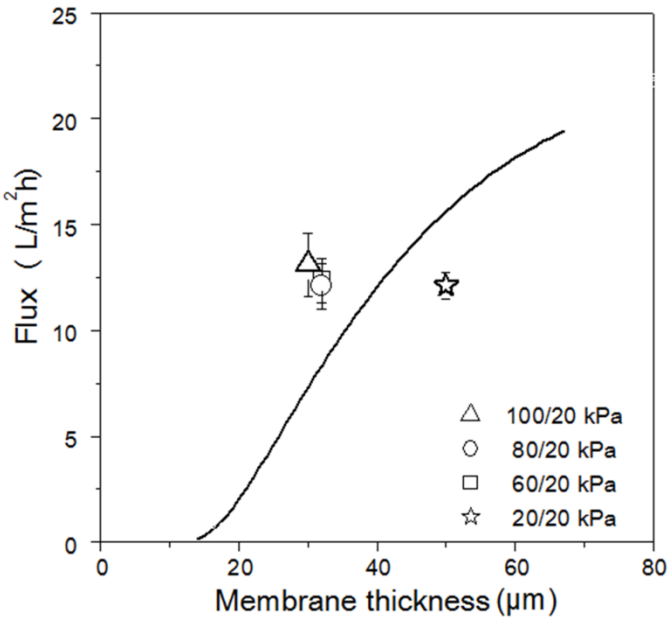

Figure 3.6 Tested and modeled water fluxes as a function of membrane thickness using the ideal gas law assumption (line: modeled fluxes; symbol: tested fluxes).

Estimation of P_{air} using force balance analysis

Force balance analysis at the pore surface

At the steady state of the MD test, both sides of the liquid-gas interface at the pore entrance must satisfy the principles of conservation of mass, momentum, and energy. Taking the liquid-gas interface as the control volume and assuming it was too thin to accumulate mass within it, conservation of mass for this control volume requires [38]:

$$\rho_l (w_{l,n} - \frac{dZ_i}{dt}) = \rho_v (w_{v,n} - \frac{dZ_i}{dt}) \tag{17}$$

where ρ_l and ρ_v are the liquid and vapor densities, respectively; $\omega_{l,n}$, $\omega_{v,n}$, and dZ_i/dt are the velocities of the liquid, vapor, and the liquid-gas interface at the normal direction,

respectively. Including the effects of hydraulic pressures and surface tension forces, the force and momentum balance normal to the interface requires [38]:

$$P_{fluid} - P_{pore} = \sigma(\frac{1}{R_1} + \frac{1}{R_2}) + \rho_v(w_{v,n} - \frac{dZ_i}{dt})w_{v,n} - \rho_l(w_{l,n} - \frac{dZ_i}{dt})w_{l,n} \quad (18)$$

where P_{fluid} is the hydraulic pressure of the liquid stream (P_f was used at the feed side and P_d at the distillate side); σ is the surface tension between the liquid and gas at the pore entrance; and R_1 and R_2 are the curvature surface radius on both the liquid and gas sides, respectively. Because the motion of the interface was limited by the heat transfer to it, the interface motion was relatively slow and the liquid and vapor momentum terms on the right side of Eq. 19 were neglected [38]. Therefore, Eq. 19 was simplified to the Young-Laplace equation [37, 38]:

$$P_{fluid} - P_{pore} = \sigma(\frac{1}{R_1} + \frac{1}{R_2}) \quad (20)$$

For a water drop on a flat membrane surface, Eq. 20 was converted to [38, 39]:

$$P_{fluid} - P_{pore} = \frac{2\sigma\cos\theta}{r} \quad (21)$$

where θ is the angle formed among liquid, membrane material, and gas inside the membrane pores under the applied hydraulic pressure (θ_f was used at the feed side and θ_d at the distillate side). If the θ values were known, P_{pore} (sum of P_{air} and P_i) could be calculated, thus P_{air} (P_i can be calculated using Eq. 3).

To estimate θ at steady-state for each MD test, the movement of air inside the membrane pores and the structure of the liquid-gas interface will be discussed. In DCMD, membrane compaction was measured, leading to a P_{pore} (estimated using the

ideal gas law) greater than P_f and P_d (*20* kPa). Thus the liquid-gas interface on the feed and distillate sides may enter into the respective liquid stream. The convexed interface was then flattened by the flowing liquid by taking away the air portion inside the liquid stream until θ (θ_f and θ_d) reached nearly 90^o (Fig. 3.7a), where P_{pore} equals P_f and P_d (Eq. 20). PEDCMD may have followed the same process as DCMD until steady-state was reached at the distillate side, where P_{pore} equaled P_d and θ_d reaches nearly 90^o (Fig. 3.7b). To maintain equilibrium at the feed side, the feed water may have infiltrated into the membrane pores (since $P_f > P_d$ and $P_d = P_{pore}$), leading to θ_f less than 90^o (Fig. 3.7b). In VEDCMD, the air inside membrane pores was observed to bubble into the distillate-side stream, thus decreasing P_{pore}. Steady-state conditions at the liquid-gas interface on the distillate side may have been reached when P_{pore} decreased to P_d, and θ_d equaled 90^o (Fig. 3.7b). Similar to PEDCMD, water in the feed-side stream may have infiltrated into the pores to maintain equilibrium at the feed side (since $P_f > P_d$ and $P_d = P_{pore}$). Thus, θ_f may have been less than 90^o at steady-state on the feed side (Fig. 3.7b). Overall, although different dynamic processes were present in DCMD, PEDCMD, and VEDCMD, the same conclusion ($P_{pore} = P_d$) was reached. Zhang et al. [13] used the same assumption in their VEDCMD system assuming that the air inside the membrane pores bubbled out to the distillate side until the pressure inside membrane pores was equal to the pressure on the distillate side.

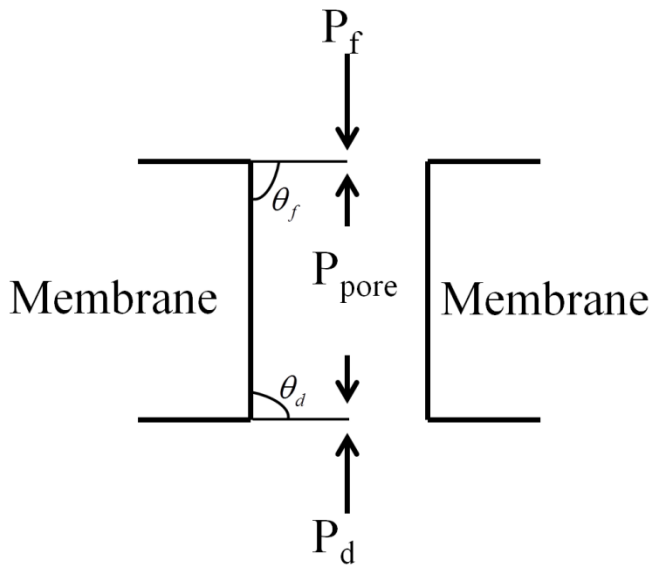

(a)

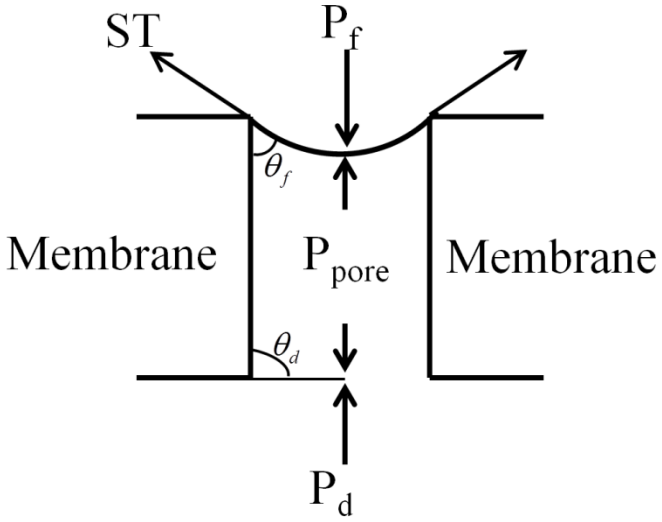

(b)

Figure 3.7 Force balance at the liquid-gas interface in: (a) DCMD; (b) PEDCMD and VEDCMD (ST: surface tension).

Estimation of P_{air} using the $P_{pore} = P_d$ assumption

Using the assumption that P_{pore} equaled P_d, the ΔP caused by a vacuum or positive pressure could be differentiated and much higher fluxes were predicted in VEDCMD than in PEDCMD over the investigated thickness range (Fig. 3.8). Comparing the measured water fluxes in PEDCMD to the predicted water fluxes at a thickness near 30 μm, it was seen that the Schofield model gave an excellent fit for water flux in PEDCMD. However, the predicted water fluxes in VEDCMD at thicknesses ranging from 55 to 65 μm (membrane thickness after the VEDCMD test; Fig. 3.3) were all overestimated compared to the measured water fluxes with errors ranging from 40 to 70%. Therefore, it was likely that the actual P_{air} was greater than P_d which reduced the predicted water flux in VEDCMD. The reason the P_{pore} equal to P_d assumption did a poor job of predicting VEDCMD flux may be because of an unstable liquid-gas interface in Fig. 3.7. The decreasing DO on both the feed and distillate sides of the system (Fig. 3.5) and the accumulation of air bubbles in the distillate loop suggested that air may have passed through the membrane continuously at the steady-state and disturbed the liquid-gas interface. A pressure gradient was likely present inside the membrane pores under VEDCMD conditions. Thus, P_{pore} was more likely equal to the average pressure of the feed and distillate-side pressures ($P_{pore} = (P_f+P_d)/2$). To verify this, the estimated P_{pore} was incorporated into the Schofield model to predict water flux of VEDCMD (Section 3.3.4).

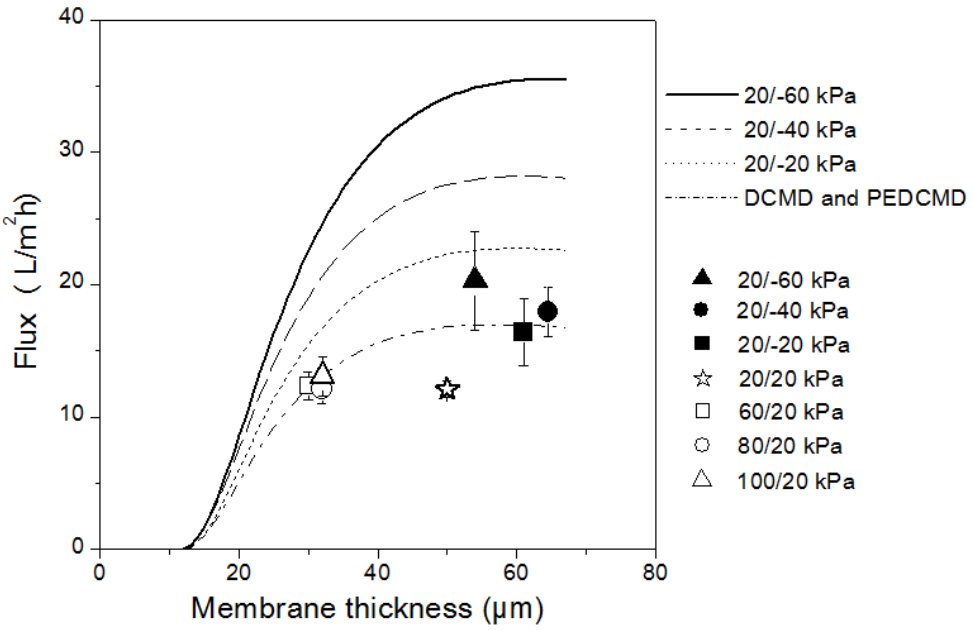

Figure 3.8 Tested and modeled water fluxes as a function of membrane thickness using $P_{pore} = P_d$ assumption (line: modeled fluxes; symbol: tested fluxes).

Using pressure gradient assumption to estimate P_{air} in VEDCMD

Using the assumption that $P_{pore} = (P_f+P_d)/2$, the predicted water fluxes at the membrane thicknesses ranging from 55 to 65 μm were more consistent with the measured water fluxes (Fig. 3.9), leading to errors in flux prediction under 20%. Therefore, once the hydraulic pressures and vacuums on the feed and distillate sides were known, P_{air} in VEDCMD could be identified accordingly.

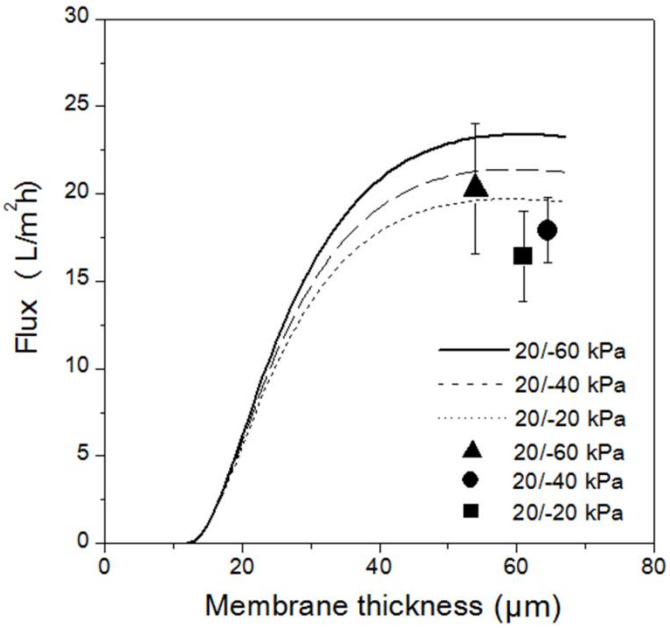

Figure 3.9 Tested and modeled water fluxes as a function of membrane thickness using the pressure gradient assumption for VEDCMD (line: modeled fluxes; symbol: tested fluxes).

3.4. Conclusion

DCMD water fluxes were investigated in three DCMD configurations, namely the traditional DCMD, PEDCMD, and VEDCMD. VEDCMD had much greater fluxes than the other two configurations. Dominant factors contributing to the higher water flux were identified including less membrane compaction and smaller air pressure inside the membrane pores. The pressure gradient was thought to have minimal effect on water flux no matter in PEDCMD or VEDCMD. Membrane compaction was observed in PEDCMD followed by DCMD, while nearly no compaction was observed in VEDCMD. Water flux remained unchanged at initial stage of membrane compaction, then dropped significantly as compaction increased. The magnitude of air pressure inside the membrane pores was

also estimated and was found to equal the hydraulic pressure at the distillate side in DCMD and PEDCMD and an average of the feed and distillate-side hydraulic pressures in VEDCMD.

Acknowledgement

The authors would like to thank the U.S. Department of Energy Geothermal Technologies Program (Grant No. DE-EE00003231) for the financial support of this work.

Nomenclature and Units

A	Membrane surface area (m^2)
d_f	Spacer filament size (m)
d_h	Hydraulic diameter of the flow channel (m)
dz_i/dt	Velocity of the liquid-gas interface at the normal direction (m/s)
h	Heat transfer coefficient (W/m^2 K)
$h_{(f,d)}$	Heat transfer coefficient in boundary layer on the feed or distillate side (W/m^2 K)
H	Channel height (m)
k_{dc}	Parameter in Eq. 17
k_f	Thermal conductivity of the fluid (W/m K)
l_m	Mesh size of the spacer (m)
m	Mass of membrane sample (kg)
M	Molecular weight of vapor (kg/kmol)
N	Overall flux (L/m^2 h)

$N_{(k,m,v)}$ Flux due to Knudsen diffusion, Molecular diffusion, or viscous flow (L/m^2h)

N_{pore} Membrane pore number

Nu Nusselt number

P_{air} Air pressure inside the membrane pores (Pa)

P_{fluid} Hydraulic pressure of the liquid stream (Pa)

P_i Water vapor pressure (Pa)

P_{pore} Sum of P_{air} and P_i (Pa)

Pr Prandtl number

Q_{cond} Membrane conductive heat loss (W/m^2)

r Membrane pore radius (m)

r_o Original membrane pore radius (m)

R Universal gas constant (J/mol K)

Re Reynolds number

$R_{(1,2)}$ Curvature surface radius on the liquid or gas side (m)

$T_{(dout\ ,\ din)}$ Distillate-side temperature at the outlet or inlet of the membrane module (K)

$T_{(f,d)}$ Bulk temperature of the feed or distillate solution (K)

T_m Average membrane temperature (K)

$T_{(mf,\ md)}$ Membrane surface temperature on the feed or distillate side (K)

x_{NaCl} Molar fraction of NaCl inside the solution

δ Membrane thickness (m)

ΔP Pressure gradient (Pa)

ε Membrane porosity

ε_o Original membrane porosity

ε_s Spacer porosity

θ Angle formed among liquid, membrane, and gas inside the membrane pores (^{o})

$_{(f,d)}$ θ at the feed or distillate side (^{o})

θ_s Hydrodynamic angle of the spacer (^{o})

μ Vapor dynamic viscosity (kg/m s)

$\dot{m}$ Fluid flow rate (kg/min)

$\rho_{(l, s, v)}$ Density of liquid, polymer material, and vapor density (kg/m^3)

σ Surface tension between liquid and gas at the pore entrance (N/m)

τ Membrane tortuosity

τ_o Original membrane tortuosity

$\omega_{(l,n, v,n)}$ Velocity of the liquid or vapor at the normal direction of the liquid-vapor interface (m/s)

Reference

[1] L.M. Camacho, L. Dumée, J. Zhang, J. Li, M. Duke, J. Gomez, S. Gray, Review: Advances in Membrane Distillation for Water Desalination and Purification Applications, Water, 5 (2013) 94-196.

[2] A.G. Fane, R.W. Schofield, C.J.D. Fell, The efficient use of energy in membrane distillation, Desalination, 64 (1987) 231-243.

[3] K. W. Lawson, D.R. Lloyd, Review: Membrane distillation, J. Membr. Sci. , 124 (1997) 1-25.

[4] J. Walton, H. Lu, C. Tumer, S. Solis, H. Hein, Solar and waste heat desalination by membrane distillation, in: Desalination and Water Purification Research and Development Program Report No. 81, College of Engineering, University of Texas at El Paso, El Paso, Texas, 2004.
[5] S. Al-Obaidani, E. Curcio, F. Macedonio, G. Di Profio, H. Al-Hinai, E. Drioli, Potential of membrane distillation in seawater desalination: Thermal efficiency, sensitivity study and cost estimation, J. Membr. Sci., 323 (2008) 85-98.
[6] G. Zuo, R. Wang, R. Field, A.G. Fane, Energy efficiency evaluation and economic analyses of direct contact membrane distillation system using Aspen Plus, Desalination, 283 (2011) 237-244.
[7] H. Susanto, Review: Towards practical implementations of membrane distillation, Chem. Eng. Process. , 50 (2011) 139-150.
[8] M. Khayet, Membranes and theoretical modeling of membrane distillation: A review, Adv. Colloid Interface Sci., 164 (2011) 56-88.
[9] J.L. Cartinella, T.Y. Cath, M.T. Flynn, G.C. Miller, K.W. Hunter, A.E. Childress, Removal of natural steroid hormones from wastewater using membrane contactor processes, Environ. Sci. Technol., 40 (2006) 7381-7386.
[10] S. Bonyadi, T.S. Chung, Flux enhancement in membrane distillation by fabrication of dual layer hydrophilic–hydrophobic hollow fiber membranes, J. Membr. Sci., 306 (2007) 134–146.
[11] R.W.Schofield, G. A, Fane,, C.J.D. Fell, Gas and vapour transport through microporous membranes. II. Membrane distillation, Journal of Membrane Science, 53 (1990) 173-185.
[12] T.Y. Cath, V.D. Adams, A.E. Childress, Experimental study of desalination using direct contact membrane distillation: a new approach to flux enhancement, J. Membr.Sci., 228 (2004) 5-16.
[13] J. Zhang, J. D. Li, M. Duke, Z. Xie, S. Gray, Performance of asymmetric hollow fiber membranes in membrane distillation under various configurations and vacuum enhancement, J. Membr.Sci., (2010) 517-528.

[14] R.W. Schofield, G. A, Fane, C.J.D. Fell, Gas and vapour transport through microporous membranes. I. Knudsen-Poiseuille transition, J.Membr.Sci, 53 (1990) 159-171.

[15] S. Adnan, M. Hoang, H. Wang, Z. Xie, Commercial PTFE membranes for membrane distillation application: Effect of microstructure and support material, Desalination 284, (2012) 297-308.

[16] M. Qtaishat, T. Matsuura, B. Kruczek, M. Khayet, Heat and mass transfer analysis in direct contact membrane distillation, Desalination 219, (2008) 272-292.

[17] R.W.Schofield, A.G.Fane, C.J.D.Fell, Heat and mass transfer in membrane distillation, Journal of Membrane Science, 33 (1987) 299-313.

[18] L Martínez-Díez, M.I. Vázquez-González, A method to evaluate coefficients affecting flux in membrane distillation, J. Membr. Sci., 173 (2000) 225–234.

[19] J. Zhang, J. D. Li, S. Gray, Effect of applied pressure on performance of PTFE membrane in DCMD J. Membr. Sci., 369 (2011) 514-525.

[20] K.W. Lawson, M.S. Hall, D.R. Lloyd, Compaction of microporous membranes used in membrane distillation. I. Effect on gas permeability, J. Membr. Sci., 101 (1995) 99-108.

[21] J. Zhang, N. Dow, M. Duke, E. Ostarcevic, J. Li, S. Gray, Identification of material and physical features of membrane distillation membranes for high performance desalination, J. Membr. Sci. , 349 (2010) 295-303.

[22] R. Mishra, S.P. Tripathy, D. Sinha, K.K. Dwivedi, S. Ghosh, D.T. Khathing, M. Muller, D. Fink, W.H. Chung, Optical and electrical properties of some electron and proton irradiated polymers, Nucl. Instrum. Methods Phys. Res., Sect. B 168, (2000) 59-64.

[23] Qing-lin Huang, Chang-fa Xiao, Xiao-yu Hu, X.-f. Li, Study on the effects and properties of hydrophobic poly(tetrafluoroethylene) membrane, Desalination, 277 (2011) 187-192.

[24] M. Mulder, Basic principles of membrane technology, Kluver Academic Publishers, Dordrecht, Netherlands, 1991.

[25] J. A. Ruskowitz, A.E. Childress, Salt-Gradient Solar Pond and Membrane Distillation System for Water Desalination Powered by Renewable Energy, in: Thesis, University of Nevada, Reno, Reno, Nevada, 2012.
[26] V.D. Alves, I.M. Coelhoso, Effect of membrane characteristics on mass and heat transfer in the osmotic evaporation process, J. Membr. Sci., 228 (2004) 159-167.
[27] S. Srisurichan, R. Jiraratananon, A.G. Fane, Mass transfer mechanisms and transport resistances in direct contact membrane distillation process, J. Membr. Sci., 277 (2006) 186-194.
[28] S. Nakao, Review: Determination of pore size and pore size distribution 3. Filtration membranes, J. Membr. Sci., 96 (1994) 131-165.
[29] M. Khayet, T. Matsuura, Determination of surface and bulk pore sizes of flat-sheet and hollow-fiber membranes by atomic force microscopy, gas permeation and solute transport methods, Desalination 158, (2003) 57-64.
[30] H.Yasuda, J.T.Tsai, Pore size of microporous polymer membranes, J. Appl. Polym. Sci., 18 (1974) 805-819.
[31] Z. Ding, R. Ma, A.G. Fane, A new model for mass transfer in direct contact membrane distillation, Desalination 151, (2002) 217-227.
[32] K.W. Lawson, D.R. Lloyd, Membrane Distillation. II. Direct contact MD, J. Membr.Sci. , 120 (1996) 123-133.
[33] J. Phattaranawik, R. Jiraratananon, Direct contact membrane distillation: effect of mass transfer on heat transfer, J. Membr. Sci., 188 (2001) 137-143.
[34] J. Phattaranawik, R. Jiraratananon, A.G. Fane, C. Halim, Mass flux enhancement using spacer filled channels in direct contact membrane distillation, J. Membr. Sci., 187 (2001) 193-201.
[35] A.R.D. Costa, A.G. Fane, D.E. Wiley, Spacer characterization and pressure drop modelling in spacer-filled channels for ultrafiltration, J. Membr. Sci., 87 (1994) 79-98.
[36] J. Phattaranawik, R. Jiraratananon, A.G. Fane, Effect of pore size distribution and air flux on mass transport in direct contact membrane distillation, J. Membr. Sci., 215 (2003) 75-85.

[37] Kevin W. Lawson, Matthew S. Hall, D.R. Lloyd, Compaction of microporous membranes used in membrane distillation. I. Effect on gas permeability, Journal of Membrane Science, 101 (1995) 99-108.
[38] V. P.Carey, Liquid-vapor phase-change phenomena: an introduction to the thermophysics of vaporization and condensation processes in heat transfer equipment second ed., Taylor and Francis Group, LLC, New York, USA, 2008.
[39] P.C. Carman, Flow of Gases Through Porous Media, Butterworth Scientific Publications, London, UK, 1956.

Chapter 4

4 MEMBRANE FOULING AND CLEANING IN DICRECT-CONTACT MEMBRANE DISTILLATION (DCMD)

Abstract

Membrane fouling has been recognized as a main obstacle that impedes the implementation of full-scale direct-contact membrane distillation (DCMD). Typical foulants in DCMD include $CaCO_3$, $CaSO_4$, SiO_2, and NaCl. The $CaCO_3$ scalant was commonly removed with HCl solutions in DCMD but the volatile properties of HCl may increase the distillate conductivity. Thus, membrane cleaning using citric acid and Na_2EDTA solutions were investigated when treating the Walker Lake water, in which $CaCO_3$ was the major scalant. The citric acid solution was found to be able to completely restore membrane performance. The $CaSO_4$ scalant was successfully removed when treating the synthetic calcium sulfate solution using deionized water (DI water), which was different from the typical cleaning solutions reported in the literature. Membrane cleaning specifically focused on SiO_2 removal in DCMD has not been investigated; therefore, five cleaning solutions (DI water and NaOH solutions (62.5, 125, 250 mM at ambient temperature and 125 mM at 40 ^oC)) and a two-stage cleaning process (125 mM NaOH at 40 ^oC followed by 26.8 mM Na_2EDTA at ambient temperature) were tested for remaining SiO_2 when treating the synthetic silica feed solution. It was found that the two-stage cleaning process completely restored membrane performance. The 2% by weight HCl solution was used to remove the scalants (mainly NaCl) when treating the hypersaline solution; however, severe membrane wetting occurred after membrane

cleaning. After membrane drying, the maximum water flux (94%) and the water recovery (90%) were restored.

Keywords: Membrane distillation; Fouling; Membrane cleaning

4.1. Introduction

4.1.1. Membrane distillation

Membrane distillation (MD) is a thermally-driven process that produces potable water via separation through a phase change process. The driving force of MD is the vapor pressure gradient across a membrane that results from the temperature difference across the membrane. The heat required to maintain the temperature of the feed solution (30-90 ^{o}C [1, 2]) can be supplied directly by low-grade heat sources, such as waste industrial heat, solar heating, and low-temperature geothermal water, which has led to an increase in interest in MD in recent years. Of all types of MD, direct-contact MD (DCMD) is the most commonly used configuration in lab-scale research [3]. DCMD was operated under atmospheric pressure with two solutions at different bulk temperatures circulated on either side of a hydrophobic membrane [1, 2]. DCMD membranes are typically made of polyvinylidenefluoride, polypropylene, or polytetrafluoroethylene with pore sizes ranging from 0.2 to 1.0 μm [3-5]. Because the driving force of DCMD did not decrease significantly with increasing feed-water salinity, DCMD has been used to treat various feed water [1, 6-8], and achieves nearly 100% rejection of salt and organic [1, 9, 10]. However, membrane fouling remaining a major obstacle to the implementation of full-scale DCMD [11, 12].

4.1.2. Membrane fouling and cleaning in DCMD

Membrane fouling is defined as the accumulation of foulants (organics, inorganics, and/or microorganisms) at the membrane surface or inside the pores of a membrane [13]. Membrane fouling caused by inorganics is also called membrane scaling [13] and the inorganics are referred to as scales [13, 14] or scalants [14]. Most literature reports concerning membrane fouling deal with pressure-driven membrane processes that are operated under hydraulic pressures using different membranes and feed waters than are used with DCMD. Thus, pressure-driven membrane processes are expected to have different fouling phenomena than DCMD processes. Membrane fouling in DCMD has been observed when treating tap water [15], groundwater [16], reverse osmosis brines [17, 18], and other specialized solutions [19]. Foulants on the membrane surface may alter the membrane's surface properties (e.g., hydrophobicity) and pore structures, hinder water transport to the membrane surface, and add an additional thermal resistance factor that in turn lowers the temperature at the membrane surface [12, 20, 21]. Membrane fouling caused by organics does not lead to significant flux decline in DCMD and organic foulants were found to be loosely packed on the membrane surface [22]. Inorganics, such as iron and manganese, also have minimal effects on water flux [18, 23]. Sparingly soluble salts, such as calcium carbonate ($CaCO_3$), calcium sulfate ($CaSO_4$), and silica (SiO_2) were frequently observed as major scalants leading to flux decline and ultimately lower water recovery [12, 13, 18, 24]. When treating hypersaline solutions, sodium chloride (NaCl) was observed as the major scalant [12].

Calcium carbonate

Although different forms of calcium carbonate ($CaCO_3$) exist in nature, the major scalant in DCMD has been recognized as calcite [25]. Calcite has a compact and hexagonal structure that results in a tendency for the calcite crystals to adhere to surfaces [18], thus it mainly accumulates on the membrane surface rather than penetrating into the membrane pores [20]. Because the solubility of $CaCO_3$ decreases with increasing temperature [18], $CaCO_3$ is also often observed in the feed container and on the connecting tubes that have higher temperatures than the membrane module [18]. The $CaCO_3$ scalant can be alleviated by pretreatment processes such as softening and coagulation [16, 21], or by acidifying the feed solution to a pH near 4 [11, 18, 21]. The pretreatment process require large amounts of chemicals, yet scalants were still observed on the membrane surface after chemical coagulation followed by sand filtration or microfiltration [21]. Although acidification of the feed water limited the formation of $CaCO_3$, membrane scaling caused by other compounds (e.g., silica) may still be observed [20]. To clean the membrane scaled by $CaCO_3$, 2-5 wt.% hydrochloride acid (HCl) solutions have been used in DCMD systems[15, 18, 20, 21], but an increase in the distillate conductivity was observed in some reports due to pore wetting [18] or passing of the volatile HCl to the distillate side [15, 20, 21]. Both acidic solutions and metal chelating agents (e.g., ethylenediaminetetraacetic acid (EDTA) and citric acid) are frequently used for $CaCO_3$ removal in pressure-driven membrane processes [26, 27], but only HCl solutions were used for membrane cleaning in DCMD and no relevant reports investigating these metal chelating agents and DCMD membrane performance are currently available in the literature to the best of the authors' knowledge.

Calcium sulfate

Calcium sulfate ($CaSO_4$) was found to be a more severe scaling problem than $CaCO_3$ in DCMD based on the sharp flux decline when $CaSO_4$ was formed [24]. The major form of $CaSO_4$ scalants has been recognized as gypsum [25], which can have needle-shaped crystal structures [18, 28] and may penetrate into membrane pores after depositing on the membrane surface [20]. The gypsum scalants in the membrane pores may dissolve into the cleaning solution during membrane cleaning, leading to a hydrophilic membrane surface and even passing of the feed solution to the distillate side when performing DCMD tests [20]. Membrane breaks caused by $CaSO_4$ crystals were also observed in some reports [11, 24]. Control of $CaSO_4$ is a major challenge in both pressure-driven membrane processes and MD because the formation of $CaSO_4$ is not pH sensitive and thus cannot be prevented by acidifying the feed solution [28]. Both metal chelating agents [17] and NaCl solutions [29, 30] have been reported to effectively clean membranes scaled by $CaSO_4$ in DCMD. Considering the relatively high solubility (2-2.5 g/L at 25 ^{o}C [31]) of $CaSO_4$, pure water may also serve as an effective and economical cleaning solution.

Silica

Silica (SiO_2) is abundant in natural waters, and membrane scaling has been observed with both high and low silica concentrations of feed solutions. Silica scaling can result in rapid flux decline and may irreversibly deteriorate the membrane material [32, 33]. The types of silica scalants are strongly pH dependent, with colloidal silica (an accumulation of silicic acid) dominating at low pH and silicates (e.g., Mg_2SiO_4, Ca_2SiO_4)

being more prevalent at high pH (> 8) [18, 33]. Silica can also adsorb onto the surface of insoluble metal compounds (e.g., $Mg(OH)_2$, $MgCO_3$) in alkaline conditions and increase the degree of membrane scaling [18]. Aggregates of opaque milky-to-white films were observed for colloidal silica scalants, which may block the mass transfer of water to the membrane surface [33]. Silica scalants showed poor removal through chemical cleaning [32, 34]. In pressure-driven membrane processes, the addition of anti-scalants to inhibit silica scalant formation [32, 33, 35] and the use of pretreatment processes to reduce silica concentrations before the membrane processes [33, 36] have been reported to mitigate the silica scaling phenomenon, but a proper type of anti-scalant or coagulant and an optimal dosage are needed, making the membrane processes difficult to control [32, 35]. Although sonification was successfully used to remove silica scalants from microfiltration membranes [37], increased solute permeation was observed and the effectiveness of sonification was strongly affected by the intensity and direction of the ultrasonic beam [38]. No specific study has been carried out on silica removal in DCMD. Although a HCl solution was used to remove a mixture of calcium scaling and colloidal silica [18], and an EDTA solution was used to remove a mixture of $CaSO_4$ and SiO_2 scalants[17], no full recovery of water flux was obtained in each study after membrane cleaning.

Sodium chloride

Sodium chloride (NaCl) has been reported to cause rapid flux decline when homogeneous precipitation of NaCl crystals on the membrane surface occur [12]. Due to the high solubility of NaCl in water (360 g/L at 25 ^{o}C [39]), precipitation of NaCl only

occurs when the feed solution becomes highly concentrated during a water treatment process or is originally a hypersaline solution. The NaCl scalant in DCMD has been recognized as halite [25], which has a cubic crystal structure. To prevent membrane scaling, crystallizers have been incorporated into the DCMD system to collect the crystals that will otherwise deposit on membrane surface [11, 40]. However, proper operating conditions must be identified to prevent deposition of crystals in the membrane module or connecting tubes instead of the crystallizer [40]. No investigation of chemical cleaning of the NaCl scaled membrane in DCMD is currently available to the authors' knowledge. Although DCMD is believed to be better when treating hypersaline feed waters compared to pressure-driven membrane processes (the driving force of DCMD does not decrease significantly with feed-water salinity [6-8, 41]), the performance of a cleaned MD membrane after treating the hypersaline feed waters has not yet been evaluated.

4.1.3. Objective

Due to the various problems and uncertainties associated with cleaning scaled membranes in DCMD systems, the main objective of this study is to identify effective cleaning solutions for removal of typical scalants ($CaCO_3$, $CaSO_4$, SiO_2, and NaCl) in DCMD. To achieve this, four feed solutions containing different scalants were tested in bench-scale DCMD systems. The membrane performance of each feed solution before and after membrane cleaning was compared to determine the effectiveness of each cleaning solution.

4.2. Materials and methods

4.2.1. Feed solutions

Four feed solutions were investigated in the study: Walker Lake water, calcium sulfate solution, silica solution, and synthetic Great Salt Lake water. The Walker Lake (Nevada, U.S.A) water was collected onsite while the other solutions were synthesized using deionized water (DI water) and reagent grade salts. Compositions of each feed solution are given in Table 1. The calcium sulfate solution was prepared with SO_4 and Ca concentrations four times greater than well water reported by the Eastern Municipal Water District of California, U.S.A. [42] and NaCl was used to adjust the ionic strength of the calcium sulfate solution to be consistent with four times the ionic strength of the well water. The concentration of Si in the silica solution was four times the concentration in the same well water and the ionic strength was adjusted using NaCl and $MgCl_2$ to keep it four times the ionic strength of the well water. The pH of the silica solution was adjusted using the HCl solution (12.1 N). The Great Salt Lake water was synthesized according to the reported ion compositions by Encyclopedia Britannica [43].

Table 4.1 Composition of feed solutions.

	Composition		TDS (g/L)	pH
	Salt	Concentration (g/L)		
Walker Lake* water	Na^+	5.04	16.07	9.4
	K^+	0.270		
	Ca^{2+}	0.0103		
	Mg^{2+}	0.189		
	Cl^-	3.53		
	SO_4^{2-}	3.57		
	alkalinity	3.46		
Well Water	$CaCl_2.2H_2O$	5.12	8.125	6.7
	Na_2SO_4	2.70		
	NaCl	0.270		
Well Water	$Na_2SiO_3.9H_2O$	2.55	13.75	6.0
	$MgCl_2.6H_2O$	3.85		
	NaCl	6.80		
	HCl	0.548		
Great Salt Lake water	NaCl	213	289.1	7.4
	$MgSO_4.7H_2O$	42.1		
	$MgCl_2.6H_2O$	25.4		
	KCl	7.75		
	$NaHCO_3$	0.345		
	$CaCl_2.2H_2O$	0.884		

* cited from [45]

4.2.2. DCMD experiments

A bench-scale DCMD system was used in the study. Vacuum (near -20 kPa as gauge pressure) was introduced to the distillate side of the membrane to expedite membrane scaling when treating the calcium sulfate solution and the silica solution. The system schematics are given in the literature [44]. Four liters of the feed solution was circulated counter-currently at the feed-side membrane surface and four liters of DI water at the distillate-side membrane surface The flow rates of both streams were kept at 1.5 L/min. The feed stream of each Walker Lake, calcium sulfate, and silica solutions was

maintained at 40-45 ^{o}C using a hot bath (Model 280, Precision Scientific, Winchester, VA) and the distillate stream was held at 20-25 ^{o}C using a re-circulating chiller (Model M-33, Thermo-electron, Newington, NH). The Great Salt Lake water was tested at 60 ^{o}C and 40 ^{o}C on the feed and distillate sides of the membrane, respectively, to achieve a temperature difference of 20 ^{o}C across the membrane for all four tests. Temperatures were monitored using dual-channel digital thermometers (DigiSense DualLog R, Cole-Parmer, Vernon Hills, IL) with thermocouples located at the inlets and outlets of the membrane module. The module had an effective membrane surface area of 118 cm^2. As water vapor passed through the membrane from the feed to the distillate, the excess water from the distillate reservoir overflowed into a beaker on an analytical balance and the overflow rate was used to calculate water flux. A conductivity meter (Jenway 4320, Jenway Ltd., UK) was used in the distillate tank to monitor distillate conductivity. Flat-sheet polytetrafluoroethylene membranes from GE Osmonics (Minnetonka, MN) were used in the tests. The membranes are compatible with strong acids and aggressive solutions according to the manufacturer. The scalant analysis on the membrane surface was performed using scanning electron microscopy (SEM; S-3000N, HITACHI, Japan) coupled with energy dispersive spectrometry (EDS; Genesis, EDAX, USA). The OLI Stream Analyzer 9.0 (OLI Systems Inc., Morris Plains, NJ) was used to estimate the salts that may precipitate out of the feed solution during the DCMD test. The aqueous thermodynamic model based on published data and the Helgeson equation of state were used in the analyzer for polynomial fits, which takes into considerations of volume, heat capacity, and temperature and pressure properties of water comparing to the standard-state equation which only includes the temperature and pressure properties [45].

4.2.3. Cleaning experiments

The membrane cleaning experiments were performed after the water flux dropped below 3 L/m^2-hr (more than 75% of flux decline). The cleaning procedure included first circulating 2 L of the cleaning solution on the feed side of the membrane at a flow rate of 2 L/min for 30 min; next, the membrane was flushed using ~10 L of DI water for each Walker Lake, calcium sulfate, and silica solutions, and a 2 hr tap water flushing of the membrane was used for the Great Salt Lake water. Two cleaning solutions were tested to clean the membrane scaled by the Walker Lake water: 1) a citric acid solution (240 mM) and 2) a disodium ethylenediamine tetraacetate solution (Na_2EDTA; 29 mM) combined with 58 mM NaOH. DI water was also tested to clean the membranes scaled by the calcium sulfate solution. The silica scaled membranes were cleaned with DI water, NaOH solutions (62.5, 125, and 250 mM at ambient temperature and 125 mM at 40 ^oC), and a two-stage procedure of NaOH (125 mM at 40 ^oC) followed by an Na_2EDTA solution (26.8 mM combined with 62.3 mM NaOH). A 2 wt.% HCl solution was used to clean the membrane scaled by the Great Salt Lake water. Membrane performance parameters (water flux and batch recovery) were evaluated before and after each cleaning cycle.

4.3. Results and discussions

4.3.1. Walker Lake water

The simulation results using the OLI Stream Analyzer predicted that $CaCO_3$ would become oversaturated first in the feed solution, followed by hydromagnesite ($Mg_5(CO_3)_4(OH)_2 \cdot 4H_2O$), which reached saturation at a water recovery near 90%. The SEM-EDS results further confirmed the elements of the two scalants. Therefore, it is

highly likely that $CaCO_3$ is the major scalant that caused flux decline at the low water recoveries.

Water flux and batch recovery before membrane cleaning are given in Fig.4. 1. The slight differences between the two runs are attributed to slight differences between membrane batches and Walker Lake water batches. Minimal flux decline was observed during the first 10 hours, indicating that little membrane scaling occurred during this period. After 10 hours of operation, gradual flux declines were observed during the following tens of hours until a stable flux of near 2 LMH was reached. It is likely that calcite nucleation occurred near 10 hours of operation, and then the gradual flux decline was due to membrane scaling caused by gradual deposition of the $CaCO_3$ scalant on the membrane surfaces. It was also noted that $CaCO_3$ was prone to precipitate in the feed bulk solution rather than on the membrane surface, a phenomenon observed by others [21]. The sticky property of $CaCO_3$ prevented $CaCO_3$ from moving to the membrane surface, and thus led to a gradual deposition of $CaCO_3$ on the membranes surface rather than the rapid scaling more traditionally observed. This is the likely reason that a gradual flux decline was observed instead of a sharp flux decline. A similar phenomenon has also been observed in the literature [18]. At the end of each test prior to membrane cleaning, a water recovery of near 50% was achieved.

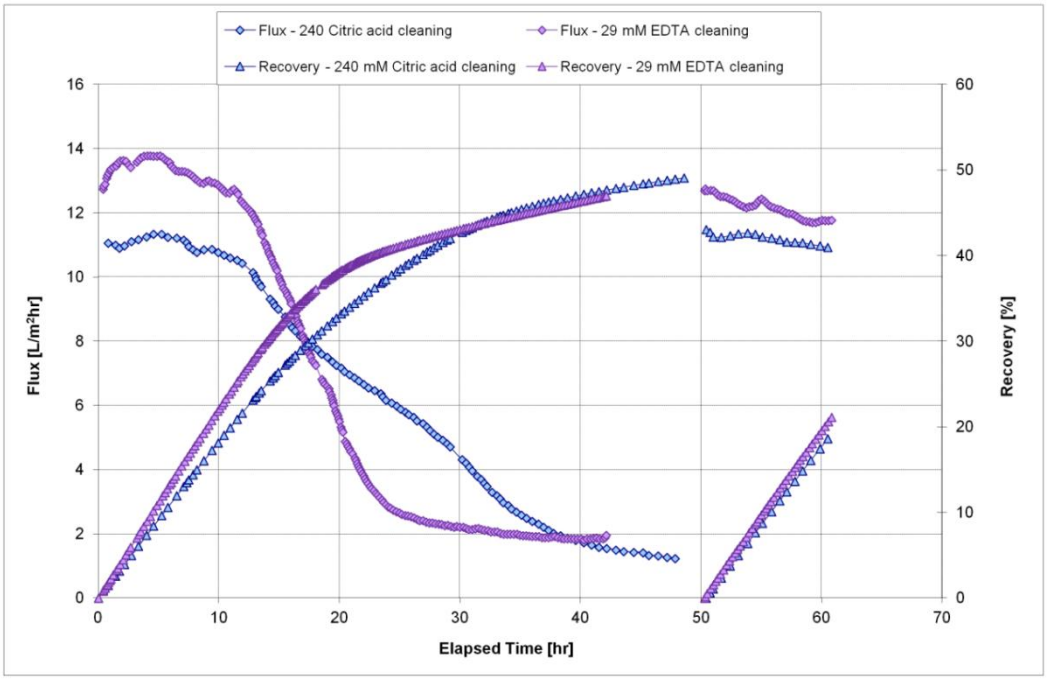

Figure 4.1 Membrane performances before and after membrane cleaning for Walker Lake water.

The maximum water flux was fully restored after the membrane cleaning with the citric acid solution, while only 90% flux restoration was observed with the Na_2EDTA solution (Fig. 4.1). One possible explanation for this was that the citric acid solution was at a much higher concentration (240 mM) of citric acid than Na_2EDTA (29 mM), thus more scalants could be removed by the citric acid solution. SEM images of the virgin membrane surfaces compared to after cleaning with both solutions are shown in Fig. 4.2. A small amount of scalants were observed on the surface of the Na_2EDTA cleaned membrane (Fig. 4.2c), while the membrane surface cleaned with the citric acid solution appears free of scalants. EDS analysis further confirmed less scalant on the citric acid-cleaned membrane. It should be noted that the membrane polymeric structure after cleaning with the Na_2EDTA solution is quite similar to the structure of the virgin

membrane, while the polymeric structure of the citric acid-cleaned membrane surface has a noticeably different appearance. However, the observed physical differences of the membrane surfaces do not appear to negatively impact the membrane performance, considering the full restoration of the maximum water flux after cleaning with the citric acid solution. Because citric acid is non-volatile, there is less of a risk for citric acid to pass through the membrane compared to the membrane cleaning using the HCl solutions. Membrane samples treated with multiple citric acid cleaning cycles were able to maintain 99.9% salt rejection. Therefore, the 240 mM citric acid solution is recommended for $CaCO_3$ scalant removal in the future.

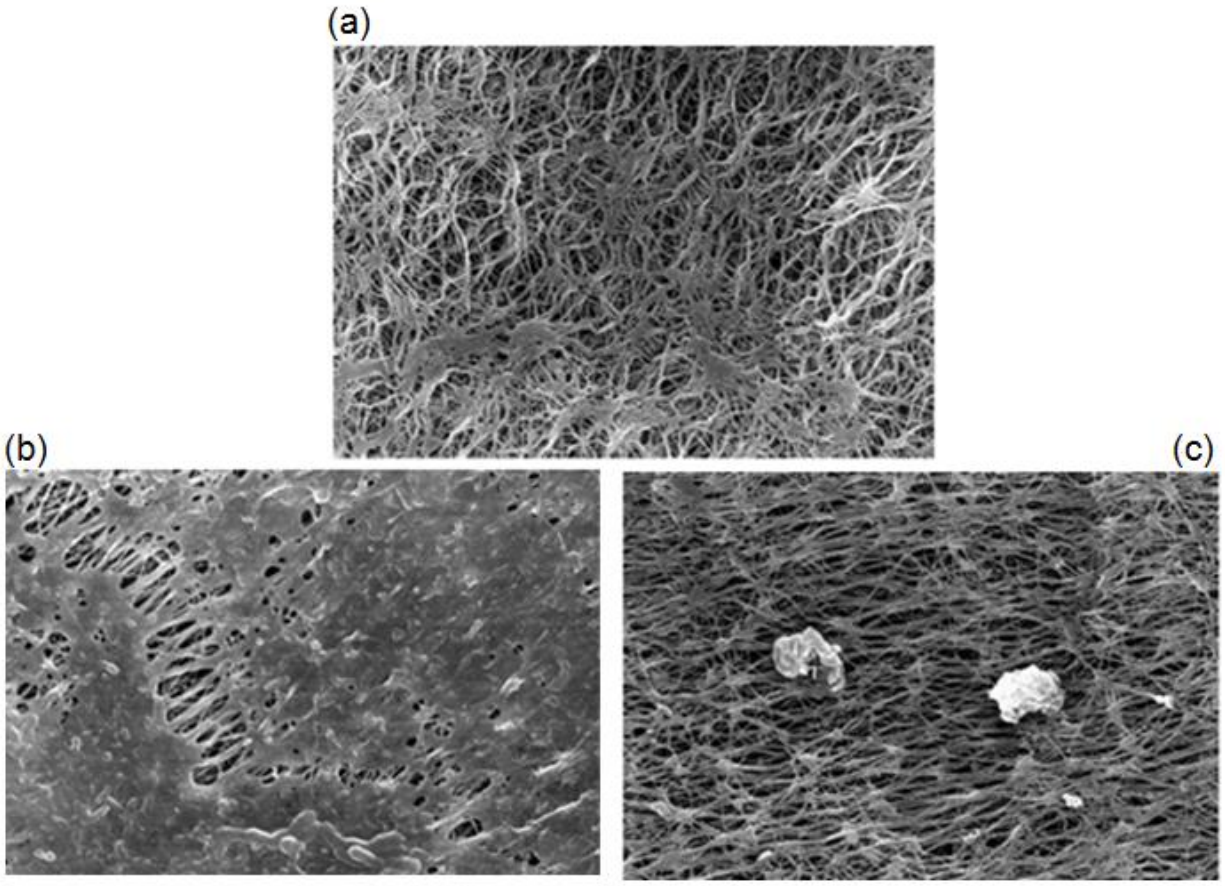

Figure 4.2 SEM images of virgin membrane and membranes cleaned using citric acid solution and Na_2EDTA solution.

4.3.2. Calcium sulfate solution

Results from the OLI software suggest that gypsum was oversaturated in the feed solution before beginning the DCMD test with the $CaSO_4$ solution. It also suggested that anhydrous calcium sulfate had a scaling tendency of 0.93 (a scaling tendency of 1.0 is considered saturated) before the test. Due to concentration polarization effects, it is highly likely that the concentration of anhydrous calcium sulfate on the membrane surface will be greater than the concentration in the bulk solution, thus anhydrous calcium sulfate may also be saturated at the membrane surface at the beginning of the test. Typical calcium sulfate structure was observed on the membrane surface based on the SEM image (data not shown) and the SEM-EDS analysis results revealed only Ca, S, and O elements on the membrane surface, indicating that $CaSO_4$ scalants had fully covered the membrane surface by the end of the test.

During the DCMD test but prior to membrane cleaning, the feed solution remained clear during the first hour, at which time precipitates were observed as the feed solution was further concentrated. A constant water flux was observed during the first 4 hr of the test (Fig. 4.3), suggesting that no membrane scaling had occurred during this period. Instead, the 4 hr period is likely the induction time for the nucleation of $CaSO_4$ scalants: a long induction time for the nucleation of $CaSO_4$ scalants has also been reported by Nghiem et al. [24]. After that, formation of $CaSO_4$ scalants caused a rapid flux decline that is consistent with what has been reported in the literature [24]. After 6 hr, the water flux was less than 2 L/m^2-hr and the flux began to decrease slowly; the water recovery decreased to 25-30% by the end of the test. After cleaning with DI water, the membrane performance was completely restored (Fig. 4.3). Preliminary tests

achieved similar membrane performances using NaOH (50 and 100 mM) and Na_2EDTA (29 and 58 mM) solutions for membrane cleaning. The distillate conductivity was stable at 2 µS/cm before and after membrane cleaning, suggesting good salt rejection during the DCMD test with no pore wetting. Therefore, DI water without additional chemicals is sufficient for $CaSO_4$ removal, which differs from cleaning solutions reportedly used in the literature [29, 30]. However, this result is not surprising considering the high solubility of $CaSO_4$ (e.g., 2-2.5 g/L at 25 ^oC [31]).

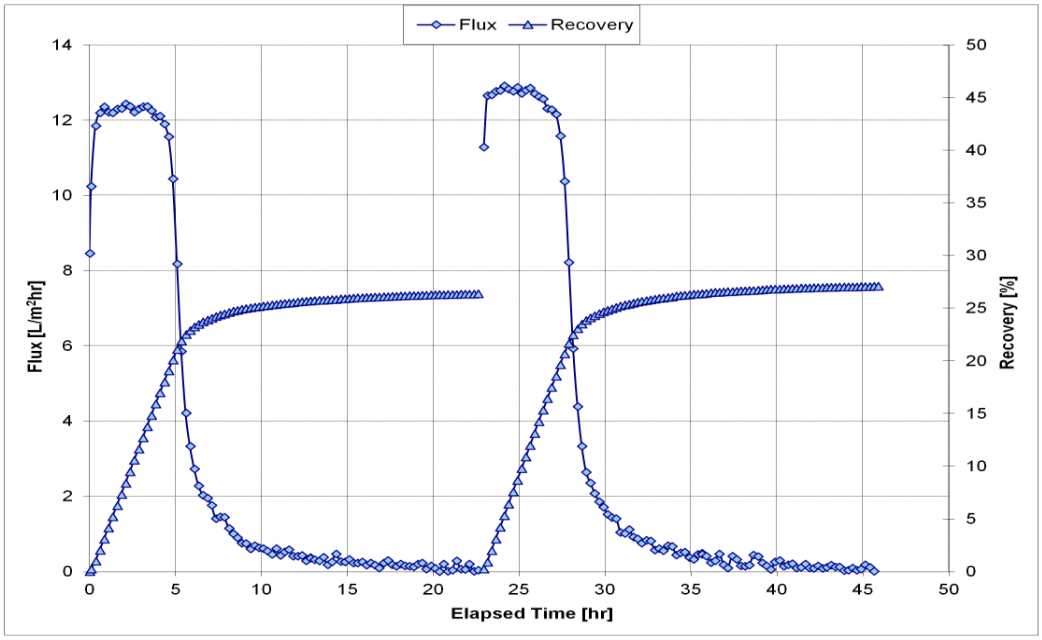

Figure 4.3 Flux and conductivity of the 6 cycle experiment, 13 and 26.8 mM Na_2EDTA cleaning procedures.

4.3.3. Silica feed solution

Results from the OLI software suggested that SiO_2 was oversaturated in the feed solution during the test and was also the only scalant that was saturated. The SEM-EDS analysis revealed that the membrane surface was fully covered by the scalants at the end of the test. A compact layer of scalants on the membrane surface was observed which had a typical structure of SiO_2. In addition, magnesium scalant was also detected but may have much less quantity than the SiO_2 scalant because of the much lower concentrations in the feed solution (Table 4.1). Therefore, the membrane surface was fully covered by the scalants at the end of the test.

DI water cleaning

Water flux and batch recovery before and after membrane cleaning using DI water are given in Fig. 4.4. Slow flux declines were observed in both tests, which differs from what has been reported in the literature for reverse osmosis membrane processes, where rapid flux decline occurred [32, 33]. The faster flux decline caused by the SiO_2 scalant in RO is likely because RO membranes have much smaller pore sizes than MD membranes, thus membrane pore blockage may easily occur in RO but not in MD. The high applied pressure in RO may also attribute to the faster rate of membrane scaling. After membrane cleaning, the maximum water flux reached 5 L/m^2-hr, which is only 42% of the maximum water flux before cleaning. Also, the batch recovery reached only 19% after membrane cleaning, which is much lower than the batch recovery before membrane cleaning (60%). Therefore, DI water is not effective for the SiO_2 scalant removal.

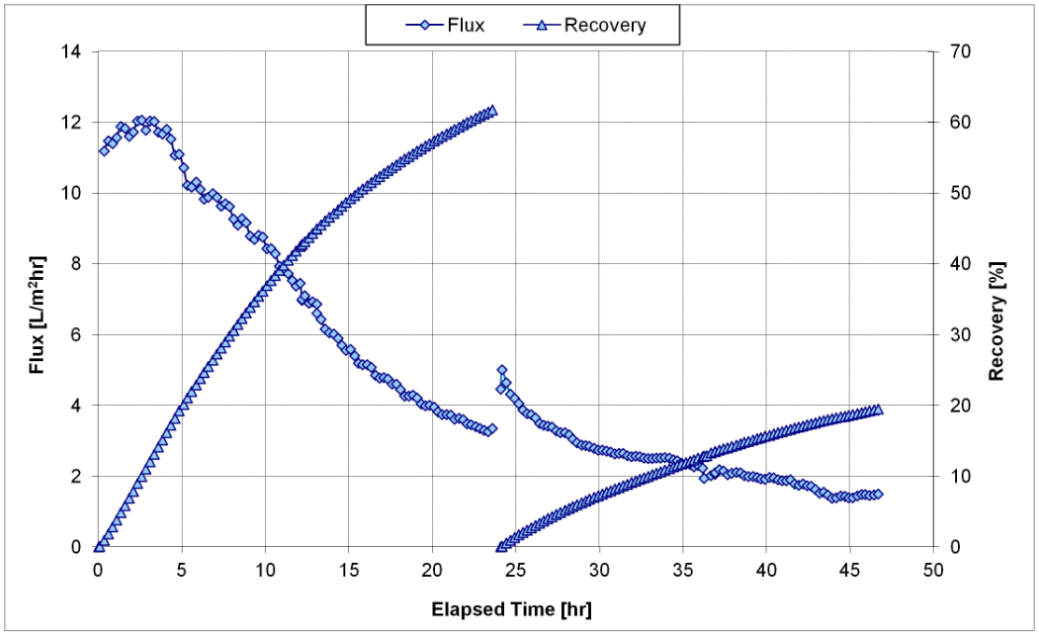

Figure 4.4 Flux and recovery of the 2 cycle experiment, DI water cleaning.

NaOH solution cleaning

Fig. 4.5 gives the membrane performances before and after membrane cleaning using NaOH solutions. The membrane cleaned by the NaOH solution with the lowest concentration (62.5 mM) has only 20% water recovery, and the membrane performance is quite similar to the membrane performance after cleaning using DI water (Fig. 4.4). Therefore, the addition of 62.5 mM NaOH did not improve membrane cleaning compared to DI water itself. Increasing the NaOH concentration to 125 mM led to the maximum water flux of 7 L/m^2-hr and a water recovery of 22% after membrane cleaning, compared to the maximum water flux of 12 L/m^2-hr and a water recovery of 55% before cleaning. Although the 125 mM NaOH solution also did not fully remove the SiO_2 scalant on the membrane surface, a better membrane performance after cleaning was achieved compared to the membrane performance after cleaning using DI water or 62.5 mM NaOH

solution. The membrane cleaned by 250 mM NaOH solution had a continuous increasing of the distillate conductivity until 2 mS/cm during the test. Posterior inspection of the membrane revealed surface damage due to the highly corrosive property of NaOH at such a high concentration. Therefore, the most effective solution among the three NaOH solutions for the SiO_2 scalant removal was the 125 mM NaOH solution and this solution was used for further analysis.

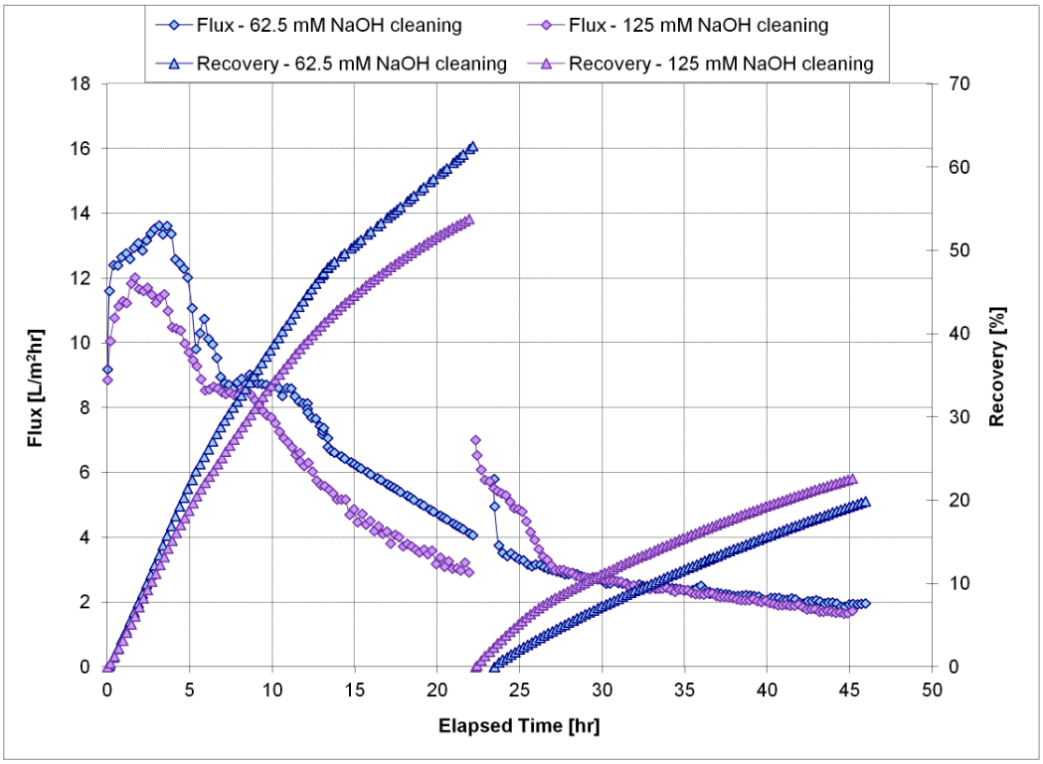

Figure 4.5 Flux and recovery of the 2 cycle experiment, NaOH solution cleaning.

NaOH solution cleaning at 40 ^{o}C

Water flux and batch recovery before and after membrane cleaning using only NaOH solution (125 mM) at 40 ^{o}C and a two-stage cleaning process with NaOH solution

(125 mM) at 40 ^{o}C followed by Na_2EDTA solution (26.8 mM combined with 62.3 mM NaOH) at ambient temperature are given in Fig. 4.6. Unlike the cleaning solutions investigated previously, the maximum water fluxes were fully restored after cleaning with both solutions, thus the increase in temperature seems to improve cleaning. It is likely that the following chemical reaction between NaOH and SiO_2 was facilitated at elevated temperatures:

$$SiO_2 + 2NaOH \rightarrow Na_2SiO_3 + H_2O \quad [46] \qquad (1)$$

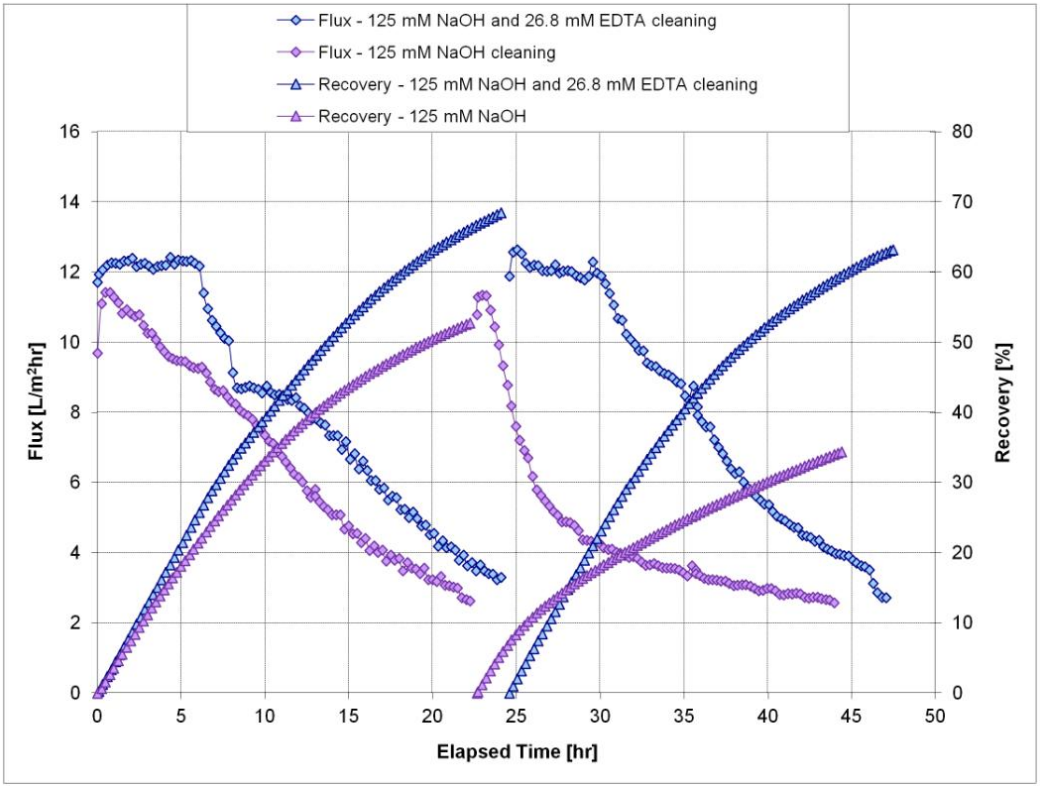

Figure 4.6 Flux and recovery of the 2 cycle experiment, comparison of different cleaning procedure (NaOH vs NaOH plus Na_2EDTA at 40 ^{o}C).

However, after membrane cleaning using only the NaOH solution, there was an immediate onset of flux decline, leading to a water recovery of 35%, which is lower than the water recovery of a virgin membrane (52%). The fast drop of water flux is likely because of the fast formation of the SiO_2 scalant on the membrane surface. It is likely that the majority of the SiO_2 scalant was removed from the membrane following cleaning, thus restoring water flux to its initial level; however, the residual scalant that did remain on the membrane served as nucleation sites for crystallization, leading to more rapid scalant formation and earlier onset of flux decline after cleaning.

In comparison, the membrane performance after cleaning using the two-stage cleaning process is quite similar to that before cleaning with both water recoveries at approximately 65%. Therefore, the two-stage cleaning process improved membrane cleaning in comparison with only NaOH solution. The improved cleaning is likely attributed to the NaOH (62.5 mM) contained in the Na_2EDTA solution. It is likely that NaOH reacted with the SiO_2 residuals (Eq. 4.1) on the membrane surface after the first-stage cleaning and fully removed the SiO_2 residuals. Although Fig. 4.5 suggests the 62.5 mM NaOH solution did not improve membrane cleaning compared to DI water, it is likely that the 62.5 mM NaOH solution removed a small portion of the SiO_2 scalant, but this removal was not significant enough to lead to obvious improvements of water recovery and the maximum water flux. The possibility of Na_2EDTA reacting with SiO_2 is quite small since complicated procedures involving high temperatures (up to 200 ^oC) and extensive amounts of time (> 40 hr) have been used to couple silica with EDTA in the literature [47]. However, Na_2EDTA may attribute to the removal of the magnesium scalants on the membrane through the metal chelating process. It is very unlikely that the

NaOH solutions will emove the magnesium scalant, although magnesium scalant was detected using the SEM-EDS analysis (Section 4.3.3).

4.3.4. Great Salt Lake water

Results from the OLI software suggested that both NaCl and $CaSO_4$ salts reached saturation in the Great Salt Lake water at a water recovery of 4%. Because more NaCl is present in the feed solution, the NaCl scalant is expected to have a more significant effect on membrane performance than the $CaSO_4$ scalant. The SEM-EDS analysis revealed that the membrane surface was fully covered by salt scalants, wth Na and Cl observed as the major scalant elements, followed by small quantities of Ca, Mg, K, and S. To completely remove all the scalants, the 2 wt.% HCl solution was used for membrane cleaning. HCl is commonly used for Ca and Mg scalant removal, and it was hypothesized that the HCl solution would effectively remove the NaCl scalant based on the high solubility of NaCl in the aqueous HCl solution.

Water flux and batch recovery before and after membrane cleaning are given in Fig. 4.7. With a virgin membrane the water flux dropped immediately at the beginning of the test, indicating the onset of membrane scaling at a TDS of 250 g/L of the feed solution. This is consistent with previous reports in the literature [12]. After 3.5 hr of the DCMD test, a rapid flux decline was observed that was likely caused by the homogeneous precipitation of NaCl crystals on the membrane surface [12]. The feed solution had a TDS of 330 g/L at the beginning of the rapid flux decline, which is comparable to reported results from the literature [12]. Only 67% of the maximum water flux was restored after the first membrane cleaning and only 39% restoration after the

second membrane cleaning, which is lower than the performance of the virgin membrane. To investigate whether the lower maximum water fluxes were because of ineffective membrane cleaning, the membrane surfaces after cleaning were investigated through the SEM-EDS analysis. Results suggested that the membrane surfaces were free of scalants with exception of few Si elements, which likely came from the environment (air or tap water) since no silica was used in the feed water preparation. Therefore, the 2 wt.% HCl solution effectively removed the scalants on the membrane surface, and determined that other factors led to the incomplete restoration of the maximum water flux. Because membrane wetting has been observed after cycles of membrane cleaning for the calcium carbonate scalant removal, leading to decreased water flux and lower flux restoration [15, 20, 21, 48], it is likely that membrane wetting also occurred in the current study. The increased distillate conductivity after each cycle of membrane cleaning also supports that membrane wetting may have occurred during membrane cleaning.

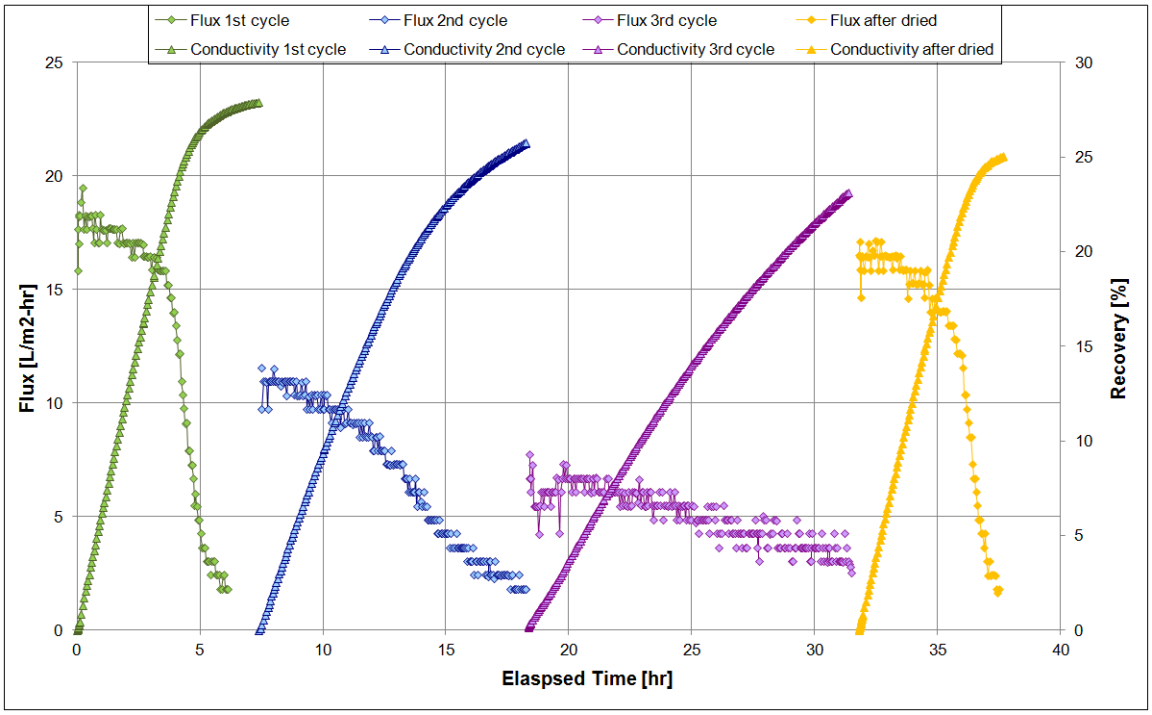

Figure 4.7 Flux and recovery of the Great Salt Lake water treatment.

As scalants fully covered the membrane surface at the end of the DCMD test, the scalants such as the NaCl crystals may have entered into the pores at the upper layer of the membrane. Penetration of the salt scalants into the interior membrane pores up to a depth of 100 μm has been observed by others [20]. Therefore, the scalants deposited inside the upper layer of the membrane may readily dissolve into the cleaning solution, leading to membrane wetting of the membrane surface during membrane cleaning. Reduced water flux caused by membrane wetting has been observed in the literature [15, 20], which is likely becausethat the wetted membrane layer acted as an additional boundary layer, which reduced the mass and heat transfers from the feed bulk solution to the evaporation surface of water vapor, leading to a reduced water flux. To eliminate membrane wetting, the membrane after cleaning was dried inside an oven at 105 ^{o}C until

the mass of the membrane sample remained constant, suggesting a fully dried membrane without water present inside. The non-wetted membrane was tested again using a new batch of the feed solution, and 94% of the maximum water flux was restored after membrane drying (Fig. 4.7). This supports the hypothesis of membrane wetting leading to the decreased maximum water flux. Batch recoveries of 26% and 23% were achieved, respectively, after the first and second membrane cleaning, which were comparable and slightly lower than the water recovery before membrane cleaning (28%). This was likely because the lower maximum water flux led to a lower rate of membrane scaling, and longer operation time before membrane cleaning was needed. After membrane drying, water recovery of 25% was achieved, corresponding to 90% of the water recovery before membrane cleaning.

It should be noted that a dramatic increase of the distillate conductivity (up to 90 μS/cm) was observed at the beginning of the test after membrane drying. The early increase of the distillate conductivity is likely because of the "wash out" of the salts that were dried inside the membrane pores during the membrane drying process.. However, the salt rejection of the DCMD test could still reach near 100% at the initial stage of the DCMD test.

4.4. Conclusions

Membrane cleaning in DCMD when treating feed solutions containing typical scalants ($CaCO_3$, $CaSO_4$, SiO_2, and NaCl) was investigated in this study. The 240 mM citric acid solution was found to effectively remove the $CaCO_3$ scalant and completely restored the membrane performance. The $CaSO_4$ scalant was easily removed using only

DI water without need for additional chemicals. The SiO_2 scalant was difficult to remove, and a two-stage cleaning process using 125 mM NaOH solution at 40 ^oC and 26.8 mM Na_2EDTA solution was used to fully remove the SiO_2 scalant and restore the membrane performance. NaCl was observed as the major scalant when treating the hypersaline solution from the synthetic Great Salt Lake water, and was effectively removed by the HCl solution. However, severe membrane wetting occurred after cleaning, leading to reduced water flux. After membrane drying, 94% of the maximum water flux and 90% of water recovery were achieved. The identification of effective membrane cleaning solutions in this study may make a contribution to the full-scale implementation of MD in the future.

Acknowledgments

The authors acknowledge the financial supports of California Department of Water Resources (Grant NO. 46-7446-R-08) and U.S. Department of Energy Geothermal Technologies Program (Grant No. DE-EE00003231).

Reference

[1] K.W. Lawson, D.R. Lloyd, Review: Membrane distillation, J. Membr. Sci., 124 (1997) 1-25.

[2] A.M. Alklaibi, N. Lior, Transport analysis of air-gap membrane distillation, J. Membr. Sci. 255 (2005) 239-253.

[3] L.M. Camacho, L. Dumée, J. Zhang, J. Li, M. Duke, J. Gomez, S. Gray, Review: Advances in Membrane Distillation for Water Desalination and Purification Applications, Water, 5 (2013) 94-196.

[4] A.M. Alklaibi, N. Lior, Membrane-distillation desalination: status and potential, Desalination, 171 (2004) 111-131.
[5] J. Zhang, N. Dow, M. Duke, E. Ostarcevic, J. Li, S. Gray, Identification of material and physical features of membrane distillation membranes for high performance desalination, J. Membr. Sci., 349 (2010) 295-303.
[6] S. Lee, J. Choa, M. Elimelech, Influence of colloidal fouling and feed water recovery on salt rejection of RO and NF membranes, Desalination, 160 (2004) 1-12.
[7] E. Curcio, E. Drioli, Membrane Distillation and Related Operations - A Review, Sep. Purif. Rev., 34 (2005) 35-86.
[8] M. Khayet, Membranes and theoretical modeling of membrane distillation: A review, Adv. Colloid Interface Sci., 164 (2011) 56-88.
[9] K.W. Lawson, D.R. Lloyd, Membrane Distillation. II. Direct contact MD, J. Membr.Sci. , 120 (1996) 123-133.
[10] J.L. Cartinella, T.Y. Cath, M.T. Flynn, G.C. Miller, K.W. Hunter, A.E. Childress, Removal of natural steroid hormones from wastewater using membrane contactor processes, Environ. Sci. Technol., 40 (2006) 7381-7386.
[11] M. Gryta, M. Tomaszewska, K. Karakulski, Wastewater treatment by membrane distillation, Desalination, 198 (2006) 67-73.
[12] K.L. Hickenbottom, T.Y. Cath, Sustainable operation of membrane distillation for enhancement of mineral recovery from hypersaline solutions, J.M.Sci, 454 (2014) 426-435.
[13] S. Shirazi, C. Lin, D. Chen, Inorganic fouling of pressure-driven membrane processes - A critical review, Desalination, 250 (2010) 236-248.
[14] H.L Yang, C. Huang, J.R. Pan, Characteristics of RO foulants in a brackish water desalination plant, Desalination, 220 (2008) 353-358.
[15] M. Gryta, Long-term performance of membrane distillation process, J. Membr.Sci., 265 (2005) 153-159.
[16] M. Gryta, Pretreatment of feed water for membrane distillation, Chemical Papers, 62 (2008) 100-105.

[17] C.R. Martinetti, A.E. Childress, T.Y. Cath, High recovery of concentrated RO brines using forward osmosis and membrane distillation, J. Membr. Sci., 331 (2009) 31-39.
[18] D. Qu, J. Wang, B. Fan, Z. Luan, D. Hou, Study on concentrating primary reverse osmosis retentate by direct contact membrane distillation, Desalination, 247 (2009) 540-550.
[19] M.T. M. Gryta, J. Grzechulska, A.W. Morawski, Membrane distillation of NaCl solution containing natural organic matter, Journal of Membrane Science, 2001 (2001) 279-287.
[20] M. Gryta, Fouling in direct contact membrane distillation process, J. Membr. Sci., 325 (2008) 383-394.
[21] M. Gryta, Desalination of thermally softened water by membrane distillation process, Desalination, 257 (2010) 30-35.
[22] R.J. Surapit Srisurichan, A.G. Fane, Humic acid fouling in the membrane distillation process, Desalination, 174 (2005) 63-72.
[23] M. Gryta, Effect of iron oxides scaling on the MD process performance, Desalination, 216 (2007) 88-102.
[24] L.D. Nghiem, T. Cath, A scaling mitigation approach during direct contact membrane distillation, Sep. Purif. Technol., 80 (2011) 315-322.
[25] J. Mericq, S. Laborie, C. Cabassud, Vacuum membrane distillation of seawater reverse osmosis brines, Water Res., 44 (2010) 5260-5273.
[26] L. Mo, X. Huang, Fouling characteristics and cleaning strategies in a coagulation-microfiltration combination process for water purification Desalination, 159 (2003) 1-9.
[27] A Maskooki, T. Kobayashi, S.A. Mortazavi, A. Maskooki, Effect of low frequencies and mixed wave of ultrasound and EDTA on flux recovery and cleaning of microfiltration membranes, Sep. Purif. Technol., 59 (2008) 67-73.
[28] Y.A. Le Gouellec, M. Elimelech, Calcium sulfate (gypsum) scaling in nanofiltration of agricultural drainage water, J. Membr. Sci., 205 (2002) 279-291.
[29] F. He, J. Gilron, H. Lee, L. Song, K. Sirkar, Potential for scaling by sparingly soluble salts in crossflow DCMD, in, 2008, pp. 68-80.

[30] F He, K.K.Sirkar, J. Gilron, Studies on scaling of membranes in desalination by direct contact membrane distillation: $CaCO_3$ and$mixedCaCO_3/CaSO_4$ systems Chem. Eng. Sci., 64 (2009) 1844-1859.
[31] E. Bock, On the solubility of anhydrous calcium sulphate and of gypsum in concentrated solutions of sodium chloride at 25 °C, 30 °C, 40 °C, and 50 °C, Canadian J. Chemistry, 39 (9) (1961) 1746-1751.
[32] D. Lisitsin, D. Hasson, R. Semiat, Critical flux detection in a silica scaling RO system, Desalination, 186 (2005) 311-318.
[33] W. Den, C. Wang, Removal of silica from brackish water by electrocoagulation pretreatment to prevent fouling of reverse osmosis membranes, Sep. Purif. Technol., 59 (2008) 318-325.
[34] T. Koo, Y.J. Lee, R. Sheikholeslami, Silica fouling and cleaning of reverse osmosis membranes Desalination, 139 (2001) 43-56.
[35] G. Braun, W. Hater, C. zum Kolk, C. Dupoiron, T. Harrer, T. Götz, Investigations of silica scaling on reverse osmosis membranes, Desalination, 250 (2010) 982-984.
[36] R. Sheikholeslami, I.S. Al-Mutaz, S. Tan, S.D. Tan, Some aspects of silica polymerization and fouling and its pretreatment by sodium aluminate, lime and soda ash, Desalination, 150 (2002) 85-92.
[37] S. Kang, K. Choo, Use of submerged microfiltration membranes for glass industry wastewater reclamation: pilot-scale testing and membrane cleaning, Desalination, 189 (2006) 170-180.
[38] T. Tran, S. Gray, B Bolto, T.D. Farmer, T.F. Collings, Ultrasound enhancement of microfiltration performance for natural organic matter removal, Organic Geochemistry, 38 (2007) 1091-1096.
[39] J. Burgess, Metal ions in solution, Halsted Press, New York: Ellis Horwood, 1978.
[40] G. Chen, Y. Lu, W.B. Krantz, R. Wang, A.G. Fane, Optimization of operating conditions for a continuous membrane distillation crystallization process with zero salty water discharge, J. Membr. Sci., 450 (2014) 1-11.
[41] K. W. Lawson, D.R. Lloyd, Review: Membrane distillation, J. Membr. Sci. , 124 (1997) 1-25.

[42] E.M.W. District, Your Water Quality Consumer Confidence Report for 2004 http://www.emwd.org/modules/showdocument.aspx?documentid=1125, in, 2005.
[43] F.T. Mackenzie, "Hydrosphere." Encyclopaedia Britannica Encyclopaedia Britannica Online Academic Edition ed., Encyclopaedia Britannica Inc., 2014.
[44] T.Y. Cath, V.D. Adams, A.E. Childress, Experimental study of desalination using direct contact membrane distillation: a new approach to flux enhancement, J. Membr.Sci., 228 (2004) 5-16.
[45] J. A. Ruskowitz, A.E. Childress, Salt-Gradient Solar Pond and Membrane Distillation System for Water Desalination Powered by Renewable Energy, in: Thesis, University of Nevada, Reno, Reno, Nevada, 2012.
[46] N.N. Greenwood, A. Earnshaw, Chemistry of the elements, Pergamon Press, Oxford, 1984.
[47] E. Repo, T.A. Kurniawan, J.K. Warchol, M.E.T. Sillanpää, Removal of Co (II) and Ni(II) ions from contaminated water using silica gel functionalized with EDTA and/or DTPA as chelating agents, J. Hazard. Mater, 171 (2009) 1071-1080.
[48] J. Ge, Y. Peng, Z. Li, P. Chen, S. Wang, Membrane fouling and wetting in a DCMD process for RO brine concentration, Desalination, 344 (2014) 97-107.

Chapter 5

5 CONCLUSIONS

5.1. Research Synopsis

This dissertation represents several investigations into the performance and enhancement of the DCMD process. These include: 1) simplified flux prediction using a novel membrane structural parameter in DCMD; 2) mechanistic investigation of factors attributing to improved water flux in VEDCMD; and 3) evaluation of membrane fouling and effective membrane cleaning solutions for various types of feed waters.

5.2. Summary of simplified flux prediction in DCMD

The flexibility of MD to operate at high water fluxes when treating waters with low fouling potential or at low water fluxes with high fouling potential waters makes it an attractive option for many situations. Because of the wide potential operating range, an *a priori* water flux prediction model is desirable, but existing mass transfer models are complicated with inconsistent mass transfer mechanism assumptions and coupled membrane property parameters. Therefore, a method to simplify the flux prediction of MD using uncoupled membrane properties was developed. Ten single-layer MD membranes were characterized and the water fluxes were determined in DCMD under the same experimental conditions. A new membrane structural parameter, C_m, was also proposed that contains uncoupled membrane properties and can be measured using simple and reliable instruments at low costs. The correlation analysis between water flux and C_m was performed and a correlation coefficient of 0.714 was obtained, suggesting

that C_m is a good structural parameter for estimating water flux. Using linear regression, a flux prediction model was developed based on C_m. Compared to the commonly used dusty gas model, better flux predictions were achieved. The new model can be used to predict water fluxes of membranes with a broad range of pore size (0.1 to 0.9 μm), although its accuracy decreases for membranes with low porosities and very small pore sizes (<0.1 μm).

5.3. Summary of evaluation of VEDCMD

Improved DCMD water flux has been reported in the literature when vacuum was applied in the membrane module, but only qualitative analyses of the factors attributing to the enhanced water flux were given. To identify the dominant factors affecting water flux, membrane performances in traditional DCMD, PEDCMD, and VEDCMD were investigated. The same membrane type was used in each test and experimental conditions were kept the same expect for adjustments to the feed- and distillate-side pressures. The experimental results agreed with the literature, with VEDCMD having the highest water flux followed by DCMD and PEDCMD, which had similar water fluxes. The effect of each of the main parameters in the dusty gas model for water flux were investigated, and it was found that water flux decreased with increased membrane compaction or air pressure inside the membrane pores (P_{air}); the pressure gradient present in PEDCMD and VEDCMD had minimal effect on water flux. Membrane properties before and after testing were characterized, and severe membrane compaction was identified in PEDCMD, followed by DCMD, and only minimal compaction occurred in VEDCMD. Therefore, less membrane compaction is one of the dominant factors attributing to the

improved water flux in VEDCMD. To identify the magnitude of P_{air} in each MD test, assumptions from the literature regarding P_{air} (ideal gas law; $P_{air} = P_d$) and from the force balance analysis at the membrane pore entrance were evaluated. Model results suggest a higher P_{air} in DCMD and PEDCMD (equal to P_d) than the P_{air} in VEDCMD (equal to the average of the feed and distillate-side pressures); therefore, a smaller P_{air} is the other dominant factor attributing to higher water flux in VEDCMD.

5.4. Summary of evaluation of membrane fouling and cleaning in DCMD

Membrane fouling has become one of the main obstacles inhibiting the full implementation of MD, yet no systematic investigation of effective membrane cleaning solutions for removal of typical scalants was available for DCMD. Using multiple feed waters that included the most common scalants experienced by DCMD ($CaCO_3$, $CaSO_4$, SiO_2, and NaCl), the membrane performance before and after several cleaning protocols was investigated. It was found that citric acid, a metal chelating agent, was able to fully restore the membrane performance after cleaning membranes scaled with $CaCO_3$. For $CaSO_4$, DI water without additional chemicals fully restored the membrane performance after membrane cleaning. A two-stage process with an NaOH solution at elevated temperature followed by an EDTA solution was identified to fully restore performance after membrane cleaning for SiO_2 scalants. An HCl solution completely removed membranes fouled by hypersaline feed water with NaCl as the major scalant, but low maximum water flux was observed after membrane cleaning. It was determined that membrane wetting occurred with HCl cleaning, and more than 90% restoration of membrane performance was achieved after membrane drying.

5.5. Environmental significance

MD is an emerging membrane separation process that can be coupled with low-grade thermal energies for potable water production. If an MD unit is operated in conjunction with a waste heat source, the cost of energy for heating the feed water is negligible. In the case of thermally polluted water, such as the produced water from oil and gas industry, MD can directly treat the water. This ability to utilize low-grade thermal energies has made MD an attractive alternative to pressure-driven membrane processes.

MD alone or hybrid MD-RO systems for the treatment of RO brines can improve water recovery in desalination processes and will produce highly concentrated waste streams. In some cases, the minerals contained in the waste streams may be further extracted and then marketed. In addition to a more concentrated waste streams, seawater desalination with MD systems avoids the need for pretreatment processes, such as coagulation and flocculation, that are frequently used with RO systems. Therefore, MD for seawater desalination can reduce chemical consumption and prevent damage to the ocean environment associated with the disposed brines [1].

Because the driving force of MD does not decrease significantly with increasing feed-water salinity, MD can be also used to treat waters with high total dissolved solids. These types of waters would be either uneconomical or unfeasible to treat using pressure-driven membrane processes. For example, MD can be installed at a mining site or a salt lake site and serve as a pretreatment process for the extraction of valuable metals (e.g., lithium) from the water. It is generally too expensive to extract the valuable metals from water with low concentrations of the target metals, but after MD pretreated, the metals

can be highly concentrated to facilitate their extraction. MD can also help to approach the zero-discharge target if coupled with crystallizers when treating hypersaline solutions. The hypersaline feed solution will first be concentrated using MD, and then NaCl can be crystallized inside the crystallizer and removed from the feed water. The water leaving the crystallizer can then be concentrated again using the MD system, and additional NaCl crystals removed.

Overall, the capability of MD to be powered by low-grade thermal energy, the high contaminant rejection, and the small decrease of the driving force when treating hypersaline feed waters makes MD an attractive water treatment technology. Versatile applications of MD have been reported in the literature. However, there is still lack of commercially available MD modules that can be used outside of the lab, and more studies are needed focusing on the module design area. In addition, the low water flux of MD, especially the AGMD, which has been studied in the pilot scale, is another concern. To make MD competitive when treating feed waters with low fouling potentials, where pressure-driven membrane processes are commonly used, it is necessary to improve water flux of the MD membranes. Therefore, more studies on manufacturing MD membranes with high water fluxes are desirable. Membrane scaling and wetting are also concerns for long-term operation of MD, thus approaches to prevent these from occurring, such as modifying the MD membranes or identifying proper experimental conditions, are still needed.

Reference

[1] J. Morillo, J. Usero, D. Rosado, H.El Bakouri, A. Riaza, F. Bernaola, Comparative study of brine management technologies for desalination plants, Desalination, 336 (2014) 32-49.